

1-1-2004

Extraction of paleohydrology and paleoclimate proxies from vadose zones and paleolake records in the southwestern Great Basin

Weiquan Dong
University of Nevada, Las Vegas

Follow this and additional works at: <https://digitalscholarship.unlv.edu/rtds>

Repository Citation

Dong, Weiquan, "Extraction of paleohydrology and paleoclimate proxies from vadose zones and paleolake records in the southwestern Great Basin" (2004). *UNLV Retrospective Theses & Dissertations*. 2591. <http://dx.doi.org/10.25669/z7m5-pt8n>

This Dissertation is protected by copyright and/or related rights. It has been brought to you by Digital Scholarship@UNLV with permission from the rights-holder(s). You are free to use this Dissertation in any way that is permitted by the copyright and related rights legislation that applies to your use. For other uses you need to obtain permission from the rights-holder(s) directly, unless additional rights are indicated by a Creative Commons license in the record and/or on the work itself.

This Dissertation has been accepted for inclusion in UNLV Retrospective Theses & Dissertations by an authorized administrator of Digital Scholarship@UNLV. For more information, please contact digitalscholarship@unlv.edu.

EXTRACTION OF PALEOHYDROLOGY AND PALEOCLIMATE PROXIES FROM
VADOSE ZONES AND PALEOLAKE RECORDS IN THE
SOUTHWESTERN GREAT BASIN

by

Weiquan Dong

Bachelor of Science
Chengdu University of Technology, China
1987

Master of Science
Institute of Geochemistry, Chinese Academy of Sciences, China
1990

A dissertation submitted in partial fulfillment
of the requirements for the

Doctor of Philosophy Degree in Geoscience
Department of Geoscience
College of Sciences

Graduate College
University of Nevada, Las Vegas
August 2004

UMI Number: 3175374

INFORMATION TO USERS

The quality of this reproduction is dependent upon the quality of the copy submitted. Broken or indistinct print, colored or poor quality illustrations and photographs, print bleed-through, substandard margins, and improper alignment can adversely affect reproduction.

In the unlikely event that the author did not send a complete manuscript and there are missing pages, these will be noted. Also, if unauthorized copyright material had to be removed, a note will indicate the deletion.

UMI[®]

UMI Microform 3175374

Copyright 2005 by ProQuest Information and Learning Company.

All rights reserved. This microform edition is protected against unauthorized copying under Title 17, United States Code.

ProQuest Information and Learning Company
300 North Zeeb Road
P.O. Box 1346
Ann Arbor, MI 48106-1346



Dissertation Approval
The Graduate College
University of Nevada, Las Vegas

JULY 23, 2004

The Dissertation prepared by

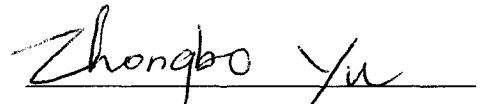
WEIQUAN DONG

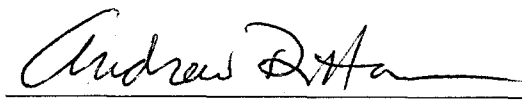
Entitled

EXTRACTION OF PALEOHYDROLOGY AND PALEOCLIMATE PROXIES FROM
VADOSE ZONES AND PALEOLAKE RECORDS IN SOUTHWESTERN GREAT BASIN

is approved in partial fulfillment of the requirements for the degree of

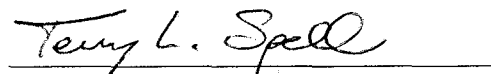
DOCTOR OF PHILOSOPHY DEGREE IN GEOSCIENCE

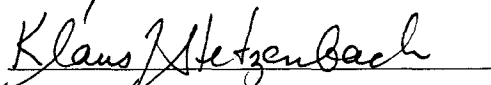

Examination Committee Chair


Examination Committee Member


Dean of the Graduate College


Examination Committee Member


Examination Committee Member


Graduate College Faculty Representative

ABSTRACT

Extraction of Paleohydrology and Paleoclimate Proxies from Unsaturated Zones and Paleolake Records in the Southwestern Great Basin

by

Weiquan Dong

Dr. Zhongbo Yu, Examination Committee Chair
Assistant Professor of Geology
University of Nevada, Las Vegas

Thick vadose zones in arid regions recorded past climate changes up to 100 ka, so they are unique archives for continental paleoclimate change and groundwater recharge during the late Quaternary. Despite extensive research on flow and transport in arid regions, the transport properties and general response of arid vadose zones to climate regimes are still not well understood. Some of these issues are addressed with four distinct studies in this dissertation. The first study investigates effects of soil texture, vegetation coverage, and macropores on soil moisture variation at Nevada Test Site (NTS). The simulations show that bare soils have higher soil water content than vegetated soils. Effects of macropore flow on soil water content are insignificant.

The second study evaluates the impacts of climate change on solute transport in arid vadose zones. Undisturbed soil cores were collected at ground surface, directly below where tension infiltrometer measurements were made. The water fluxes and Br dispersion coefficients at investigated matric heads were very high due to the coarseness of the soils

and possibly due to preferential flow pathways. These high water fluxes are more likely to occur in ephemeral washes. However, higher fluxes through the surface soil would be more likely during wetter climates.

The third study simulates paleolake extent in Owens Valley in the last 18 ka. A coupled catchment-lake model is developed in this study, and used to reconstruct the observed paleolake levels for Owens Lake and Searles Lake. Finally, a quantitative time-series of paleoclimate information was obtained.

The fourth study models the actual measured chloride profile in Amargosa Desert Research Site (ADRS) with the modified version of the HYDRUS-1D computer code by using variable boundary conditions. The paleoinformation estimated from the third study, and chloride concentration in Greenland ice core (GISP2) are used to prepare the atmospheric boundary file. The simulated chloride profile is in agreement with the measured chloride profile, and simulated water flux at ADRS is ~ 0.016 mm/year upward at the base of the profile.

Transport properties and general response of vadose zones to climate regimes are addressed by these four independent studies.

TABLE OF CONTENTS

ABSTRACT	iii
LISTS OF TABLES	vii
LISTS OF FIGURES	viii
ACKNOWLEDGMENTS.....	x
CHAPTER 1 INTRODUCTION	1
1.1. Simulations on Soil Moisture Variation in Arid Regions	2
1.2. Bromide Displacement Experiments.....	2
1.3. Paleolake Extent in Owens Valley	3
1.4. Chloride Transport in Vadose Zone of ADRS	5
References	7
CHAPTER 2 SIMULATIONS ON SOIL WATER VARIATION IN ARID REGIONS	12
2.1. Abstract	12
2.2. Introduction	13
2.3. Soil Hydrologic Model (SHM)	17
2.3.1. Infiltration-Runoff Calculation	19
2.3.2. Subgrid Spatial Variability.....	20
2.3.3. Parameterization of Macropore Flow.....	21
2.4. Study Sites.....	24
2.5. Model Validation.....	29
2.6. Hydrologic Data	30
2.7. Results	33
2.7.1. Soil Texture.....	34
2.7.2. Macropores.....	37
2.7.3. Vegetation	42
2.8. Summary and Conclusions.....	49
References	53
CHAPTER 3 SOLUTE TRANSPORT IN ARID VADOSE ZONES	62
3.1. Abstract	62
3.2. Introduction	63
3.3. Materials and Methods	66
3.3.1. Site Description	66
3.3.2. Collection of Undisturbed Cores.....	68
3.3.3. Experimental Setup	68

3.4. Modeling Approaches	71
3.5. Results and Discussion.....	74
3.5.1. Infiltration Data Analysis	74
3.5.2. Br Transport Characteristics.....	76
3.5.3. Discussion	86
3.6. Conclusions and Further Work	91
References	93
CHAPTER 4 SIMULATION OF PALEOLAKE EXTENTS IN OWENS VALLEY	102
4.1. Abstract	102
4.2. Introduction	103
4.3. Owens River System	106
4.4. Description of Model and Modeling Strategies	109
4.5. Calibration of Catchment-Lake Model	113
4.6. Input Parameters.....	116
4.7. Results	119
4.7.1. Simulation on Modern Lakes	119
4.7.2. Simulations on Lakes at Last Glacial Maximum (LGM).....	119
4.7.3. Simulations on Lakes at 15 ka.....	122
4.7.4. Simulations on Lakes at 12 ka.....	122
4.7.5. Simulations on Lakes at 9 ka.....	123
4.7.6. Simulations on Lakes at 6 ka.....	123
4.8. Sensitivity Analysis.....	124
4.9. Discussion	125
4.10. Conclusions and Future Work.....	129
References	131
CHAPTER 5 SIMULATION OF CHLORIDE TRANSPORT	141
5.1. Introduction	141
5.2. Site Description	144
5.3. Numerical Modeling	146
5.4. Input Parameters.....	148
5.5. Results	150
5.6. Uncertainty Analyses	151
5.7. Conclusions and Further Work	154
References	155
CHAPTER 6 CONCLUSIONS.....	162
APPENDIX I PERMISSION OF ELSEVIER SCIENCE	166
VITA	168

LISTS OF TABLES

Table 2.1. List of variables used in this study.	35
Table 2.2. Estimated macroporosity for different radii.	42
Table 2.3. Summary of simulated volumetric water content over the 2-m soil profile. ...	46
Table 3.1. In-situ measured water flow rates (cm^3/hour) with tension infiltrometer at the ADRS.	75
Table 3.2. Calculated parameters with the data in Table 3.1.	77
Table 3.3. Input parameters and fitted parameters with the one-region model.	80
Table 3.4. Fitted parameters with the two-region model.	85
Table 4.1. Proxy data in the southwest United States in the last 18 ka.	121
Table 4.2. Simulated lake extent and elevation of lake levels in Owens Valley in the last 18 ka.	125
Table 5.1. Hydraulic properties of representative soil at ADRS.	149
Table 5.2. The parameters related chloride profile used in this study.	149

LISTS OF FIGURES

Figure 2.1. Hydraulic conductivity for silty loam with and without macropores.	25
Figure 2.2. Location map of the study area at the Nevada Test Site.....	26
Figure 2.3. Water content profile for the borehole U3fd-N2.	28
Figure 2.4. Comparison of the measured volumetric water content and the simulated volumetric water content.	31
Figure 2.5. Simulated soil water content for bare soils without macropores at the top 10 cm and 30 cm.....	36
Figure 2.6. Simulated soil water content for sand with macropores at the top 10 cm and 30 cm.	39
Figure 2.7. Simulated soil water content for loamy sand with macropores at the top 10 cm and 30 cm.....	40
Figure 2.8. Simulated soil water content for silty loam with macropores at the top 10 cm and 30 cm.	41
Figure 2.9. Simulated soil water content for sand with vegetative cover only and both vegetative cover and macropores at the top 10 cm and 30 cm.	43
Figure 2.10. Simulated soil water content for loamy sand with vegetative cover only and both vegetative cover and macropores at the top 10 cm and 30 cm.	44
Figure 2.11. Simulated soil water content for silty loam with vegetative cover only and both vegetative cover and macropores at the top 10 cm and 30 cm.	45
Figure 3.1. Location map of the ADRS.	67
Figure 3.2. Schematic of the experimental setup used in this study.	69
Figure 3.3. Calculated hydraulic conductivities based on the in-situ measurements; a. shows the hydraulic conductivity for soils close to plants, b. shows the hydraulic conductivity for the bare soils.	78
Figure 3.4. Observed data and fitted curves with the one-region model of CXTFIT2 at saturated conditions were plotted with pore volumes.	79
Figure 3.5. Observed data and fitted curves with the one-region model of CXTFIT2 at the matric head of -2 cm were plotted with pore volumes.....	82
Figure 3.7. Observed data and fitted curves with the one-region model of CXTFIT2 at the matric head of -10 cm were plotted with pore volumes.....	84
Figure 3.8. Observed data and fitted curves with the two-region model of CXTFIT2 were plotted with pore volumes.	86
Figure 4.1. Location map of Owens River system.....	108
Figure 4.2. $\delta^{18}\text{O}$ for core OL84B (solid line with dot), $\delta^{18}\text{O}$ from GISP2 (solid line), and elevation of lake surface for Searles Lake (dashed line) in the last 20 ka...	109
Figure 4.3. A comparison of observed runoff and simulated runoff in Mono Lake drainage basin.....	114
Figure 4.4. a. A plot of simulated and measured temperature profile in Mono Lake; b. Simulated evaporation and observed evaporation for Mono Lake.....	115

Figure 4.5. Inputs of cloud cover, solar radiation for the simulations at 18 ka, 15 ka, 12 ka, 9 ka, and 6 ka.	117
Figure 4.6. Inputs of wind speed for the simulations at at 18 ka, 15 ka, 12 ka, 9 ka, and 6 ka.	118
Figure 4.7. Simulated lake extents (dotted area) in the last 18 ka, and hillshed (Gray scale) and stream network (solid lines) derived from DEM data.	120
Figure 4.8. a. Simulated temperature (solid line with dots) and estimated temperature based on pollen (solid line) in Owens Lake; b. Simulated precipitation (solid line with dots) and estimated precipitation based on pollen (solid line) in Owens Lake.	127
Figure 5.1. Location map of the ADRS.	145
Figure 5.2. Measured chloride and soil water content profiles.	146
Figure 5.3. The data used to prepare atmospheric boundary input file for HYDRUS-1D.	150

ACKNOWLEDGMENTS

The projects in this dissertation were funded by the U.S. Dept. of Energy through the Harry Reid Center for Environmental Studies, Geologic Society of America Graduate Student Grant, and Graduate Student Association Grant, University of Nevada, Las Vegas.

After any four year endeavor one certainly hopes there will be many people to thank for their help and friendship. I feel fortunate that this is indeed the case with this dissertation.

From the beginning each member of my committee has been interested and actively involved in my research. Dr. David K. Kreamer offered thoughtful comments based on his expertise in hydrology and hydrogeology. Dr. Andrew D. Hanson provided extremely helpful assistance from both technical and conceptual aspects. I'd like to thank Dr. Terry L. Spell for his help and discussions during my study. I also appreciate Dr. Klaus J. Stetzenbach for his generous financial support and service as graduate faculty representative over the years.

Most of all, I am indebted to my advisor and mentor Dr. Zhongbo Yu for providing invaluable guidance throughout my graduate study. He has achieved the perfect balance between providing guidance and independence. I am also grateful to Dr. Zhongbo Yu for his generous financial support.

I would like to thank all of the ADRS research team, and especially Dr. Brian Andraski for the cooperation and help that allowed me to perform my study at the ADRS.

Many thanks go to Dr. Michael Young for generous help to allow me to perform my experiments in his laboratory.

I gratefully acknowledge Dr. Bridget R. Scanlon for providing the modified version of the HYDRUS-1D computer code, Dr. Steven W. Hostetler for providing the lake model code, and Dr. Richard L. Orndorff for providing the surface hydrology model.

Many thanks to John Goreham, Clay H. Crow, Kazumasa Lindley, and Caixiao Guo for their assistance on experiments, to Shuxia Wu, Feng Pan, for their help on my field measurements and collection of undisturbed soil cores.

The text of Chapter 2 is a reprint of material as it appeared in Journal of Hydrology. The co-authors on this publication, Zhongbo Yu, directed and supervised the research which forms the basis for this chapter; Dennis Weber provided logical supports for this research. Chapter 3 is the outcome of a collaborative effort with Zhongbo Yu, Michael Young, and Klaus J. Stetzenbach. Chapter 4 is also the result of a collaborative study with Zhongbo Yu, Richard L. Orndorff, and Klaus J. Stetzenbach.

Many thanks go to Drs. Norbert Thonnard, Larry D. McKay for their guidance and supports when I was in the University of Tennessee, Knoxville. I greatly appreciate Dr. Devendra Lal for his teaching me real science. Thanks to Dr. Duofu Chen for our productive collaboration.

Finally, thanks to my family. My parents and Qian's parents have provided long-distance love and support throughout. As I try to figure out how to express my gratitude to Qian I find I am at a loss for words. I am not sure I would have, or could have done this without her. She has provided constant support and encouragement. In addition to being a wonderful wife and a fantastic mother for Anya, she is my best friend.

CHAPTER 1

INTRODUCTION

Predicting future hydrologic conditions requires a better understanding of present and past hydrometeorologic processes and of related climatic and hydrologic variability. Also, there is a critical need for designing a disposal site for radioactive wastes that will be safe for a time frame of 10 ka. One of the best ways to approach these two problems is to study Quaternary paleoclimatic and paleohydrologic records (Kutzbach, 1980; Winograd, 1981). Changes in hydrology, including unsaturated zone percolation, saturated zone hydrology, and groundwater discharge, are closely related to climate changes. Therefore, inferences related to paleohydrology can be drawn from paleoclimatic studies. Links between paleoclimate and paleohydrology offer a basis for evaluating and predicting the effects of climate changes on hydrology in the past and in the future.

Low precipitation rates and high evapotranspiration rates commonly result in low rates of water movement and thick vadose zones in arid regions, thus the arid vadose zones have been considered very suitable for waste disposal sites (Winograd, 1981; Scanlon, 1991). Despite extensive research on flow and transport in arid regions, the transport properties and general response of arid vadose zones to climate regimes are still not well understood. In this dissertation, with field, laboratory, and numerical approaches, these problems were addressed by studying effects of soil textures, vegetation cover, and

macropores on soil moisture variation (Chapter 2), impacts of climate changes on bromide transport (Chapter 3), paleoclimate and paleohydrology change in Owens Valley (Chapter 4), and chloride transport in vadose zones of Amargosa Desert Research Site (ADRS), United States Geologic Survey (Chapter 5).

1.1. Simulations on Soil Moisture Variation in Arid Regions

Soil hydraulic properties are intrinsic factors in controlling flow and transport in vadose zones. Macropores are one of the common soil structural properties, as they play an important role in the movement of water and chemicals owing to occasional rapid fluxes through them. Although macropore flows are not common in desert soils because of very low effective precipitation, they do occur in desert soils under certain circumstances (Devitt and Smith, 2002). So it is important to evaluate contributions of macropores to soil moisture and water flow in desert soils. In this study, a soil hydrologic model (SHM) was developed for simulating soil water movement through the unsaturated zone at the Nevada Test Site (NTS). A parameterization scheme with dual processes of matrix and macropore was adopted to derive *effective* hydraulic conductivity for the SHM. Effects of soil texture and vegetation coverage on soil water content were evaluated in this study.

1.2. Bromide Displacement Experiments

A quantitative description of water movement and solute transport in soils is necessary for a variety of reasons, including groundwater recharge, ecosystem processes, and waste management. Beside intrinsic factors of soil hydraulic properties, external

factors such as climate conditions have significant effects on water movement and solute transport. The conclusion that desert vadose zones are suitable for waste disposal is based on present climate conditions. However, the region was strongly influenced by pluvial climate conditions during the Quaternary Period (Quade et al., 2003; Anderson and Wells, 2003). Although extensive research on flow and transport has been conducted in arid regions, the transport properties and general response of arid vadose zones to wetter climate regimes are still not well understood. Therefore, it is necessary to study those processes in soils under alternative possible climate scenarios.

Since it is very difficult to perform field scale experiments to study such problems, miscible displacement experiments were used in this study to examine the effects of a high effective precipitation on water movement and solute transport. Miscible displacement experiments have been used by many researchers to quantitatively and qualitatively describe effects of soil structure, water flux, and water content on solute transport (Ersahin et al., 2002; Langner et al., 1999; Wilson et al., 1998; Mayes et al., 2003). In this study, field measurements with a tension infiltrometer were incorporated into an investigation of the transport of nonreactive bromide (Br) under matric heads (soil water pressure) of 0, -2, -5 and -10 cm using undisturbed soil columns collected from Amargosa Desert Research Site (ADRS).

1.3. Paleolake Extent in Owens Valley

Quantitative paleoclimate information is needed for evaluating past and predicting future effects of climate changes on hydrology. Paleoclimate proxies have been extracted from a variety of sources such as tree rings, ice cores, and marine and continental

sediments (e.g., Stuiver et al., 1995; Spaulding, 1985; Shackleton, 1967). Excepting ice core records, most of these records can only provide indirect and qualitative estimates of paleoprecipitation. However, lake levels in closed basins are the most sensitive indicators of the water balance between precipitation and evapotranspiration in the watershed (Street-Perrott and Harrison, 1985). Lakes fluctuate in volume on both seasonal and interannual time scales in response to variations in the water balance over the lake and its catchment. These volume fluctuations are reflected in the lake level fluctuations in closed basin lakes, and in the rate change of overflow in open lakes. Studies of the lakes in the Owens River system, California, have shown that lake levels primarily record annual precipitation amounts and almost quantitatively document changes in precipitation within their catchments, thus these lakes are sometimes termed as “natural rain gauges” (Smith and Bischoff, 1997). Thus lake records of continental closed basins provide a unique opportunity to extract quantitative paleoprecipitation. There were more than a hundred lakes located in closed basins in the western United States during the Late Wisconsin (25 ka to 10 ka), but only about 10% of the lakes are perennial and of substantial size today (Smith and Street-Perrott, 1983). This dramatic change on the hydrologic system is a result of changes in one or more elements of the climate including precipitation, temperature, evaporation, wind, cloud cover, and humidity.

The Owens River system, California, located at the western margins of the Great Basin, has the most complete continental Quaternary paleoclimate record in the world, and it is one of the best locations for studying paleoclimate change (Smith and Bischoff, 1997). Although studies on the lakes in the Owens River system have shown that their water levels primarily record annual precipitation amounts within their catchment, the

interpretation on paleoclimatic changes is generally limited to either wetter or drier climate, and offers little about the specific nature of the climate change. The reason for this is that the lake level in a particular basin is a complicated function of intrabasin and extrabasin climate and basin topography. One of the best approaches for extracting quantitative paleoclimatic proxies from these lake records, is through numerical modeling.

A variety of models have been used to simulate the paleorecord of closed basin lakes in arid and semiarid areas (e.g., Kutzbach, 1980; Benson, 1981; Benson, 1986; Hostetler and Bartlein, 1990; Hostetler and Benson, 1990; Hostetler et al., 1993, 1994). Physically-based lake models, which explicitly represent the physical processes governing the energy and water balances of the lake, offer a more robust way to predict climate induced changes in water volume, level, and outflow of the lakes. A suitable lake model for paleolake level studies should require a minimum of site-specific parameters (Hostetler and Giorgi, 1993). In this dissertation, a coupled catchment-lake hydrologic model was developed to evaluate how the hydrology responds to climate changes (e.g., mean annual temperature and mean annual precipitation) in the Owens River system since the last glacial maximum (LGM). The simulated paleoclimatic proxies were evaluated with a variety of lake records.

1.4. Chloride Transport in Vadose Zone of ADRS

The low water fluxes in arid environments result in thick vadose zones, providing an archive of continental paleoclimate (Tyler et al., 1996). How to precisely extract the paleoclimate information from arid vadose zones has not been resolved yet. Edmunds and

Walton (1980) first recognized that paleoclimate could be reconstructed from vadose zone chemistry. Cook et al. (1992) reported that the unsaturated chloride profiles from Cyprus and northern Senegal record the past 400 yr climate changes. The time scales for vadose zones responding to atmospheric forces are much longer in arid regions than in humid regions (Allison and Hughes, 1983; Phillips, 1994; Scanlon et al., 1997). For example, paleoclimate records up to 120 ka in vadose zones of southern Nevada were reported by Tyler et al. (1996). Low water fluxes and water content in arid vadose zones significantly reduce the effects of diffusion, thus resulting in excellent preservation of tracers in the infiltrating water (Phillips, 1994; Allison et al., 1994). Among available tracers, chloride is most widely used as chloride mass balance (CMB), because of its conservative property and easy analytic technique. In order to apply CMB, the following assumptions must be satisfied (Scanlon, 1991): (1) one-dimensional, vertical, downward piston-type flow; (2) atmospheric fallout as only source of chloride; (3) mean annual precipitation and constant chloride concentration of precipitation through time; (4) steady-state chloride flux equal to the chloride accession rate in rainfall. However, little is known of the temporal changes in the fallout of chloride during pre-historic records, and the assumption of piston-type flow has been questioned at many sites. Previous studies have shown that the climate changed many times since the LGM. When precipitation or chloride mass deposition varies over time, the steady flow assumption is violated and a nonuniform profile results. Previous studies concluded that climate changes in the late Quaternary might be responsible for the nonuniform chloride “bulge” (Scanlon, 1991; Phillips, 1994). Therefore, in order to model chloride transport in vadose zones since the LGM, all assumptions above have to be clarified.

In this study, a modified version of the HYDRUS-1D computer code (Simunek et al., 1998; Scanlon et al., 2003) was applied to forward model vertical chloride transport in the vadose zone of ADRS, southern Nevada since the LGM. By using variable boundary conditions, the unclear assumptions for the CMB were avoided. The variable boundary conditions were prepared based on independent estimates of paleoprecipitation and paleotemperature (Chapter 4), and chloride deposition rate (Mayeski et al., 1994). By comparing the simulated results to the actual measured chloride profile, the independent estimate of paleoprecipitation and/or chloride deposition rates were evaluated. In this way, chloride profile variations in the unsaturated zone can be quantitatively linked to the variations of paleoprecipitation.

References

- Allison, G.B., and Hughes, M.W., 1983. The use of natural tracers as indicators of soil-water movement in a temperate semi-arid region. *J. Hydrol.* 60, 157-173.
- Allison, G.B., Gee, G.W., and Tyler, S.W., 1994. Vadose-zone techniques for estimating groundwater recharge in and semiarid regions. *Soil Sci. Soc. Am. J.* 58, 6-14.
- Anderson, D.E., and Wells, S.G., 2003. Latest Pleistocene lake highstands in Death Valley, California, in Enzel, Y., Wells, S.G., and Lancaster, N., eds., *Paleoenvironments and paleohydrology of the Mojave and southern Great Basin Deserts: Boulder, Colorado, Geological Society of America Special Paper 368*, 115-128.

- Benson, L., 1981. Paleoclimatic significance of lake-level fluctuations in the Lahontan Basin. *Quat. Res.* 16, 390-403.
- Benson, L., 1986. [Monograph] The sensitivity of evaporation rate to climate change; results of an energy-balance approach. *Water-Resources Investigations - U. S. Geological Survey, Report: WRI 86-4148*, 40 pp.
- Cook, P.G., Edmunds, W.M., and Gaye, C.B., 1992. Estimating paleorecharge and paleoclimate from unsaturated zone profiles. *Water Resour. Res.* 28, 2721-2731.
- Devitt, D.A., and Smith, S.D., 2002. Root channel macropores enhance downward movement of water in a Mojave Desert ecosystem. *J. Arid Environments* 50, 99-108.
- Edmunds, W.M., and Walton, N.G.R., 1980. A geochemical and isotopic approach to recharge evaluation in semi-arid zones, past and present. *Arid zone Hydrology, Investigations with Isotopes Techniques*, pp.47-68. IAEA, Vienna.
- Ersahin, S., Papendick, R.I., Smith, J.L., Keller, C.K., and Manoranjan, V.S., 2002. Macropore transport of bromide as influenced by soil structure differences. *Geoderma* 108, 207-203.
- Hostetler, S.W., and Bartlein, P.J., 1990. Simulation of lake evaporation with application to modeling lake level variations of Harney-Malheur Lake, Oregon. *Water Resour. Res.* 26, 2603-2612.
- Hostetler, S.W., and Benson, L.V., 1990. Paleoclimatic implications of the high stand of Lake Lahontan derived from models of evaporation and lake level. *Climate Dynamics* 4, 207-212.

- Hostetler, S.W., and Giorgi, F., 1993. Use of output from high-resolution atmospheric models in landscape-scale hydrologic models; an assessment. *Water Resour. Res.* 29,1685-1695.
- Hostetler, S.W., Bates, G.T., and Giorgi, F., 1993. Interactive coupling of a lake thermal model with a regional climate model. *J. Geophys. Res. D, Atmospheres* 98, 5045-5057.
- Hostetler, S.W., Giorgi, F., Bates, G.T., and Bartlein, P.J., 1994. Lake-atmosphere feedbacks associated with paleolakes Bonneville and Lahontan. *Science* 263, 665-668.
- Kutzbach, J.E., 1980. Estimates of past climate at Paleolake Chad, North Africa, based on a hydrological and energy-balance model. *Quat. Res.* 14, 210-223.
- Langner, H.W., Gaber, H.M., Wraith, J.M., Huwe, B., and Inskeep, W.P., 1999. Preferential flow through intact soil cores: effects of matric head. *Soil Sci. Soc. Am. J.* 63, pp. 1591-1598.
- Mayes, M.A., Jardine, P.M., Mehlhorn, T.L., Bjornstad, B.N., and Ladd, J.L., 2003. Transport of multiple tracers in variably saturated humid region structured soils and semi-arid region laminated sediments. *J. Hydrol.* 275, 141-161.
- Mayewski, P.A., Meeker, L.D., Whitlow, S., Twickler, M.S., Morrison, M.C., Bloomfield, P., Bond, G.C., Alley, R.B., Gow, A.J., Grootes, P.M., Meese, D.A., Ram, M., Taylor, K.C., and Wumkes, W., 1994. Changes in atmospheric circulation and ocean ice cover over the North Atlantic during the last 41,000 years. *Science* 263, 1747-1751.

- Phillips, F. M., 1994. Environmental tracers for water movement in desert soils: A regional assessment for the American southwest. *Soil. Sci. Soc. Am. J.* 58, 15-24.
- Quade, J., Forester, R.M., and Whelan, J.F., 2003. Late Quaternary paleohydrologic and paleotemperature change in southern Nevada, in Enzel, Y., Wells, S.G., and Lancaster, N., eds., *Paleoenvironments and paleohydrology of the Mojave and southern Great Basin Deserts*: Boulder, Colorado, Geological Society of America Special Paper 368, 165-188.
- Scanlon, B.R., and Goldsmith, R.S., 1997. Field study of spatial variability in unsaturated flow beneath and adjacent to playas, *Water Resour. Res.* 33, 2239-2252.
- Scanlon, B.R., 1991. Evaluation of moisture flux from chloride data in desert soils. *J. Hydrol.* 128, 137-156.
- Scanlon, B.R., Keese, K., Reedy, R.C., Simunek, J., and Andraski, B.J., 2003. Variations in flow and transport in thick desert vadose zones in response to paleoclimatic forcing (0-90 kyr): Field measurements, modeling, and uncertainties. *Water Resour. Res.* 39, SBH 3-1-17.
- Shackleton, N.J., 1967. Oxygen isotope analyses and Pleistocene temperatures re-addressed. *Nature* 215, 15-17.
- Simunek, J., Sejna, M., and van Genuchten, M.T., 1998. The HYDRUS-1D software package for simulating the one-dimensional movement of water, heat, and multiple solutes in variably-saturated media, version 2.0, IGWMC - TPS - 70, 202 pp., Int. Groundwater Model. Cent., Colo. Sch. of Mines, Golden, Colo.
- Smith, G.I., and Bischoff, J.L., 1997. Core OL-92 from Owens Lake: Project rationale, geologic setting, drilling procedures, and summary. In "An 800,000-year

- paleoclimatic record from core OL-92, Owens Lake, Southern California" edited by Smith, G.I. and Bischoff, J.L. Special Paper 317, the Geological Society of America, Boulder, pp. 165.
- Smith, G.I., and Street-Perrott, F.A., 1983. Pluvial lakes of the western United States, in S.C. Porter, ed., The Late Pleistocene. University of Minnesota Press, Minneapolis, Minnesota, p. 53-70.
- Spaulding, W.G., 1985. Vegetation and climates of the last 45,000 years in the vicinity of the Nevada Test Site, south-central Nevada. U.S. Geological Survey Professional Paper 1329, 83 p.
- Stuiver, M., Grootes, P.M., and Brasiunas, T.E., 1995. The GISP2 $\delta^{18}\text{O}$ climate record of the past 16,500 years and the role of the sun, ocean, and volcanoes. *Quat. Res.* 44, 341-354.
- Tyler, S.W., Chapman, J.B., Conrad, S.H., Hammermeister, D.P., Blout, D.O., Miller, J.J., Sully, M.J., and Ginanni, J.M., 1996. Soil-water flux in the southern Great Basin, United States: temporal and spatial variations over the last 120,000 years. *Water Resour. Res.* 32, 1481-1499.
- Wilson, G.V., Yunsheng L., Selim H.M., Essington M.E., and Tyler, D.D., 1998. Tillage and cover crop effects on saturated and unsaturated transport of fluometuron. *Soil Sci. Soc. Am. J.* 62, 46-55.
- Winograd, I.J., 1981. Radioactive waste disposal in thick unsaturated zones. *Science* 212, 1457-1463.

CHAPTER 2

SIMULATIONS ON SOIL WATER VARIATION IN ARID REGIONS

2.1. Abstract

Significant soil water variation has often been found in the top few meters of arid soils. Understanding soil water variation in these soils is crucial to groundwater recharge estimation, rainfall runoff process, risk assessment, and water resource management. A soil hydrologic model (SHM) was developed for simulating soil water movement in the vertical direction using time steps of minutes to days. To account for the dual processes of matrix and macropore flow, a parameterization scheme of dual processes has been adopted to derive *effective* hydraulic conductivity used in the SHM simulation. The integral-balance model based on water flux at different degrees of water saturation used to calculate the macropore conductivity is more useful in quantitatively integrating the macropore contribution to the dynamic soil water fluxes. The SHM, successfully applied to humid and semiarid regions and validated at the Nevada Test Site (NTS) in this study, was used to evaluate soil water variation in an arid region. Soil texture effects on soil water content have been evaluated; results indicate that higher hydraulic conductivity soils have less soil water content. A representative vegetation type at the NTS -- *Larrea tridentate* (creosote) is included to simulate the effects of vegetative cover on the soil water content. The simulations show that the bare soils have higher soil water content than the vegetated soils, which is consistent with observations and other modeled results.

Due to low precipitation at the NTS for much of the year, effects of the macropore flow on soil water content are insignificant. However, the macropore flow could be an important factor influencing the soil water content during high precipitation events.

2.2. Introduction

Studies on soil water flow and solute transport in arid regions have been conducted in the last four decades to evaluate the processes and factors that control water movement (e.g. Winograd and Thordarson, 1975; Tyler et al., 1992; Gee et al., 1994; Tyler et al., 1996; Pohll et al., 1996; Schmeltzer et al., 1996; Albright et al., 1997; Andraski, 1997). An understanding of how these complex processes respond to the current climatic condition is required for predicting their response to potential future climatic conditions. This is important for evaluating the groundwater recharge and the potential for groundwater contamination. Results from these studies not only improve our understanding of these natural processes, but also provide valuable information of risk assessment and management of waste storage sites. Due to extremely low and highly variable precipitation and high potential evaporation, water flux in the unsaturated zone in arid regions can range from 100 ~ 1000 mm/year to less than 0.01 mm/year. The time for the response in arid regions to surface boundary conditions is much longer than in humid regions, which makes it difficult to measure the water fluxes of desert soils. Therefore, the number of projects for long-term monitoring of water content in desert soils is quite limited (Warrick et al., 1998). Most precipitation that infiltrates into desert soil is taken up by plant roots and transpired back into the atmosphere (Phillips, 1994). Thus the vegetative cover has a significant influence on desert soil water fluxes.

Furthermore, structured soils formed by fractures, shrinkage cracks, old root holes, chemical dissolution, and original heterogeneity also play a very important role in desert soil water fluxes (Scanlon, 1992). Therefore, large spatial and temporal variations of soil water content, and consequently recharge in desert soils can be expected. However, for a particular landfill or disposal site, all the above factors must be considered in order to make reliable long-term prediction of water fluxes. In order to choose the optimal combination of storage capacity and soil depth, interactions and feedback mechanisms between various controlling parameters must be analyzed. The best approach for this is numerical modeling.

Further studies are required to characterize the soil water content variation in desert soils, because the processes influencing water movement were significantly affected by temporal and spatial changes in precipitation, vegetation, and soil textures (Gee and Hillel, 1988; Andraski, 1997). The soil texture is an intrinsic factor that controls soil water variation, because the soil texture and its associated bulk density have a direct effect on porosity and vapor transport velocity. The distribution of water occurs more rapidly in a coarse-textured soil because of the steeper $K(h)$ function, as compared to a fine-textured soil (Hillel, 1998). Knowledge of the amount and distribution of water in the soil profile can aid in assessing the rate of groundwater recharge. The soil texture is also an important factor that controls soil water evaporation. Generally, sand sustains evaporation at the full potential rate only during the first day, whereas evaporation from loam continues at the climatically determined potential rate for three days, and evaporation from clay persists at this rate for as long as five days (Hillel, 1977). In this

study, the effect of three soil textures: sand, sandy loam, and silty loam on the soil water variation will be examined along with bare soil, vegetated soil, and macropore soil.

Vegetative cover can modify surface water runoff, infiltration, and evaporation. The vegetative cover has a profound effect on infiltration in arid areas by: 1) reducing rainfall impact, thereby reducing ponding, sealing, and crusting; 2) delivering the precipitation to the soil surface in a redistributed pattern, different drop sizes, and different energy levels; and 3) modifying the drying rate of the soil surface (Saxton, 1979). However, field data shows that bare soil has a higher soil water content than the vegetated soil (Levitt et al., 1996; Albright et al., 1997). Therefore, the amount of water lost through plant transpiration has a direct effect on the amount of soil water that is potentially available for groundwater recharge. In this study, the effect of a cover of the deciduous shrub – *Larrea tridentate* on the soil water was examined. This is the dominant species in the Yucca Flat study area (Beatley, 1974).

Macropores consist of a relatively small portion of the soil volume, but they play an important role in the movement of water and chemicals owing to occasional rapid fluxes through them. The macropore can be defined as large soil channeling pores that have minimum equivalent cylindrical diameters (ECDs) ranging from 0.03 to 5 mm (Chen and Wagenet, 1992). Here ECDs ranging from 0.03 to 1 mm (Luxmore et al., 1990) were used. Macropores form preferred flow pathways for infiltrating water in most soils (Jarvis and Larsson, 2001). This is macroscopically reflected by significant increases in unsaturated hydraulic conductivity when the soil is close to saturation (Clothier and Smettem, 1990; Jarvis and Messing, 1995). At the pore scale, macropore flow occurs

when the water pressure locally increases to near saturation as the water-entry pressure of the pore is exceeded (Jarvis and Larsson, 2001).

Interest in macropore flow has grown recently because: (1) macropores can promote rapid, preferential transport of water and wastes through soil (e.g., Beven and German, 1982; Bouma, 1991; Villholth and Jensen, 1998 a, b; Kamra et al., 2001); and (2) all numerical simulations of soil water fluxes are based on precise calculations of the unsaturated hydraulic conductivity, to which macropore hydraulic conductivity can significantly contribute. Field and laboratory observations suggest that part of the overall soil hydraulic conductivity is governed by macropores (McCoy et al., 1994).

Macropore flow is significant not only in both saturated and near-saturated soils, but also in the unsaturated soil (Phillip et al., 1989). Macropore flow or preferential flow can be an important factor influencing the soil water in arid soils (Scanlon, 1992; Mohanty et al., 1998). Current approaches to characterizing macropore flow in soils are to lump individual preferential flow pathways into two or more pore domains within one-dimensional numerical models (Jarvis and Larsson, 2001). Most traditional numerical simulations of water fluxes in the unsaturated zone have not explicitly included macropore flow processes. For this study, an integral-balance model based on water contents at different degrees of water saturation was used to calculate the macropore conductivity, and then the effect of the macropore on the soil water variation was examined.

In this study, a soil hydrologic model (SHM) was modified and validated at the NTS, then the modified SHM was used to simulate the soil water variation at the NTS. Because the deciduous shrub parameters in the SHM were originally developed for

humid and semi-arid regions (Capehart and Carlson, 1994), these parameters were modified by available data for the SHM application in the NTS. The derived parameters were used to evaluate the vegetation effect on the soil water variation. The modified SHM with macropore flow and modified vegetation parameters was used to evaluate how macropores in the soil could affect the soil water flow and distribution, and to simulate the temporal soil water variations. The following sections contain a description of the SHM and its parameterization schemes, a description of the study site and field data, model validation for the modified SHM, a discussion of the simulated results, and a summary.

2.3. Soil Hydrologic Model (SHM)

The SHM was developed to simulate the vertical profile of soil water content and is driven by conventional meteorological and land-use data (Capehart and Carlson, 1994; Yu et al., 2001). The SHM is a sub-model of a hydrologic model system (HMS) (Yu et al., 1999; Yu, 2000), which is used to simulate the transient variation of soil water in the vadose zone, to evaluate each component of vertical moisture flow, and to calculate near surface fluxes, such as evapotranspiration (ET) and infiltration, for each cell of the grid. The one-dimensional moisture flow in the SHM can be described (Capehart and Carlson, 1994) as

$$\frac{\partial \theta(z,t)}{\partial t} = -\frac{\partial q(z,t)}{\partial z} + S(z,t) \quad (2.1)$$

where q is the vertical moisture flux, θ is the volumetric water content, z is depth, and t is time. The term S represents a source/sink term that accounts for the rate of input and

output of moisture into the soil column. By applying Darcy's equation in conjunction with Equation 2.1, the vertical flux term in Equation 1 can be expanded as

$$-\frac{\partial q(z,t)}{\partial z} = \frac{\partial}{\partial z} \left[K(z,t) \frac{\partial \psi(z,t)}{\partial \theta} \frac{\partial \theta(z,t)}{\partial z} \right] + \frac{\partial K(z,t)}{\partial \theta} \frac{\partial \theta(z,t)}{\partial z} \cos \beta \quad (2.2)$$

where K is the hydraulic conductivity, ψ is the soil water matric potential, and β is the grid-surface slope angle. Equation 2.2 is solved using the Crank-Nicholson numerical scheme (Press et al., 1986; Capehart and Carlson, 1994) and a finite difference scheme of forward in time and backward in space.

Four schemes are available in the SHM for calculating soil hydraulic parameters (relating K and ψ to the volumetric water content): the Clapp and Hornberger (1978) method, the van Genuchten and Mualem (van Genuchten, 1980; Mualem, 1976) method, the Cosby et al. (1984) method, and the Rawls and Brakensiek (1985) method (Capehart and Carlson, 1994; Capehart and Carlson, 1997). The van Genuchten and Mualem method is used in this study and can be expressed in the following equations:

Hydraulic conductivity $K(\theta)$

$$K(\theta) = K_s (S_e)^{1/2} \left[1 - (1 - S_e^{1/m})^m \right]^2$$

Matric potential $\psi(\theta)$

$$\psi(\theta) = \psi_s (S_e^{-1/m} - 1)^{1/n}$$

Where $n = \lambda + 1$, $m = \lambda / (\lambda + 1)$, λ is the pore size parameter ($b = \lambda^{-1}$). S_e is the normalized volumetric water content expressed in terms of the soil water content at saturation θ_s , and a residual soil water content θ_r , thus S_e is defined as

$$S_e = \frac{\theta - \theta_r}{\theta_s - \theta_r} \quad (2.3)$$

2.3.1. Infiltration-Runoff Calculation

Runoff in the model is simulated as infiltration-excess runoff (Horton, 1933) and saturation-excess runoff (Dunne and Black, 1970). Before the incoming precipitation is available for calculating infiltration and runoff, part of it is partitioned into the vegetation leaf or canopy interception which is directly proportional to the fractional vegetation cover, leaf water holding capacity, and leaf area index (LAI) (Yu et al., 2001). The Green-Ampt (GA) method (Chow et al., 1988) was implemented in the model for the infiltration-runoff calculation

$$f = f(t) = \frac{dF}{dt} = K_{av} \left(1 + \frac{\Delta\psi\Delta\theta}{F} \right) \quad (2.4)$$

where f is the infiltration capacity (cm/s), K_{av} is the average saturated hydraulic conductivity (cm/s), $\Delta\psi$ is the difference in average matric pressure before and after wetting (cm), $\Delta\theta$ is the difference in average soil water content before and after wetting, and F is the cumulative infiltration for the rainfall event (cm). Three possible conditions were considered in the model for the GA method that requires data on effective rainfall intensity (I) (after plant interception), saturated hydraulic conductivity (K_s), and infiltration capacity. The infiltration capacity is calculated for each cell at each time step based on the saturated hydraulic conductivity, matric pressure, soil water content, and cumulative infiltration (Equation 2.4). Following Chu's method (1978), two surface indicators, C_u and C_p (the unponded and ponded surface indicators), respectively were implemented in the model to differentiate various soil conditions during a rainfall event.

Infiltration and evaporation are distributed over the top layers. ET occurs across the entire root zone according to a weighting function, which depends on vegetation type and

height. The Penman-Monteith method (Monteith, 1981) is used to calculate evaporation on the bare soil and ET on the vegetation canopy.

2.3.2. Subgrid Spatial Variability

Traditional modeling approaches use a single value of parameters for a point or grid cell, resulting in smoothing out the natural variability and over- or under- estimating various variables. Theoretical, numerical, and observational studies indicate that the subgrid-scale spatial variability in hydrologic parameters has a significant effect on various hydrologic processes (Yu, 2000). For instance, the simulated moisture represents an average over the grid cell. This spatial averaging over dimensions of the order of 10-100 m results in average soil water contents that are significantly lower than the actual peak intensities. This problem has been addressed by using “effective values” of soil hydraulic parameters. However, Beven (1989) questioned the physical basis for this practice. Using this approach naturally overestimates the required travel time of solute transport from vadose zone to groundwater.

Simulations capable of incorporating the spatial variability in hydrologic parameters would improve the representation of physical processes and consequently improve the fit between the simulated results and the observed data. As a first step in representing variability in hydrologic parameters, the following probability distribution is implemented in the SHM to distribute the average value among subgrid fractions within a grid cell (Yu, 2000)

$$f(p_i) = \frac{1}{P} \exp\left(-\frac{p_i}{P}\right), \int_0^{\infty} f(p_i) dP = 1 \quad (2.5)$$

where $f(p_i)$ is the fraction of a grid cell with precipitation p_i , and P is the grid cell average value of hydrologic parameters. Each subgrid fraction represents the fraction of land-

surface area having a set of particular hydrologic variables. For each subgrid fraction, the rainfall-runoff process is applied and the integrated runoff and infiltration can be obtained. For this study, the SHM was only applied at a single point, without considering the spatial variation, for the evaluation of temporal variation of soil water.

2.3.3. Parameterization of Macropore Flow

Numerical simulations of hydrologic processes (e.g., soil water) based on Equation 2.2 with various parameterizations of hydraulic properties (e.g., hydraulic conductivity) such as those equations of van Genuchten (1980) produce a very long flow timescale. This approach would overestimate the time required to allow the rainfall-induced recharge to the groundwater system and consequently underestimate the quick flow response of shallow groundwater systems (Yu et al., 1999).

A conventional approach to defining macroporosity based on pore size seems unsuccessful in quantitatively relating macroporosity to the dynamics of water flow. A definition of macroporosity based on water flux at different degrees of water saturation is more useful (Chen et al., 1993). In this study, a simple approach is used to estimate composite functions of hydraulic conductivity accounting for both macropore and matrix processes. Low macroporosity is assumed so that the effect on $\theta(\psi)$ is negligible; the rapid pressure equilibration is reached instantaneously between the soil matrix and macropores. With certain values of macroporosity (the fraction of soil volume comprised of macropores) n_m and the macropore radius probability density $f(r)$ can be calculated by using the following equation

$$f(r) = k_1 \cdot \exp(-k_2 \cdot r) \quad (2.6)$$

where r is the macropore radius, and k_1 and k_2 are fitting parameters, 0.63 and 0.60 for the fractional macroporosity $n_m = 0.01$ respectively (Brandes, 1998). So the hydraulic conductivity of macropores for each value of radius can be calculated by

$$K_{mp}(\psi) = \frac{\int_0^{\Gamma} K_{mp}(r) f(r) dr}{\int_0^{\Gamma} f(r) dr} \quad (2.7)$$

where Γ is chosen such that $\psi_{ae}(\Gamma) = \psi$, and the ψ_{ae} is air entry pressure, so that the weighted sum includes only those pores ($r < \Gamma$) that contribute to flow at a certain matric potential. Γ is calculated using the following equation

$$\Gamma = \frac{2\sigma \cos \gamma}{\rho g \psi} \quad (2.8)$$

where σ is the air-water surface tension, γ is the water/pore surface contact angle, (assumed to be 0 for water), ρ is the density of water, and g is the gravitational acceleration. Therefore, the calculated Γ from Equation 8 would be a maximum radius for the macropore.

$K_{mp}(r)$ is calculated using Hagen-Poiseuille's and Manning's equations (Chen and Wagenet, 1992). When $\Gamma < 100 \mu\text{m}$ (or 10^{-4} m), the flow in pores can be considered laminar, thus the average flow velocity (U) in the pores is calculated using the Hagen-Poiseuille equation

$$U = \frac{gr^2}{8\nu} \Delta h \quad (2.9)$$

where ν is the kinematical viscosity and Δh is the hydraulic gradient. Following Darcy's equation, the macropore conductivity can be defined

$$K_{mp}(r) = \frac{U}{\Delta h} = \frac{gr^2}{8\nu} \quad (2.10)$$

When $r > 100 \mu\text{m}$, the macropore flow is no longer laminar and the Hagen-Poiseuille equation is invalid to describe flow. In this case, the macropore flow can be described using Manning's formula (Chen and Wagenet, 1992). The average flow velocity is

$$U = \frac{1}{n} R^{2/3} |\Delta h|^{1/2} \quad (2.11)$$

where R is the hydraulic radius (for the special case of full pore flow with radius r , $R = r/2$), and n is the coefficient of roughness, ranging from 0.016 to 0.14 for open channels. Here assuming the upper limit because the scale of the wall surface roughness to pore diameter is generally large. Therefore, the macropore hydraulic conductivity can be calculated using

$$K_{mp}(r) = \frac{U}{|\Delta h|} \cong \frac{(r/2)^{2/3}}{0.14 |\Delta h|^{1/2}} \quad (2.12)$$

$K_{mx}(\psi)$ is calculated using the van Genuchten's equation (1980), which is expressed as

$$K_{mx}(\psi) = K_s \frac{\{1 - (\alpha\psi)^{n-1} [1 + (\alpha\psi)^n]^{-m}\}^2}{[1 + (\alpha\psi)^n]^{m/2}} \quad (2.13)$$

in which α , n , and m are soil parameters and $m = 1 - 1/n$. K_s is the soil hydraulic conductivity at saturation. This equation is valid over ranges of pressure values broader than that of Gardner's exponential model (van Genuchten and Nielsen, 1985). The weighted effective conductivity for each value of ψ may then be obtained

$$K_{eff}(\psi) = n_m \cdot K_{mp}(\psi) + (1 - n_m) K_{mx}(\psi) \quad (2.14)$$

With macroporosity $n_m = 0.01$ and 0.001 , the computed relations of $K_{eff}(\psi)$, $K_{mp}(\psi)$, and $K_{mx}(\psi)$ for a silty loam are shown in Figure 2.1. The effective hydraulic conductivity is

directly proportional to the macroporosity and the matric potential. The effective hydraulic conductivity increases as the matric potential increases (less negative). There are indications that pores as small as $15\ \mu\text{m}$ (equivalent to $\psi = -1.0\ \text{m}$) in radius can act as channels where macropore flow occurs (Germann, 1990). Furthermore, in Figure 2.1, when the matric potential decreases below $-1.0\ \text{m}$, the effective hydraulic conductivity does not follow the matrix conductivity because the integral-balance model for calculating the macropore conductivity has the limitation for all the matric potentials. Therefore, the low limit of macropore radius as $15\ \mu\text{m}$ was set. Because the saturated hydraulic conductivity K_s is a sum of the macropore conductivity and the matrix hydraulic conductivity at saturation, K_s is the maximum of the effective hydraulic conductivity.

2.4. Study Sites

The NTS is located approximately 105 km northwest of Las Vegas, Nevada (Figure 2.2). The study area is located within the Area 3 Radioactive Waste Management Site (RWMS) which is located within the south-central part of Yucca Flat. Yucca Flat is an alluvium-filled, topographically closed basin (Schmeltzer et al., 1996). The soil textures of all core samples within Area 3 ranged from a silty sand to a well-graded sand. The most prevalent textures in the samples from borehole UE-3bl-D1 are well-graded sand with silt and silty sand. In the samples from borehole UE-3bl-U1, the most prevalent textures are well-graded sand, well-graded sand with silt, and silty sand (Schmeltzer et al., 1996). The samples from two other boreholes (U3fd-N1 and U3fd-N2) were

classified as sand or loamy sand (Tyler et al., 1992). Soil textures of loamy sand or sand appear common at the NTS (Schmeltzer et al., 1996).

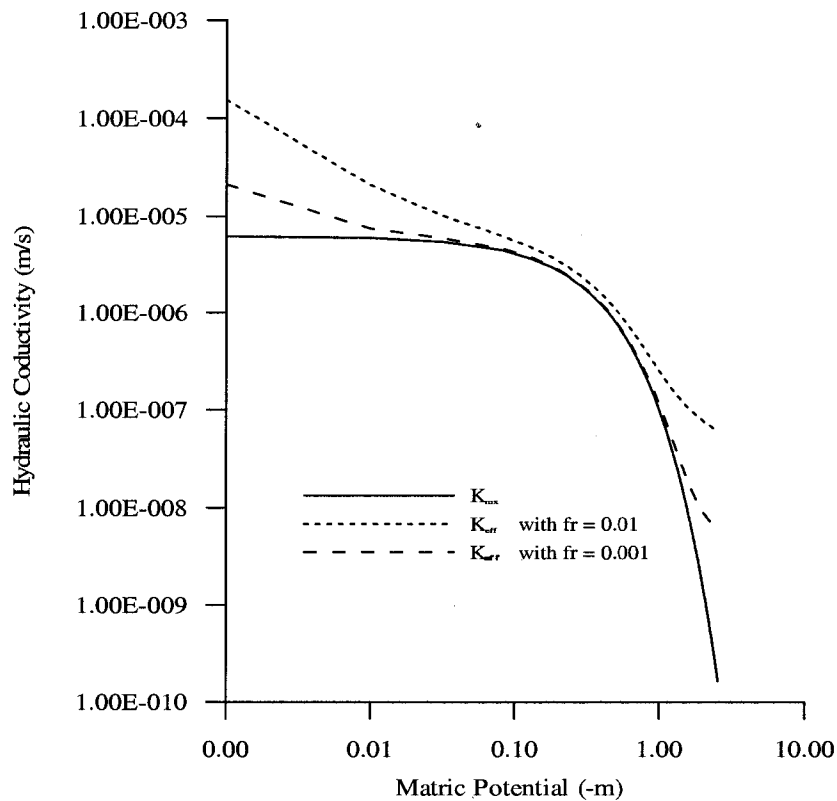


Figure 2.1. Hydraulic conductivity for silty loam with and without macropores.

Hydrologic investigation demonstrated that the undisturbed alluvium beneath the Area 3 is relatively homogeneous and that no barriers to flow, such as carbonate horizons, are present (REECo, 1994). Bulk density and porosity for core samples fall to a range of 1.16 to 1.6 g/cm³ and 0.30 to 0.54, respectively. Measured hydraulic conductivity at saturation ranges from 6×10^{-4} to 1.5×10^{-1} cm/s and mean values are on the order of 4.4×10^{-3} cm/s. Saturated water contents, θ_s , range from 29.2 to 48.2 percent and residual water contents, θ_r , range from 0.0 to 10.2 percent. Fitted van Genuchten

parameters α and n for water characteristic curve data are 0.065-0.159 and 1.47-1.29, respectively (Schmeltzer et al., 1996).

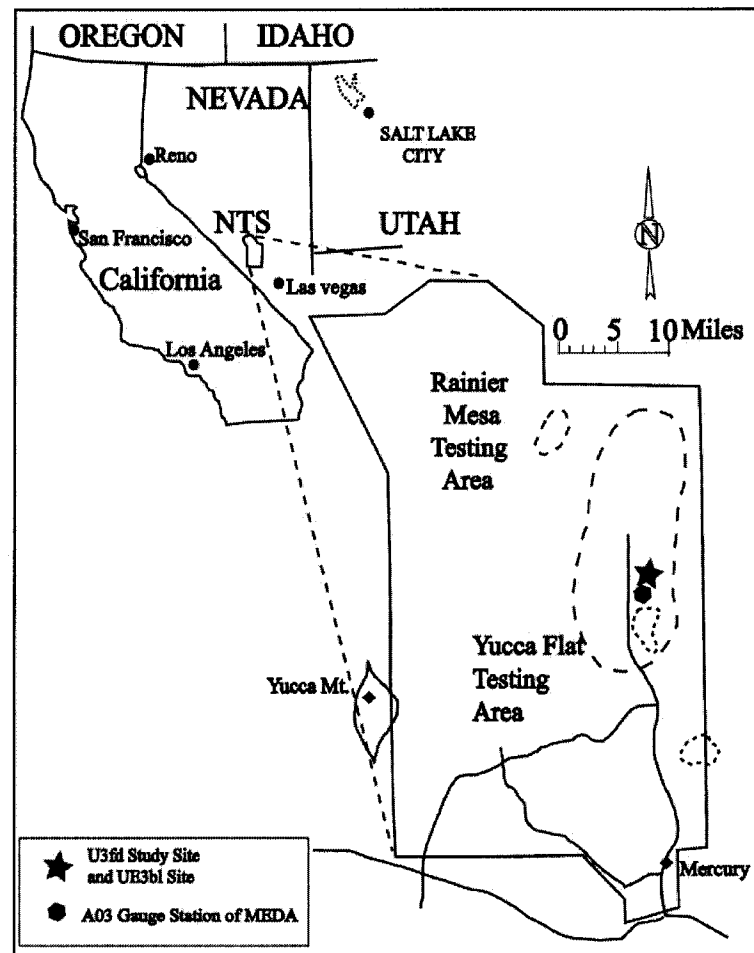


Figure 2.2. Location map of the study area at the Nevada Test Site (modified after Tyler et al., 1992).

The vadose zone characterization of alluvium at the Area 3 RWMS documented that the upper 1 to 3 m is a hydrologically active zone (Schmeltzer et al., 1996). In this region, both the magnitude and direction of fluxes are influenced by the episodic

infiltration, evaporation, and plant root uptake. The depth of this active zone varies spatially and temporally depending on soil properties, plant density and species, and recent weather conditions. Root and animal activity are found mainly in the upper 2 to 5 m. Seasonal changes in temperature contribute to the movement of water vapor in the upper few meters of the alluvium (Schmeltzer et al., 1996). Experimental and modeling studies in the similar climate of the Chihuahuan Desert of Texas have shown that the vast majority of both liquid and water vapor movement is limited to the upper 30 cm of the soil profile (Scanlon and Milly, 1994). Because the climate conditions, evaporative demand, and soil conditions of the Chihuahuan Desert are comparable to those at the NTS, Scanlon and Milly's results can be applicable to the Area 3 RWMS.

This study focused on the Area 3 RWMS. Four shallow boreholes (U3fd-N1, U3fd-N2, UE-3bl-U1, and UE-3bl-D1) were drilled (Tyler et al., 1992; Schmeltzer et al., 1996). Borehole U3fd-N1 was drilled at the lowest point within the U3fd crater to a depth of approximately 47 m; it represents a soil zone disturbed by weapons testing (Figure 2.2). Borehole U3fd-N2 was drilled 207 m north and east of the U3fd crater to a depth of 30.7 m in sediments which were unaffected by weapons testing. The water content profile (Figure 2.3) was determined by using the neutron logs at 30 cm intervals in each borehole immediately after drilling. The average volumetric water content was 0.25 for U3fd-N1 profile and 0.13 for U3fd-N2 in undisturbed soils.

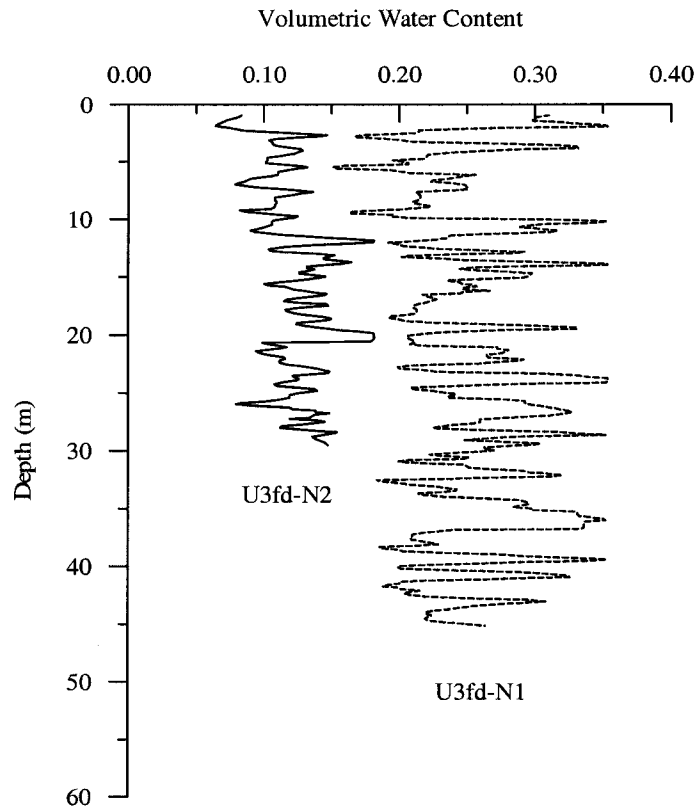


Figure 2.3. Water content profile for the borehole U3fd-N2 (modified after Tyler et al., 1992).

Because there is no major textural difference between the two sites, the higher water content in U3fd-N1 is attributed to changes in soil properties or recharge potential from the disturbed soil by weapons testing (Tyler et al., 1992). The mean volumetric water content in UE-3bl-U1 and UE-3bl-D1 is 0.10 and 0.11 respectively (Schmeltzer et al., 1996). Laboratory measurements including gravimetric water content, bulk density, saturated hydraulic conductivity, soil water potential, soil water tritium analysis, and textural classification were performed on core samples of the two boreholes (Tyler et al., 1992; Schmeltzer et al., 1996).

2.5. Model Validation

The SHM has been validated using two sets of experimental data that represent different soil and climatological conditions, one collected at Rock Springs and the other collected at Hanford, Washington (Capehart and Carlson, 1994). Both climatic conditions and soil textures at Hanford are very similar to these at the NTS, so the SHM could be applied to simulate the soil water content of soils at the NTS. Due to the lack of temporal data on soil water contents at the NTS, it is not possible to precisely test the validity of the modified SHM. However, the modified SHM with measured soil water content data of borehole samples was initially validated.

The SHM inputs include meteorology (i.e., hourly precipitation), vegetation, and soil property data. The meteorological data consist of hourly precipitation, daily average temperature ($^{\circ}\text{C}$), downwelling global solar radiation (Watts/m^2), 2 m wind speed (km/day), and clear sky fraction. The climatic input data are taken from the Area 3 Station ($\text{N}37^{\circ}00.23'$, $\text{W}116^{\circ}01.88'$, elevation 1206.9 m) (Figure 2.2) (Meteorological Data Acquisition system (MEDA) maintained by the Air Resources Laboratory/Special Operations and Research Division (ARL/SORD)) and the average of solar radiation and cloud cover data at Desert Rock from 1998 to 2000 ($\text{N}36^{\circ}37.25'$, $\text{W}116^{\circ}01.55'$, elevation 990.6 m) (SURFRAD Network, NOAA) are used for this calibration simulation. This station records 15-minute observations including precipitation, temperature, 2 m wind speed, and other meteorological recordings from 1983 to present. Vegetation inputs were prepared based on the major type plant *Larrea tridentate* (Levitt et al., 1996; Beatley, 1974).

There are relatively abundant data on soil water contents of the borehole samples from both Area 5 and Area 3 at the NTS. Based on typical soil textures and profile structures of these borehole data (Schmeltzer et al., 1996; Tyler et al., 1996), major input data for this validation were prepared and listed in Table 1 excepting the packing data which are loamy sand from 0 to 4 m deep and sand from 5 to 12 m deep. Simulated soil water content variations in top 12 m soils from 1990 to 2000 were simulated.

The simulated soil water contents and measured soil water contents are plotted with the depth of soil profile in Figure 4, where the simulated soil water contents represent the average of the measured soil water contents in the soils of upper 12 m. The average of the measured volumetric water contents and the simulated volumetric water contents are 0.067 and 0.064 respectively, so the modified SHM here is capable of modeling the soil water variation in a depth of 12 m. The following simulations focus on the top 2 m of soils using this modified SHM, because significant soil water variation occurs this range of the soil depth, and the depth of most facilities in alluvial deposits used for the burial of low-level radioactive waste (LLRW) and hazardous chemical waste is 2 to 9 m (Andraski, 1997).

2.6. Hydrologic Data

The annual precipitation of the NTS ranges from 29 mm to 230 mm over last 30 years with an average of 124 mm/yr, of which approximately 75% is generated by the cyclonic frontal system originating along the western coast of the Pacific Ocean during the winter.

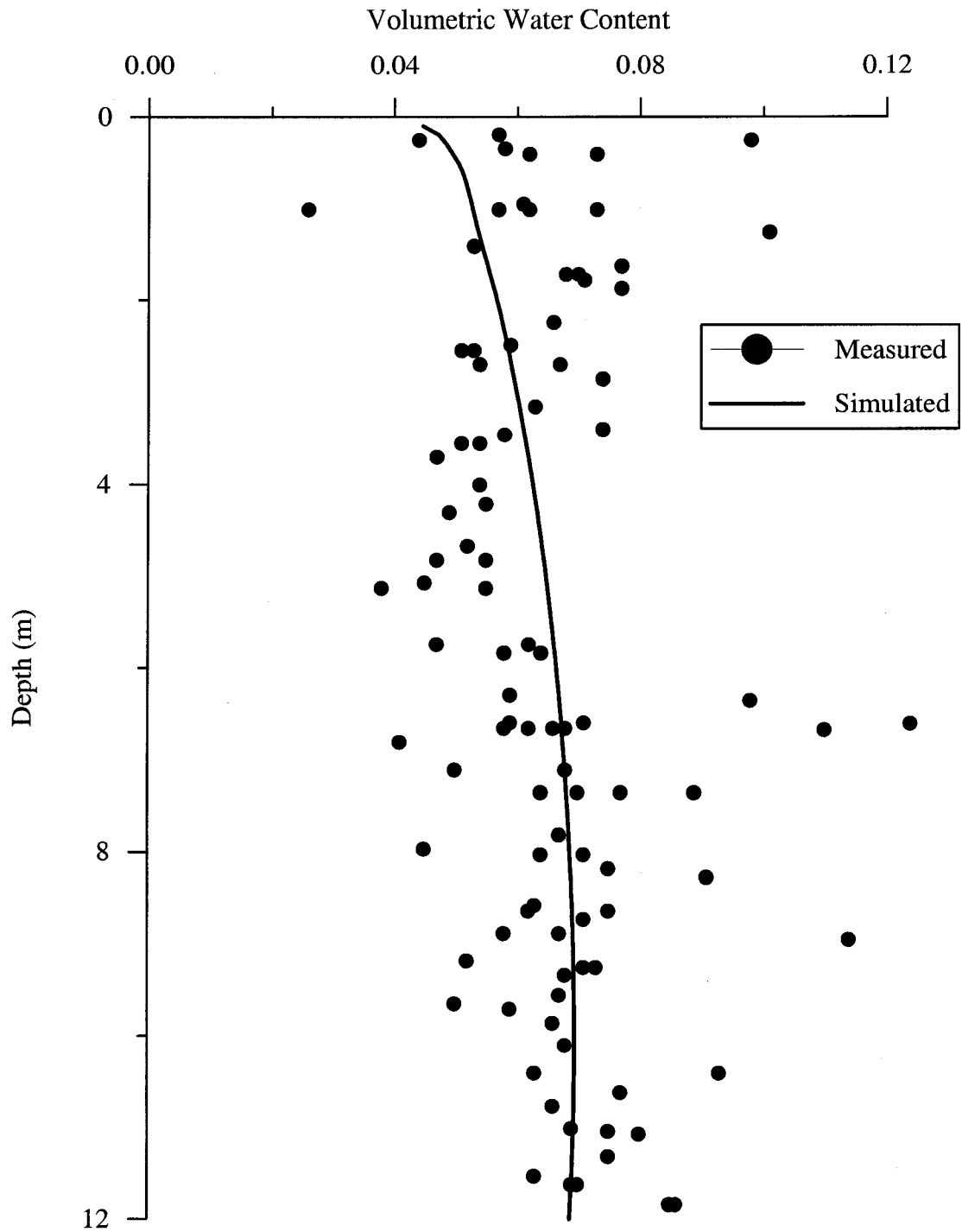


Figure 2.4. Comparison of the measured volumetric water content and the simulated volumetric water content.

The rest of the precipitation is from the summer monsoons originating from the Gulf of California and the Gulf of Mexico. For the study site, the input meteorological data were taken from surface observations of the Area 3 station.

In this study, the simulated results with the input of 1998 and 1999 meteorological data representing relatively high and low precipitation were respectively presented. In 1998 and 1999, the total precipitation was 177 and 89 mm respectively, maximum daily precipitation is 18.7 and 9.5 mm respectively, and the average maximum and minimum temperature are 72.4 and 39.7 F° respectively. The average daily wind speed is 6.9 knots from 1983 to 2000. Available solar radiation and cloud cover data for the period of 1998 to 2000 at the Desert Rock station is used for our Area 3 study. The SHM soil texture file has eleven soil texture types that include most typical soil categories; other specific texture types can be added as needed. The input files of soil profile data for the NTS were prepared based on soil data for the Subsidence Crater U3fd (Schmeltzer et al., 1996).

The input vegetation parameters for this study were chosen based on representative plant type – *Larrea tridentate* because *Larrea tridentate* is the dominant species at the 12 Yucca Flat sites (Beatley, 1974). The parameters include: the maximum leaf area index (LAI) 2.0, 30 percent vegetative cover, an average height of 1.27 m, and a minimum stomata resistance of 157 s/m (Beatley, 1974 and Levitt et al., 1999). Because the biological response of Mojave Desert plants to climate is controlled by the available water and precipitation which is low as well as being temporally and spatially variable at the NTS, plant response varies from year to year (Levitt et al., 1999). Six-year average data show that *Larrea tridentate* becomes active in March and dormant at the end of

May, while *Lycium hymenoides* becomes active in January and dormant in April (Ackerman et al., 1980). However, the total annual vegetative growth and natural vegetative cover fluctuates from year to year in response to variations in annual precipitation. Thus it is difficult to normalize general vegetation parameters. The biological response in the SHM is dependent on the growth angle, which is calculated based on time of the year (Capehart and Carlson, 1994). Major input parameters used in this study are listed in Table 2.1.

2.7. Results

All the simulations presented here are based on assumptions that soil properties have uniform distribution and no stratifications for the 2 m vertical soil profile. Each simulation uses 0.2-hour time steps and 5-cm vertical discretion in the unsaturated zone. For the simulation on the macropore flow, the macroporosity is assumed to be 0.01 percent of the total soil volume, which is based on available macroporosity data published in the literature (Table 2.2). The one-dimensional simulations assume an initial constant of 50 percent saturation distribution of soil water content. All simulations show that it takes about 120 days for the model to reach the equilibrium, thus discussions will focus on the simulated results for Days 121 to 730. The following sections will present the modeled results with different soil textures, vegetation cover, and macropore effect. The simulated results are expressed as the normalized volumetric water content (S_e) while the volumetric water content is listed in Table 2.1. The simulated volumetric water content over the period of 1998 to 1999 for three soil textures with bare cover, macropores, vegetative cover, and both macropores and vegetative cover are summarized

in Table 2.3. In general, the average volumetric water content as well as the range between maximum and minimum volumetric water contents increases as the soil hydraulic conductivity decreases. The vegetation tends to decrease the soil water content for all three soil textures, while macropores tend to increase the soil water content slightly for sand and silty loam. Because of the naturally arid regions, the minimum value is similar to its residual soil water content for all cases.

2.7.1. Soil Texture

Three soil textures: sand, loamy sand, and silty loams are used for this study because they represent the range of soil textures within Area 3. Simulations with three soil textures and bare land surfaces were driven by the observed meteorological data beginning on January 1, 1998 and ending on December 31, 1999. The simulated soil water content within the uppermost 10 cm and 30 cm of the soil column are shown in Figures 2.5a and 2.5b for three different soil textures, respectively. In general, the simulated S_e for various soil textures resemble each other except for their magnitudes, indicating that the soil water content is controlled by meteorological forces such as temperature, precipitation, and solar radiation, as well as soil texture. The soil water content shows more fluctuation in the winter of 1998 and the spring of 1999 in response to relatively high precipitation. Furthermore, S_e within the top 10-cm soil layer shows larger daily fluctuations than does with the uppermost 30-cm soil layer (Figure 2.5). The average volumetric water content is 0.05 (lowest) in sand, 0.09 in loamy sand, and 0.14 (highest) in silty loam because the sand has lower water retention and higher conductivities, resulting in faster downward drainage through the soil. Higher water retention in the silty loam leads to slower drainage. As a result, more water drains

deeper through sand while more water is held in the fine-grained soils such as silty loam and loamy sand and is subsequently lost through evaporation.

Table 2.1. List of variables used in this study.

Variable	Units	Value and source
Meteorological variables		
Average daytime temperature	K	15-minute records at Area 3 station
Cloud cover	N/A	Hourly records at the Desert Rock
Dew-point temperature	K	Daily minimum temperature at Area 3 station
Daily wind speed, u	m/s	15-minute records at Area 3 station
Precipitation, P_{total}	m	15-minute records at Area 3 station
Solar radiation	W/m ²	3-minute records at the Desert Rock
Botanical variables		
Maximum LAI, LAI _x	N/A	2.0 (Levitt et al., 1999)
Min. stomata resist, r_{stmin}	s/m	157 s/m (Kleinkopf et al., 1980)
Vegetation height	m	1.27 (Beatley, 1974)
Vegetation cover	%	30 (Beatley, 1974)
Hydrological/Envir. Variables		
Macroporosity		0.01 percent, estimated
Soil texture		Sand, loamy sand, silty loam
Saturated conductivity, K_s	m/s	6.22E-5, 1.66E-5, 3.67E-5
Saturated matric potential, ψ	m	-0.0726, -0.0869, -0.2076
Sat. vol. Water content, θ_s	m ³ /m ³	0.379, 0.437, 0.501
Residual vol. Water content, θ_r	m ³ /m ³	0.020, 0.035, 0.015
Running variables		
Depth of permeable zone	m	2.0
Space step	m	0.05
Time step	hour	0.20
Start date	N/A	01/01/1998
End date	N/A	12/31/1999

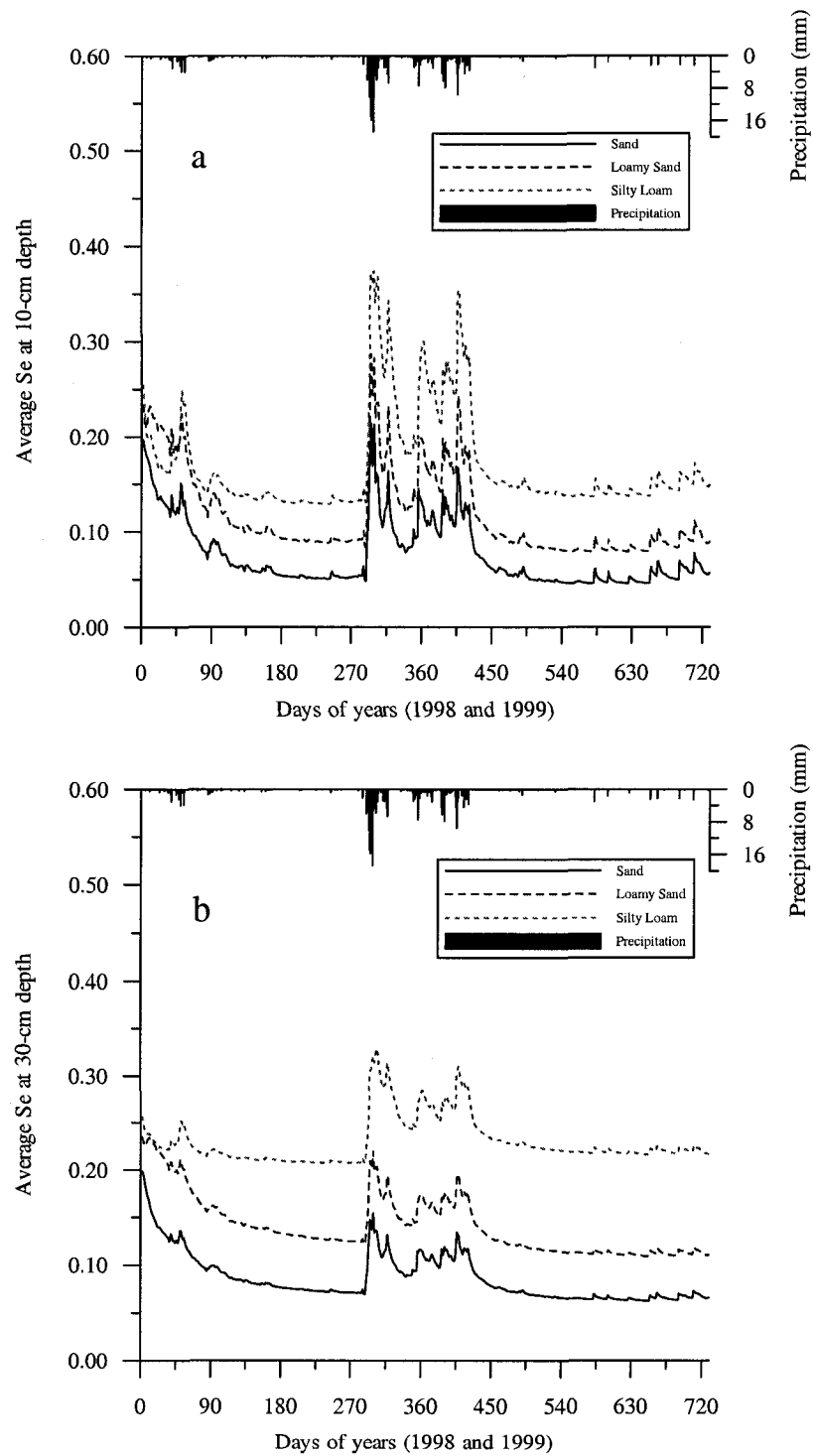


Figure 2.5. Simulated soil water content for bare soils without macropores at the top 10 cm and 30 cm.

The results suggest that the soil saturates near the surface at a rate that is primarily determined by precipitation, but the rate at which the water is transported downward through the soil is dependent upon the soil hydraulic properties. It can be seen in Figure 2.5 that the magnitude of the S_e variation becomes smaller with increases in soil depth. These results indicate that the influence of meteorological forces is reduced gradually with depth, and the influence of soil texture increases with depth. These results are similar to those reported in a humid area (Yu et al., 2001).

2.7.2. Macropores

Macropore flow can be an important mechanism influencing the temporal and vertical variation in soil water, especially in humid areas. There is no data available for the macropore flow at the NTS. In this analysis of techniques for estimating potential recharge and shallow unsaturated zone water balance near the NTS, Leary (1990) concluded that the macropore could be one of the factors influencing the shrub dormancy. Scanlon (1992) found preferential flow in fissured soils in a similar environment – the Chihuahuan Desert of Texas. Although annual precipitation is low at the NTS, the precipitation intensity can be high. For instance, the precipitation for Area 3 was 18.7 mm on October 24, 1998, and the total precipitation from October 16 to 30 of 1998 was 96.8 mm. A recent study concluded that the 100-year return-period value of a 24-hour precipitation is 89 mm (Randerson, 1997). Therefore, macropore flow could occur in the upper structured soil layers in the NTS under extremely high rainfall events. The simulations presented here are based on a hypothetical set of conditions. In these simulations, 0.01 percent macroporosity along with observed meteorological data is applied to drive the simulation with bare soil, and soil textures of sand (Figure 2.6),

loamy sand (Figure 2.7), and silty loam (Figure 2.8). The simulated results show that S_e is slightly lower for sand (Figure 2.6) and loamy sand (Figure 2.7) with macropores, than S_e without macropores during periods of low precipitation, but apparently lower during periods of high precipitation. The difference of S_e becomes greater with an increase in soil depth. However, the simulated S_e for silty loam (Figure 2.8) with macropores shows a higher S_e than silty loam without macropores. Therefore, the macropores may have different effects on the soil water content for different textures. In Table 2.3, the average volumetric content of the sand and silty loam is slightly higher with macropores than that without macropores. Inversely, the average volumetric water content of the loamy sand is lower with macropores than without macropores. From the start of the transpiration season around the middle of April to the end of the growing period around late October, the S_e of both the top 10-cm and top 30-cm soil layers for three soil textures is much lower in the soils with vegetative cover than in the bare soils. This is in agreement with the observed results for the loamy sand at Beatty (Gee et al., 1994). However, the S_e for the winter period is similar to bare soil. The actual situation may be slightly different depending on the vegetation types and growing cycle.

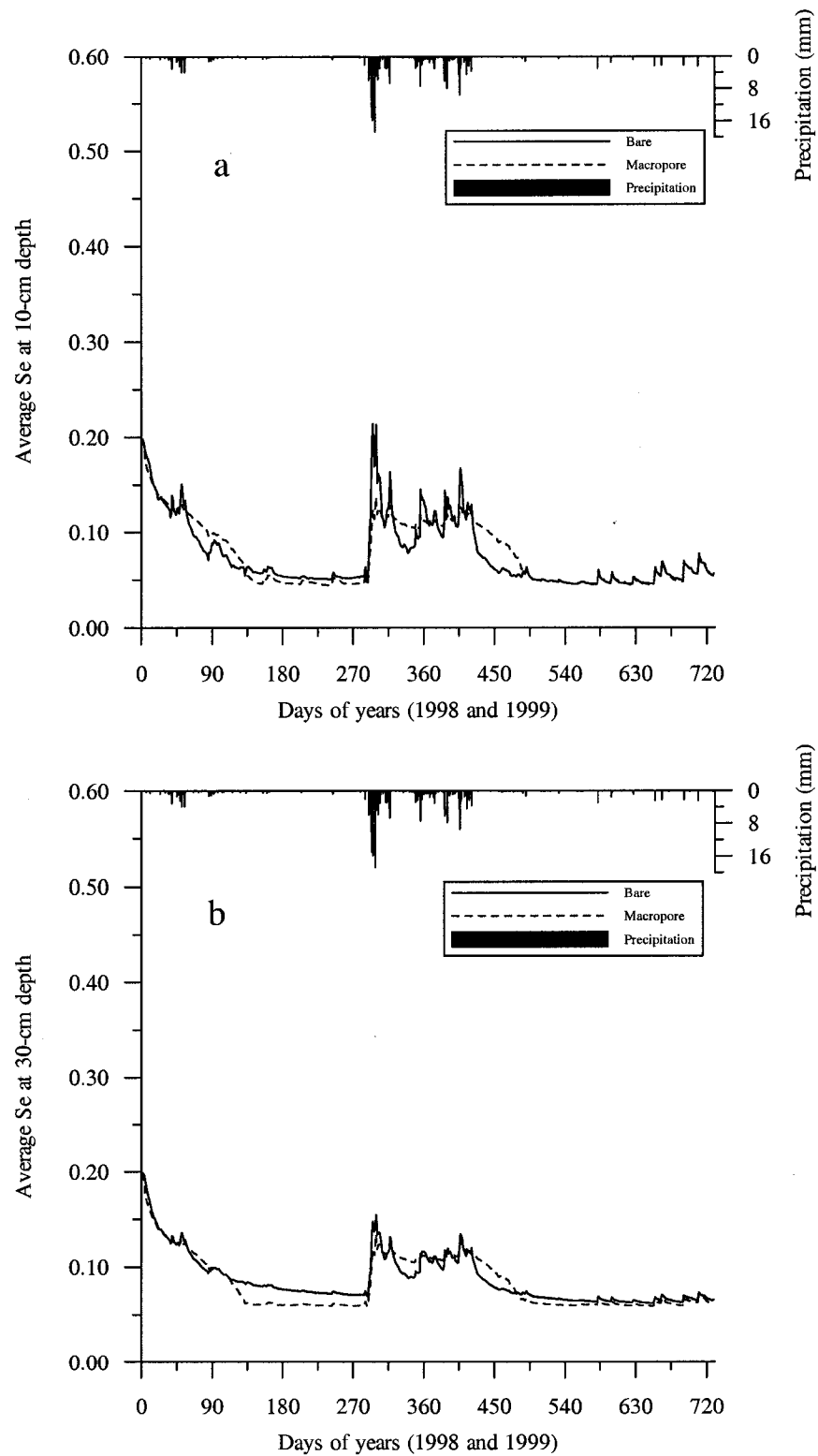


Figure 2.6. Simulated soil water content for sand with macropores at the top 10 cm and 30 cm.

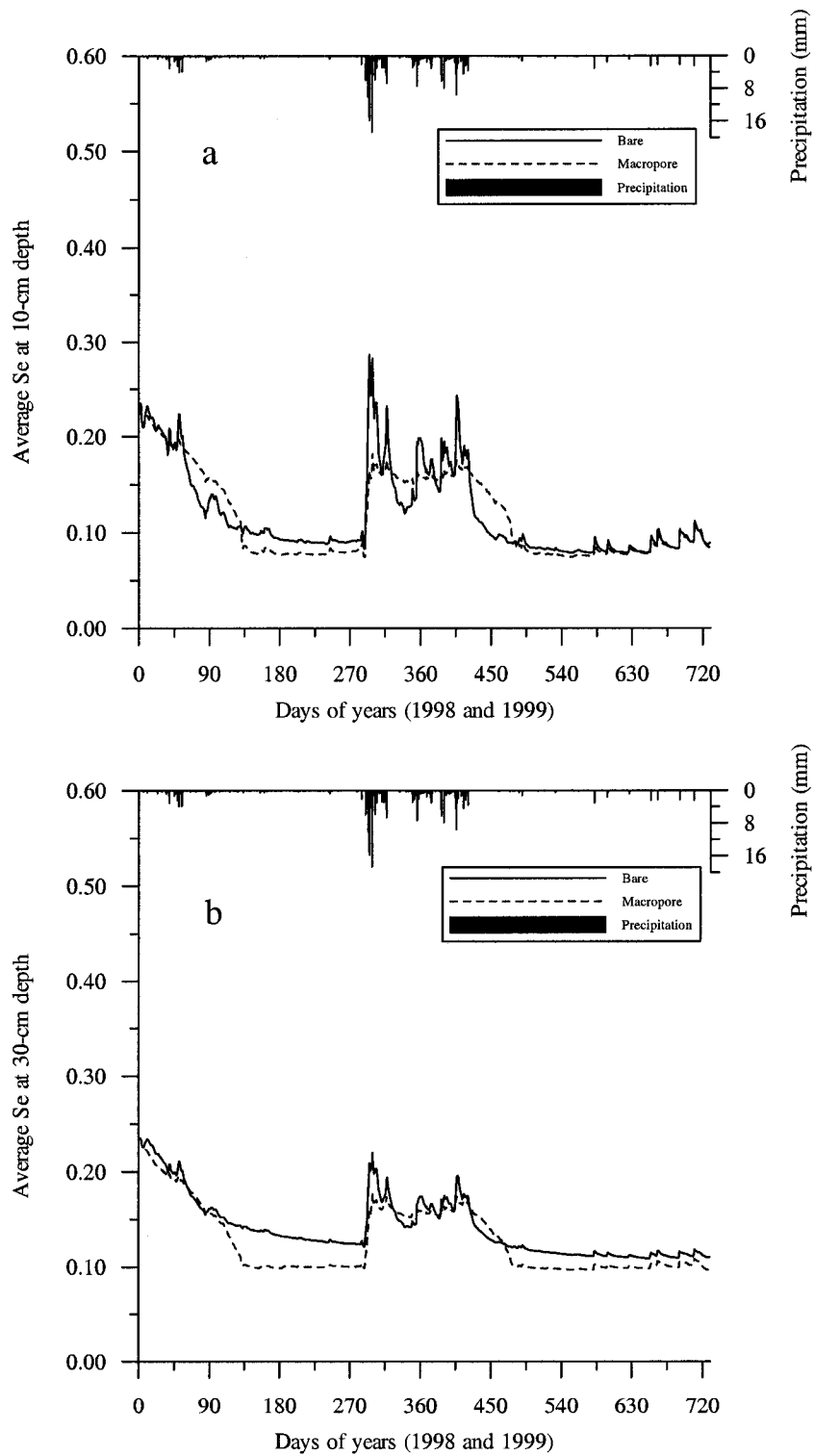


Figure 2.7. Simulated soil water content for loamy sand with macropores at the top 10 cm and 30 cm.

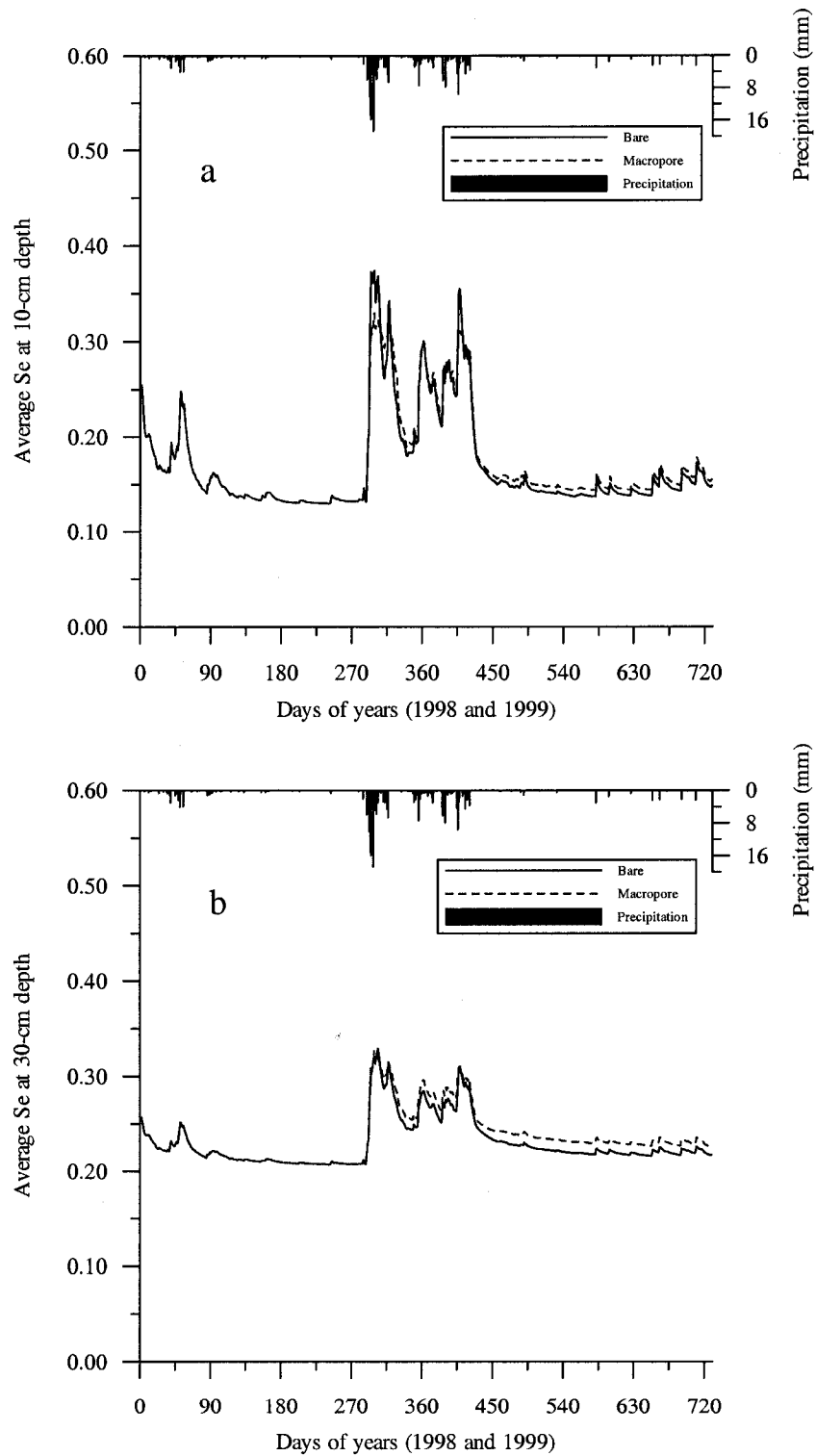


Figure 2.8. Simulated soil water content for silty loam with macropores at the top 10 cm and 30 cm.

2.7.3. Vegetation

This section examines the effect of vegetative cover and its combined effect with macropores on the soil water content variation. The simulated results are plotted on Figure 2.9 for sand, Figure 2.10 for loamy sand, and Figure 2.11 for silty loam. All simulations show S_e is significantly lower in the three types of soils with vegetative cover, than with bare soils during the period of active water uptake by roots.

Table 2.2. Estimated macroporosity for different radii.

Assumed threshold radius of macropores (μm)	Macroporosity (% of soil volume)	Reference
1500	1 ~ 4.5	Germann and Beven (1981)
750	0.04	Watson and Luxmoore (1986)
750	0.017 ~ 0.032	Wilson and Luxmoore (1988)
750	3.4	Smettem et al. (1991)
380	0.006 ~ 0.013	Dunn and Phillips (1991)
500	0.000169 ~ 0.000188	Lin and McInnes (1995)
500	0.00087 ~ 0.0219	Buttle and McDonald (2000)

Comparison among Figures 2.9, 2.10, and 2.11 indicates that the effects of the vegetative cover on the simulated S_e significantly increase from sand to loamy sand, and to silty loam. It can be also noted that the soil water reaches its minimum more quickly in sand and loamy sand than it does in silty loam. The average loss of soil water content due to vegetation in 1998 and 1999 is 5.0% for sand and loamy sand, and 9.0% for silty loam (Table 2.3). Therefore, the vegetation cover can significantly reduce the soil water content and modify the soil texture effects on the soil water variation during the transpiration period. Gee et al. (1994) concluded that differences in the accumulation and

depletion of soil water at Beatty are attributed to soil properties and the presence or absence of vegetation. This is in agreement with the simulated results.

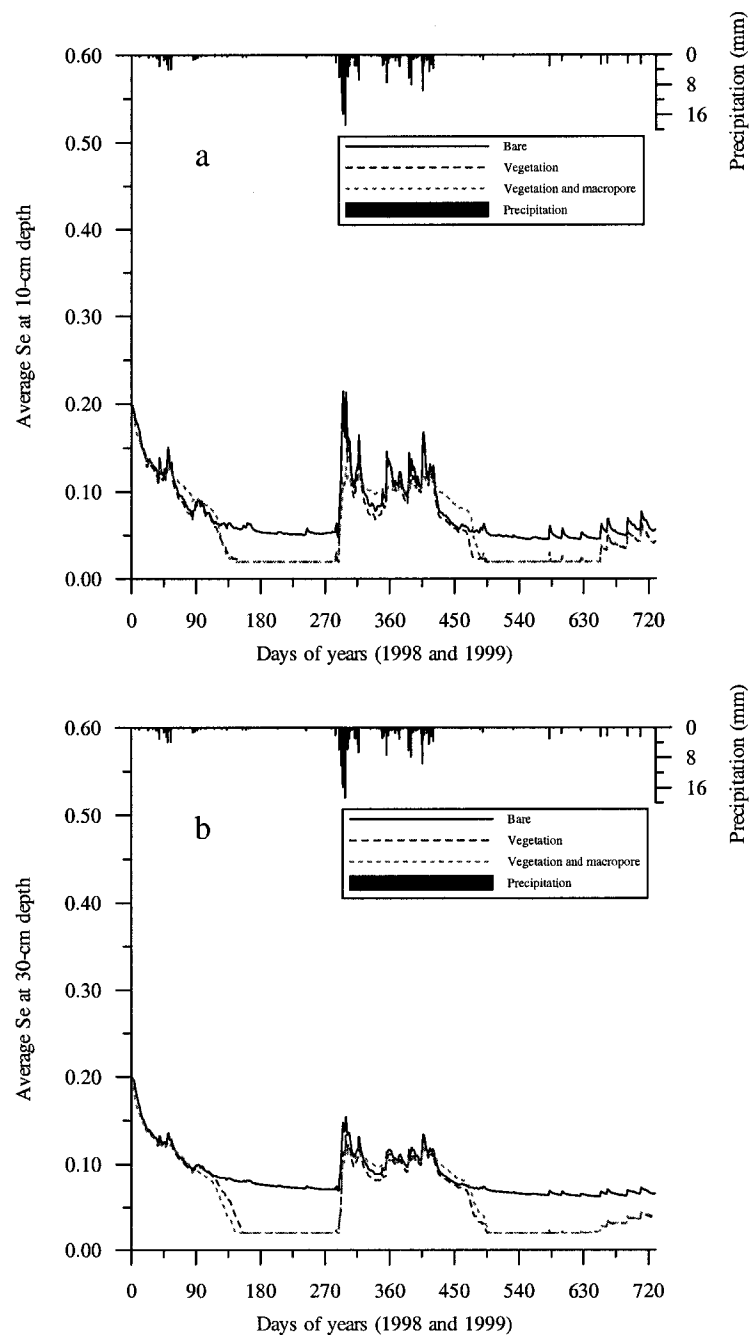


Figure 2.9. Simulated soil water content for sand with vegetative cover only and both vegetative cover and macropores at the top 10 cm and 30 cm.

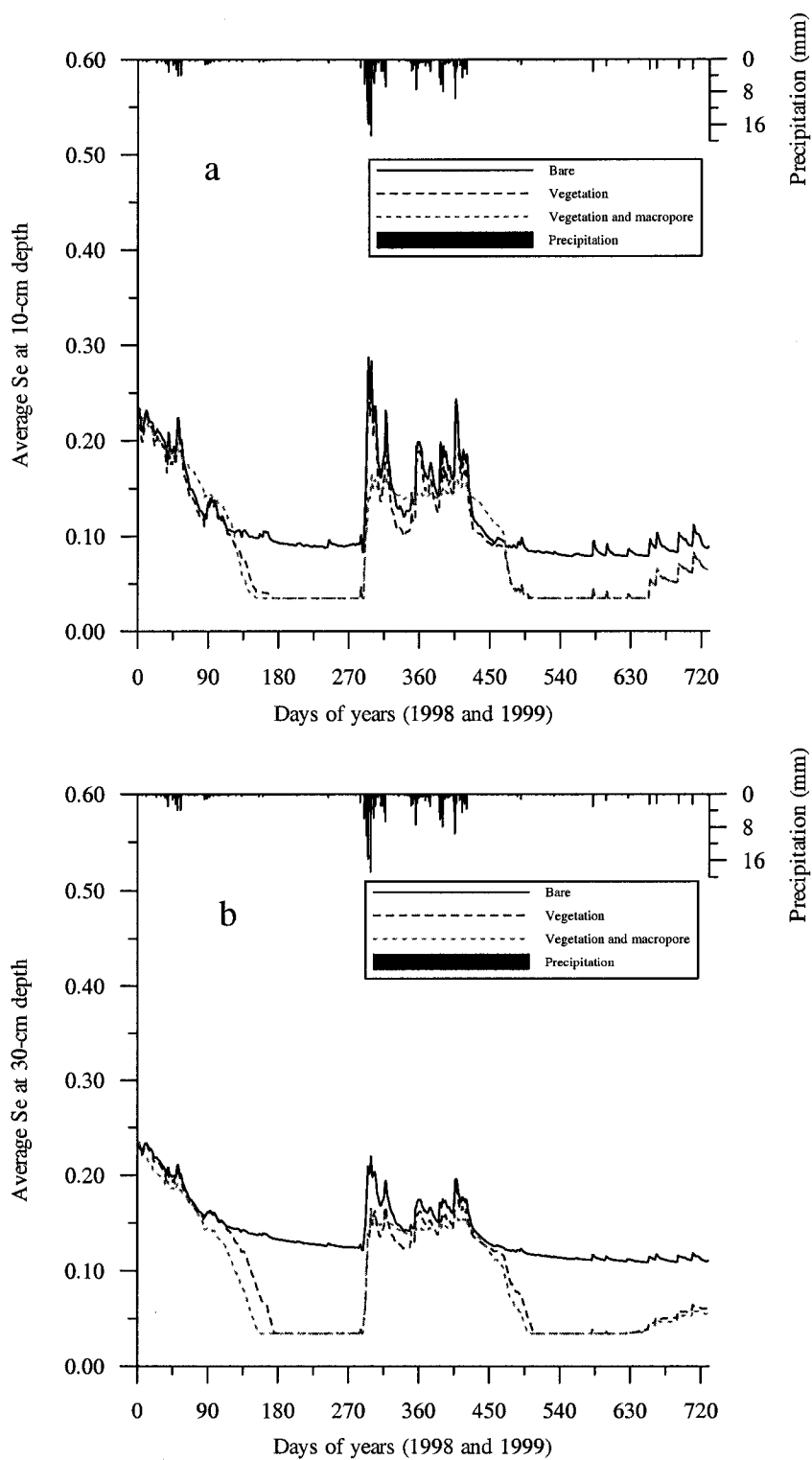


Figure 2.10. Simulated soil water content for loamy sand with vegetative cover only and both vegetative cover and macropores at the top 10 cm and 30 cm.

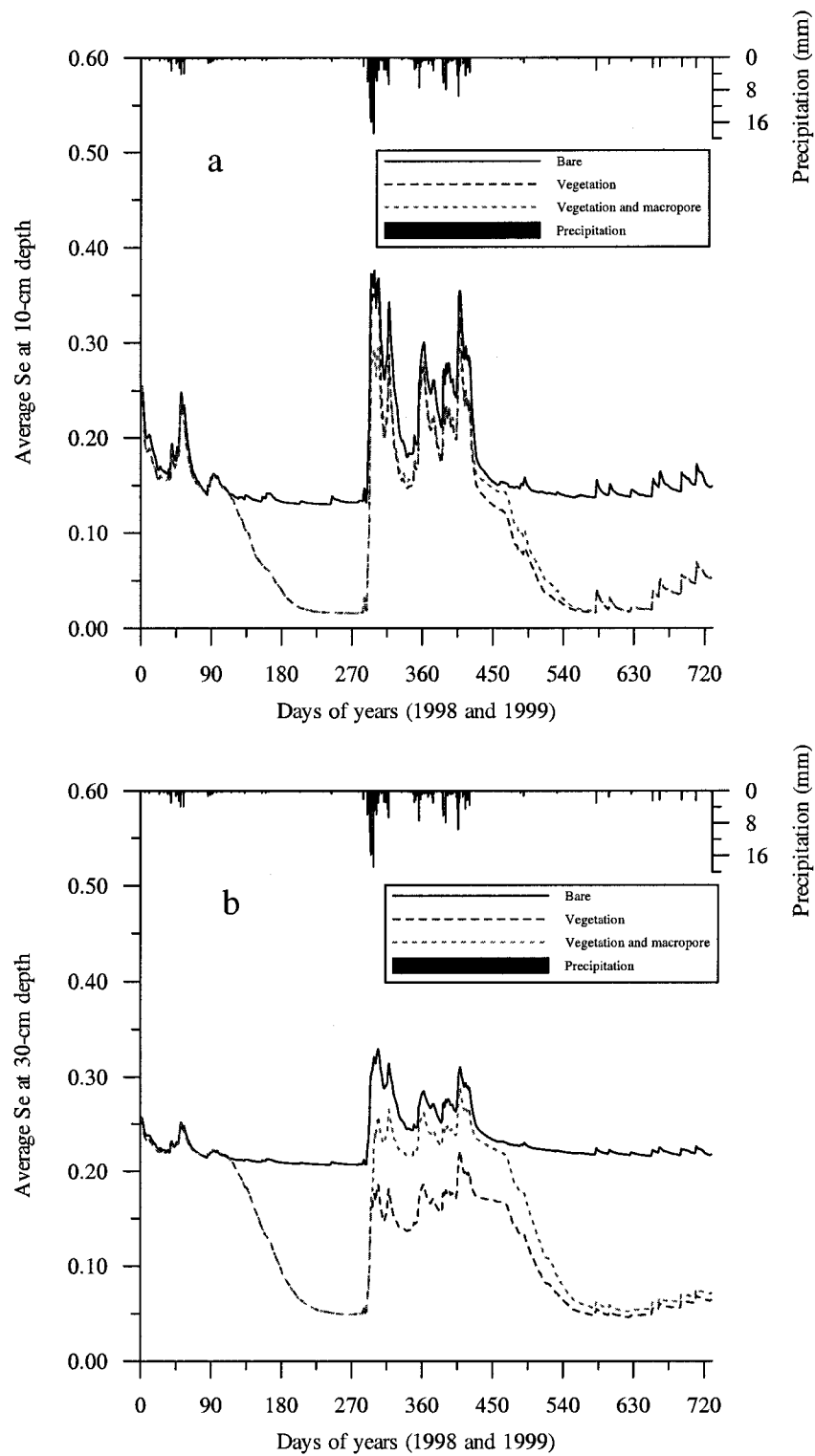


Figure 2.11. Simulated soil water content for silty loam with vegetative cover only and both vegetative cover and macropores at the top 10 cm and 30 cm.

Table 2.3. Summary of simulated volumetric water content over the 2-m soil profile.

Soil texture		θ_{av}	θ_{max}	θ_{min}	%
Sand	Bare	0.0487	0.1205	0.02	
	Macropore	0.0500	0.0913	0.02	-3.0
	Vegetation	0.0463	0.1146	0.02	5.0
	Vegetation and macropore	0.0477	0.0913	0.02	2.0
Loamy sand	Bare	0.0857	0.1610	0.0305	
	Macropore	0.0831	0.1264	0.0305	3.0
	Vegetation	0.0814	0.1563	0.0305	5.0
	Vegetation and macropore	0.0785	0.1233	0.0305	8.0
Silty loam	Bare	0.1368	0.1977	0.015	
	Macropore	0.1408	0.1751	0.015	-3.0
	Vegetation	0.1254	0.1982	0.015	9.0
	Vegetation and macropore	0.1273	0.1590	0.015	7.0

Note: % indicating water gain or loss with macropore, vegetative cover, and both macropore and vegetative cover as compared to the water content of the bare soil.

For all simulations with the *Larrea tridentate* cover, the soil water content is lower than the bare soil during the growing period (Figures 2.9, 2.10, and 2.11). This shows that mean plant community peak transpiration is different from year to year, depending on the amount and duration of precipitation in the current and previous year (Beatley, 1974). This is demonstrated in Figures 2.9, 2.10, and 2.11 where the growing season begins earlier in 1999 than in 1998, because of higher precipitation in the winter of 1998 and the spring of 1999. *Larrea* maintains active photosynthesis during the spring when temperatures are mild and water is usually available. Summer and winter seasons bring extremes of temperature and aridity that usually cause *Larrea* to become dormant. However, in the case of a cool, wet, late spring or a mild, wet fall, it is thought that *Larrea* can extend the temporal range of photosynthesis (Ackerman et al., 1980).

Therefore, the plant has its own temporal range of transpiration depending on the timing of precipitation.

The loss by evapotranspiration in Figure 2.11 is greater than in Figures 2.9 and 2.10 because the fine-grained silty loam has a higher water holding capacity than the sand and loamy sand, hence there is more water for extraction by plants. Both TDR (Time Domain Reflectometry) and TCP (Thermocouple psychrometer) measurements show that bare soil appears to reach slightly higher water contents than the vegetated soil during the wetting phase, and both bare and vegetated soils show fairly rapid drying in the upper 75 cm. This indicates significant evaporation and transpiration during the drying phase (Albright et al., 1997), which is consistent with the simulated results. Although more water is lost from the silty loam, the minimum soil water content is higher in the silty loam than in the sand and loamy sand because the soil texture controls the residual soil water. Lane et al. (1984) concluded that evaporation accounts for approximately two-thirds of the annual water loss and is the dominant process controlling the local water balance in the desert soils of the NTS and Yucca Mountain area. The simulated results show that plant transpiration increases the loss of the soil water. Thus for soil with vegetative cover at the NTS, most of water loss is through evapotranspiration.

The simulated results with both macropores and vegetative cover are very close to those with vegetative cover only. These results are also plotted on Figure 2.9 for sand, Figure 2.10 for loamy sand, and Figure 2.11 for silty loam. Results with macropores in the three textural soils show that macropores have a lesser influence on the soil water content than the vegetative cover does, which is consistent with the previous conclusion that the macropores are insignificant under present climatic conditions. However, the

water loss due to both vegetative cover and macropores is the highest in loamy sand (Table 2.3), thus the combination of the vegetation and macropores does produce different effects on the loss of the soil water content.

It is unclear how the soil texture, vegetative cover, and macropores interact with each other to influence the soil water distribution, but it seems that texture plays an important role. The difference among the three soil textures is that loamy sand has greater ranges of grain sizes than sand and silty loam. It can therefore be concluded that both the mean grain size and the distribution of the grain size are important in macropore flow. The sum of the water loss due to macropores and vegetation respectively is about the same as for both macropores and vegetative cover together, which means that macropores, vegetative cover, and soil texture interact with each other to influence the soil water content.

The simulations with combinations of vegetative cover and macropores show that macropore effect on the soil water content is secondary to the loss of soil water by transpiration. However, it seems that during vegetative dormancy, the macropore effect on the soil water content is enhanced, especially in the silty loam (Figure 2.11). Therefore, it can be concluded that the depletion of the soil water by plants is one of important contributors to the loss of soil water in the NTS soil. The macropore flow, however, may be important during high winter and spring precipitation events. All simulations in this study were performed with a uniform soil profile that is not representative of soil conditions at the NTS, therefore the simulated results cannot be quantitatively compared to the observed temporal profile data of soil water contents. However, the average of simulated can be approximately compared to measured profile

data. The average of measured volumetric water content (0.10) for Area 3 undisturbed soil at the NTS (Tyler et al., 1992 and Schmeltzer et al., 1996) compares well with the average of simulated volumetric water content (0.09) for loamy sand.

2.8. Summary and Conclusions

The modified SHM was initially validated with the measured data at study sites. The validated SHM was then used to simulate combined effects of soil texture, vegetative cover, and macropores on the soil water variation. The simulated results described above indicate that the soil texture and vegetative cover have significant effects on the soil water content, while macropores have only slight effects on the soil water content in the NTS. Soil texture determines the soil's hydraulic properties and affects the retention and flow of water in the soil, which thereby affects the soil water content. In arid environments, plant growth increases the loss of water from the soil. Structured soil macropores may play an important role in soil water content depending on soil types and environmental conditions.

Most surface soils of Area 3 in the NTS were classified as loamy sand or sandy loam (Schmeltzer et al., 1996 and Tyler et al., 1992), thus the volumetric water content (0.09) of loamy sand should represent the simulated soil water content of the surface soils at Area 3. The results compare well with the average of measured soil water content of undisturbed soils (Schmeltzer et al., 1996). The simulated volumetric water content of sand and silty loam should represent the respective lower and upper limit of soil water content in the soils at Area 3. The decrease of soil water content due to the transpiration of vegetation is 9.0% for silty loam and 5.0% for sand and loamy sand.

Soil texture is an important factor influencing soil water variation. In general, soils with high hydraulic conductivity have high infiltration and drainage rates. After the surface dries, the soil texture is one of the dominant controlling factors influencing the evaporation rate. Surface sandy soils dry more rapidly than loams and clays due to the decreasing upward capillary movement of water and lesser water storage capacity of coarse-textured soils. The overall effect of soil texture on evaporation varies with the quantity of available water. For instance, water from very light rainfall events will evaporate quickly from any soil. In contrast, if precipitation is sufficient to wet the soil below the root zone, moisture deficient conditions develop more rapidly in coarse-textured soils. This explains why sand has the lowest soil water content and silty loam has the highest soil water content. Furthermore, sand has a higher hydraulic conductivity, leading to a higher rate of water flow. This causes more water to drain into deeper soils and less water to be held in the coarse-grained soils during the high rain events.

The macropore flow increases the soil water content by 3.0% in sand and silty loam, and decreases the soil water content by 3.0% in the loamy sand. The combined effects of vegetation and macropores on the soil water content are most significant in loamy sand and insignificant in sand.

Soil with macropores has higher effective hydraulic conductivity near saturation than soil without macropores. However, macropore flow contribution to soil water content varies for different soil textures. Generally, the macropore flow is more significant in fine-grained soils. The simulated results with macropores in Figures 6 and 7 show that sand and loamy sand with macropores have a slightly lower soil water content during periods of low precipitation, but larger difference during periods of high precipitation.

This is because soils with macropores have a higher effective hydraulic conductivity near saturation. Water flows faster through soil with macropores than soil without macropores. High precipitation makes it possible for a higher S_e , and therefore a more significant macropore flow.

Under current climatic conditions, the precipitation in the NTS is low throughout most of the year, and macropore flow is insignificant. However, macropore flow could have been important in past pluvial periods and could be important for possible future high precipitation events. The simulated results in Figure 2.8 show different patterns of soil water content than those in Figures 2.6 and 2.7, especially for the simulated results of 1999. This could be explained by the premise that the soil water content is also controlled, in part, by the initial soil-water conditions. There was relatively high precipitation during the winter of 1998 and the spring of 1999, so the silty loam with a higher water holding capacity retained more water than the sand and loamy sand. Another explanation is that the same scheme of the macropore parameterization used in all the simulations may have lead to some errors.

In general, soils with higher values of hydraulic conductivity have higher infiltration and drainage rates. Bare soils have higher soil water content than vegetated soils, which is consistent with observations (Levitt et al, 1996, Gee et al., 1994) and other modeled results (Albright et al, 1997). Higher hydraulic conductivity soils have less soil water content because they drain faster and have a lower capacity for water retention. Although the macropore flow can be an important factor influencing the soil water content, it is insignificant for the NTS soils under current climatic conditions.

The parameterization of the effective hydraulic conductivity shows promise in calculating soil water contents for soils with macropores. The simulations in this study show that soil texture, vegetative cover, and macropores interact with each other to influence the soil water content in arid regions. However, due to the lack of precise knowledge concerning vegetative cover, soil properties, and the atmospheric processes of transpiration and precipitation, no direct comparison with observed data could be made. Therefore, one aspect of future work will be to characterize the soil properties in the vertical profile and lateral variability, and to collect more precise field data concerning the vegetative cover.

Recent displacement studies on the leaching of bromide and two pesticides under unsaturated steady state flow conditions show that large variability and double peak behavior in the field-scale concentrations, and mass flux of bromide and pesticides induce a small number of preferential flows in small columns from two sites (Kamra et al., 2001). Therefore it is necessary to conduct soil column experiments to study the macropore effects on the movement of solutes in arid soils. With more precise characterization of soil properties in the profile, the natural tracer data (Tyler et al., 1992, 1996), and laboratory experiments, the SHM should provide better simulation for natural process of water flow and solute transport in arid soils. The simulated results will become the basis for further understanding of soil water fluxes and solute transport in arid regions.

Acknowledgements

This project was funded by the Department of Energy under Sponsored Project (DE-RP08-00NV13813). The authors wish to acknowledge David Brandes and Chris Duffy for providing and assisting with the integral-balance model of macropore hydraulic conductivity. Many thanks to Doug Soule for providing most of the meteorological data, and to Dan Levitt for providing data used in this paper. The authors acknowledge the insightful comments and suggestions of Scott Tyler and two anonymous reviewers.

References

- Ackerman, T.L., Romney, E.M., Wallace, A., and Kinnear, J.E., 1980. Phenology of desert shrubs in southern Nye County, Nevada. In: Great Basin Naturalist Memoirs, Brigham Young University.
- Albright, W., Tyler, S., and Hokett, S., 1997. Analysis of shallow soil water flux adjacent to the Area 5 radioactive waste management site. Prepared for U. S. Department of Energy, Nevada Operation Office, DOE/NV/11508-18.
- Andraski, B.J., 1997. Soil-water movement under natural-site and waste-site conditions: A multiple-year field study in the Mojave Desert, Nevada. *Water Resour. Res.* 33, 1901 –1916.
- Beatley, J.C., 1974. Effects of rainfall and temperature on the distribution of *Larrea tridentate* (creosote bush) in the Mojave Desert of Nevada. *Ecology* 55, 245-261.
- Beven, K., 1989. Changing ideas in hydrology-the case of physically-based models. *J. Hydrol.* 105, 157-172.

- Beven, K., and Germann, P., 1982. Macropores and water flow in soils. *Water Resour. Res.* 18, 1311–1325.
- Bouma, J. 1991. Influence of soil macroporosity on environmental quality. *Adv. Agron.* 46, 1-37.
- Brandes, D., 1998. A low-dimensional dynamical model of hillslope soil water, with application to a semiarid field site. Dissertation, the Pennsylvania State University.
- Brooks, R.H., and Corey, A.T., 1964. Hydraulic properties of porous media. Colorado State Univ. Hydrology Paper 3, 27 pp.
- Buttle, J. M., and McDonald, D.J., 2000. Soil macroporosity and infiltration characteristics of a forest podzol. *Hydrological Processes* 14, 831-848.
- Capehart, W.J., and Carlson, T.N., 1994. Estimating near-surface soil water availability using a meteorologically driven soil water profile model. *J. Hydrol.* 160, 1-20.
- Capehart, W.J., and Carlson, T.N., 1997. Decoupling of surface and near-surface soil water content: a remote sensing perspective. *Water Resour. Res.* 33, 1383-1395.
- Chen, C., Thomas, D.M, Green, R.E., and Wagenet, R.J., 1993. Two-domain estimation of hydraulic properties in macropore soils. *Soil Sci. Soc. Am. J.* 57, 680-686.
- Chen, C., and Wagenet, R.J., 1992. Simulation of water and chemicals in macropore soils Part 1. Representation of the equivalent macropore influence and its effect on soilwater flow. *J. Hydrol.* 130, 105-126.
- Chow, V.T., Maidment, D.R., and Mays, L.W., 1988. *Applied hydrology*. McGraw-Hill, New York, 572 pp.
- Chu, S.T., 1978. Infiltration during an unsteady rain. *Water Resour. Res.* 14, 461-466.

- Clapp, R.B., and Hornberger, G.M., 1978. Empirical equations for some soil hydraulic properties. *Water Resour. Res.* 14, 601-604.
- Clothier, B.E., and Smettem, K.R., 1990. Combining laboratory and field measurements to define the hydraulic properties of soil. *Soil Sci. Soc. Am. J.* 54, 299-304.
- Cosby, B.J., Hornberger, G.M., Clapp, R.B., and Ginn, T.R., 1984. A statistical exploration of the relationships of soil water characteristics to the physical properties of soils. *Water Resour. Res.* 20, 682-690.
- Dunne, T., and Black, R.D., 1970. Partial area contributions to storm runoff in a small New England watershed. *Water Resour. Res.* 6, 1296-1311.
- Dunn, G.H., and Phillips, R.E., 1991. Macroporosity of a well-drained soil under no-till and conventional tillage. *Soil Sci. Soc. Am. J.* 55, 817-823.
- Gee, G.W. and Hillel, D., 1988. Groundwater recharge in arid regions: Review and critique of estimation methods. *Hydrol. Process.* 2, 255-266.
- Gee, G.W., Wierenga, P.J., Andraski, B.J., Young, M.H., Fayer, M.J., and Rockhold, M.L., 1994. Variations in water balance and recharge potential at three western desert sites. *Soil Sci. Soc. Am. J.* 58, 63-72.
- Germann, P., and Beven, K., 1981. Water flow in soil macropores. 1. An experimental approach. *Journal of Soil Science* 22, 1-13.
- Germann, P.F., 1990. Macropores and hydrologic hillslope processes. In: M.G. Anderson and T.P. Burt (Eds.), *Process Studies In Hillslope Hydrology*, pp. 327-363. John Wiley & Sons Ltd.
- Hillel, D., 1998. *Environmental soil physics*. Academic Press, San Diego, 771 pp.

- Hillel, D., 1977. Computer simulation of soil-water dynamics. Int. Dev. Res. Centre, Ottawa, Canada, 214 pp.
- Horton, R.E., 1933. The role of infiltration in the hydrologic cycle. Trans. Am. Geophys. Union 14, 446-460.
- Jarvis, N., and Messing, I., 1995. Validation of the dual-porosity model MACRO for assessing pesticide fate and mobility in soil. In: A. Walker, R. Allen, S.W. Bailey, A.M. Blair, C.D. Brown, P. Gunther, C.R. Leake, P.H. Nicholls (Eds.), Proc. BCPC Symposium Pesticide Movement to Water, Warwick, U.K., pp. 161-170.
- Jarvis, N., and Larsson, M., 2001. Modeling macropore flow in soils: Field validation and use for management purposes. In: National Research Council (Ed.), Conceptual Models of Flow and Transport in the Fractured Vadose Zone. National Academy Press, DC, pp 189-215.
- Kamra, S.K., Lennartz, B., Van Genuchten, M.Th., and Widmoser, P., 2001. Evaluating non-equilibrium solute transport in small soil columns. J. Contam. Hydrol. 48 189-212.
- Kleinkopf, G.E., Hartsock, T.L., Wallace, A., and Romney, M., 1980. Photosynthetic strategies of two Mojave Desert shrubs. In: Great Basin Naturalist Memoirs. No. 4, Brigham Young Univ.
- Lane, L.J., Romney, E.M., and Hakonson, T.E., 1984. Water balance calculations and net production of perennial vegetation in northern Mojave Desert. J. Range Management 37, 12-18.

- Leary, K.D., 1990. Analysis of techniques for estimating potential recharge and shallow unsaturated zone water balance near Yucca Mountain, Nevada. Master thesis, University of Nevada, Reno, 334 pp.
- Levitt, D.G., Sully, M.J., and Lohrstorfer, C.F., 1996. Modeling evapotranspiration from arid environments: Literature review and preliminary model results. Bechtel Nevada.
- Levitt, D.G., Sully, M.J., Dozier, B.L., and Lohrstorfer, C.F., 1999. Determining performance of an arid zone radioactive waste site through site characterization, modeling and monitoring. Water Management '99 Conference, Tucson, Arizona.
- Lin, H.S., and McInnes, K.J., 1995. Water flow in clay soil beneath a tension infiltrometer. *Soil Science* 159, 375-382.
- Luxmoore, R.J., Jardine, P.M., Wilson, G.V., Jones, J.R., and Zelazny, L.W., 1990. Physical and chemical controls of preferred path flow through a forested hillslope. *Geoderma* 46,139-154.
- McCoy, E.L., Boast, C.W., Stehouwer, R.C., and Kladvko, E.J., 1994. Macropore hydraulics: Taking a sledgehammer to classical theory. In: R. Lal, B.A. Stewart (Eds), *Soil Processes and Water Quality*, Lewis Publishers, 398 pp.
- Mohanty, B.P., Bowman, R.S., Hendrickx, J.M.H., Simunek, J., and van Genuchten, M.T., 1998. Preferential transport of nitrate to a tile drain in an intermittent-flood-irrigated field; model development and experimental evaluation. *Water Resour. Res.* 34, 1061-1076.
- Monteith, J.L., 1981. Presidential address: evaporation and surface temperature. *Q. J. R. Meteorol. Soc.* 107, 1-28.

- Mualem, Y., 1976. A new model for predicting the hydraulic conductivity of unsaturated porous media. *Water Resour. Res.* 12, 513-522.
- Philip, J.R., Knight, J.H., and Waechter, R.T. 1989. Unsaturated seepage and subterranean holes: Conspectus, and exclusion problem for circular cylindrical cavities. *Water Resour. Res.* 25, 16-28.
- Phillips, L.V., 1994. An innovative and successful approach to site investigations and remedial action. *Ground Water Management* 18, 27-39.
- Pohll, G.M., Warwick, J.J., and Tyler, S.W., 1996. Coupled surface-subsurface hydrologic model of a nuclear subsidence crater at the Nevada test site. *J. Hydrol.* 186, 43-62.
- Press, W.H., Flanger, B.P., Teulkosky, S.A., and Vetterling, W.T., 1986. *Numerical Recipes: The art of scientific computing.* Cambridge Univ. Press, Cambridge, 818 pp.
- Randerson, D., 1997. *Analysis of Extreme Precipitation Events in Southern Nevada.* Technical Memorandum ERL ARL-221. Silver Spring, Maryland: U. S. Department of Commerce, National Oceanic and Atmospheric Administration.
- REECo, 1994. *Archival literature search and conceptual model for the U3ax/bl Disposal unit.* REECo, Las Vegas, NV, DRAFT.
- Raws, W.J., and Brakensiek, D.L., 1985. Prediction of soil-water properties for hydrologic modeling. In: *Watershed Management in the Eighties*, Am. Soc. Of Civ. Eng., New York, pp. 293-299.

- Saxton, K.E., 1979. Plant characteristic effects on soil surface conditions. Infiltration Research Planning Workshop: State of the Arts. USDA-ARM-NC-4, Part 1. Peoria, IL.
- Scanlon, B.R., 1992. Moisture and solute flux along preferred pathways characterized by fissured sediments in desert soils. *J. Contam. Hydrol.* 10, 19-46.
- Scanlon, B.R., and Milly, P.C.D., 1994. Water and heatfluxes in desert soils__2: Numerical simulations. *Water Resour. Res.* 30, 721-733.
- Schmeltzer, J.S., Barker, L.E., and Blout, D.O., 1996. Site characterization data from the U-3ax/bl exploratory boreholes at the Nevada Test Site. DOE/NV/11718-003, U.S. Department of Energy, Nevada Operations Office, Las Vegas, Nevada.
- Soil Conservation Services (SCS), 1972. National Engineering Handbook, section 4, Hydrology, U. S. Govt. Off., Washington, D. C.
- Smettem, K.R.J., 1987. Characterization of water entry into a soil with a contrasting textural class: spatial variability. *Soil Science* 114, 167-174.
- Tyler, S.W., McKay, W.A., and Mihevc, T.M., 1992. Assessment of soil water movement in nuclear subsidence craters. *J. Hydrol.* 139, 159-181.
- Tyler, S.W., Chapman, J.B., Conrad, S.H., Hammermeister, D.P., Blout, D.O., Miller, J.J., Sully, M.J., and Ginanni, J.M., 1996. Soil-water flux in the southern Great Basin, United States: temporal and spatial variations over the last 120,000 years. *Water Resour. Res.* 32, 1481-1499.
- van Genuchten, M. TH., 1980. A closed-form equation for predicting the hydraulic conductivity of unsaturated soils. *Soil Sci. Soc. Am. J.* 44, 892-898.

- van Genuchten, M.T.H., and Nielsen, D.R. 1985. On describing and predicting the hydraulic properties of unsaturated soils. *Annales Geophysicae* 3, 615-627.
- Villholth, K.G., and Jensen, K.H., 1998a. Flow and transport processes in a macropous surface-drained glacial till soil I. Field investigations. *J. Hydrol.* 207, 98-120.
- Villholth, K.G., and Jensen, K.H., 1998b. Flow and transport processes in a macropous surface-drained glacial till soil II. Model analysis. *J. Hydrol.* 207, 121-135.
- Warrick, A.W., Pan, L., and Wierenga, P.J., 1998. Water flow in desert soils near buried waste repositories. In: M.B. Parlange and J.W. Hopmans (Eds.), *Vadose Zone hydrology—Cutting Across Disciplines*, Oxford University Press, New York, pp. 375-395.
- Watson, K.W., and Luxmoore, R. J., 1986. Estimating macroporosity in a forest watershed by use of a tension infiltrometer. *Soil Sci. Soc. Am. J.* 50, 578-582.
- Wilson, G.V., and Luxmoore, R.J., 1988. Infiltration, macroporosity, and mesoporosity distributions on two forested watersheds. *Soil Sci. Soc. Am. J.* 52, 329-335.
- Winograd, I.J., and Thordarson, W., 1975. Hydrogeologic and hydrochemical framework, South-central Great Basin, Nevada-California, with special reference to the Nevada test site. U. S. Geological Survey Professional Paper, Report: P 0712C, pp.C1-C23.
- Yu, Z., Lakhtakia, M., Yarnal, B., White, R., Miller, D., Frakes, B., Barron, E.J., Duffy, C., and Schwartz, F.W., 1999. Simulating the river-basin response to atmospheric forcing by linking a mesoscale meteorological model and a hydrologic model system. *J. Hydrol.* 218, 72-91.

Yu, Z., 2000. Assessing the response of subgrid hydrologic processes to atmospheric forcing with a hydrologic model system. *Global and Planetary Change* 25, 1-17.

Yu, Z., Carlson, T.N., Barron, E.J., and Schwartz, F.W., 2001. On evaluating the spatial-temporal variation of soil water in the Susquehanna River Basin. *Water Resour. Res.* 37, 1313-1326.

CHAPTER 3

SOLUTE TRANSPORT IN ARID VADOSE ZONES

3.1. Abstract

A quantitative description of water movement and solute transport in soils is necessary for a variety of reasons, including groundwater recharge, ecosystem processes and waste management. The transport of bromide (Br) under matric heads of 0, -2, -5, and -10 cm was investigated using undisturbed soil columns collected from the Amargosa Desert Research Site, located approximately 20 km east of Death Valley National Park. Undisturbed soil cores were collected at the ground surface, directly below where tension infiltrometer measurements were made. Measured water fluxes in the field ranged from 1.67 cm/hour to 38.9 cm/hour at the investigated matric heads. Experiments were conducted by introducing water containing Br tracer into a soil column maintained at steady-state conditions. Effluent was collected using a fraction collector inside of a vacuum chamber, and analyzed using a Br ion electrode. Results of breakthrough curves (BTC) exhibited asymmetries and tailing for all core samples. The observed data were well fitted to a one-region model, except for the cores at saturation, and a core at the matric head -5 cm, from which the observed data were better fitted to a two-region model. Fitted pore water velocities with the one-region model ranged from 1.2 to 56.6 cm/hr, and fitted dispersion coefficients (D) ranged from 2.2 to 100 cm²/hr. Results for the core analyzed with the two-region model indicated that D ranged from 27.6 to 70.9

cm^2/hr at saturation, and $25.7 \text{ cm}^2/\text{hr}$ at the matric head -5 cm ; fraction of mobile water (β) ranged from 0.18 to 0.65, and mass transfer coefficient (ω) ranged from 0.006 to 0.03. In summary, the water fluxes and Br dispersion coefficients at investigated matric heads were very high due to the coarseness of the soils and possibly due to preferential flow pathways. These high water fluxes are more likely to occur in ephemeral washes that collect runoff from larger contributing areas. However, higher fluxes through the surface soil would be more likely during wetter climates, like the past pluvial periods or potentially in the future. These high water fluxes and Br dispersion coefficients would lead to higher risk leaching accumulated nitrate nitrogen, which was recently discovered in arid vadose zones, to the groundwater, and have significant effects on the desert ecosystem.

3.2. Introduction

Present low effective precipitation commonly results in low rates of water movement and thick vadose zones in southern Nevada, thus these thick vadose zones have been considered very suitable for waste disposal sites (Winograd, 1983; Scanlon, 1991; Reith and Thomson, 1992). The primary objective for waste-burial facilities is to limit exposure of the public to hazardous wastes for 100 to 10,000 yr (Andraski, 1996). However, the region was strongly influenced by pluvial climate conditions during the late Quaternary Period (Quade et al., 2003; Anderson and Wells, 2003). Despite extensive research on flow and transport in arid regions, the transport properties and general response of arid vadose zones to wetter climate regimes are still not well understood. Therefore, it is necessary to study those processes in soils under possible climate scenarios. For example, a large reservoir of nitrate nitrogen recently found in subsoil zones of arid regions has

been accumulated by long-term leaching from upper soils throughout the Holocene (Walvoord et al., 2003; Stokstad, 2003). This nitrate nitrogen is readily mobilized, which poses a risk of groundwater contamination after land-use or climatic changes. Climate changes, especially the increase in precipitation, and land-use have tremendous effects on the soil moisture that controls desert ecosystems. Studies have found that a dynamic relationship exists among climate change, CO₂ content of the atmosphere, nitrogen deposition, and pedogenic inorganic carbon (Naumburg et al., 2003; BassiriRad et al., 1998; Hamerlynck et al., 2002; Huxman and Smith, 2001). A "reverse desertification" phenomenon was postulated by Idso (1986) based on the dramatic increase in desert plant water use efficiency due to the ongoing rise in CO₂ content of the atmosphere (Grunzweig et al., 2003; Eklundh and Olsson, 2003). It can be predicted that a combination of the rise in precipitation and CO₂ content of atmosphere will promote the reverse desertification.

A wetter climate means more water available to percolate into deeper soil zones; thus, processes for water movement and solute transport would significantly differ from the present situation. For example, soils would have higher overall water storage, higher possibility for a preferential flow, and lead to an overall downward hydraulic gradient. However, a wetter climate generally leads to more vegetation coverage and diversities that would uptake more water. Therefore, a dynamic relationship between climate, ecosystem, and soil water control the overall soil water storage and flow direction. Preferential flow is a transport phenomenon in which water and solutes can move through soils along preferred pathways, bypassing much of the soil matrix when the soil is near saturation (Seyfried and Rao, 1987; Singh and Kanwar, 1991; Wilson et al., 1998).

Cracks, root channels, animal burrows, and sediment bedding often found in desert soils provide an intrinsic condition leading to the preferential flow; thus, whether the preferential flow occurs depends on external conditions, largely net precipitation falling on the soil surface. Although the desert areas have low annual precipitation, a high precipitation intensity is very common. It is thus possible that the preferential flow occurs during periods of high intensity rainfall events which are more common in summer time convective storms. Because the preferential flow can result in rapid solute movement to significant depths in the vadose zone, it is important to include this transport mechanism in the prediction of solute transport in the arid vadose zone, in past and potentially the future wetter climate conditions.

Field scale experiments are ideal for studying the preferential flow and related solute transports, but they are very difficult to be implemented. Miscible displacement experiments have been used by many researchers to quantitatively and qualitatively describe effects of soil structure, water flux, and water content on solute transport (Ersahin et al., 2002; Langner et al., 1999; Wilson et al., 1998; Mayes et al., 2003). In this study, miscible displacement experiments are used to examine the effects of a high net precipitation on water movement and solute transport. Based on field measurements with a tension infiltrometer, miscible displacement experiments of nonreactive bromide (Br) under matric heads of 0, -2, -5 and -10 cm using undisturbed soil columns collected from United States Geological Survey (USGS) Amargosa Desert Research Site (ADRS) were performed.

3.3. Materials and Methods

3.3.1. Site Description

The ADRS is a USGS field laboratory for the study of arid-site processes. The site is located about 17 km south of Beatty, Nevada, and 20 km east of Death Valley National Park (Figure 3.1) (Andraski and Stonestrom, 1999). The Beatty facility was the first commercially operated low-level radioactive waste disposal site in the United States (1962-92), and is now used for the disposal of hazardous chemical wastes (1970 to present). Investigations at ADRS began in 1983 and have produced basic data on soil hydraulic properties, climate, and soil-water movement for both undisturbed and disturbed conditions. Average annual precipitation and annual pan evaporation at the ADRS is about 108 millimeters (mm) and 1900 mm respectively (Johnson et al., 2002). Average air temperatures are about 3°C in December and 33°C in July. 70% of precipitation at ADRS occurs during October through April through frontal systems. Remaining summer rainfall is predominantly through localized and short-duration convective storms (Wood and Andraski, 1995). Although annual precipitation is very low, the precipitation intensity of some rainfall events at ADRS is high. Based on the micrometeorological data collected at ADRS (Johnson et al., 2002), the intensity for three rainfall events on February 14, March 16, and July 21 of 1998 was 13.33, 17.57, and 13.03 mm/hour, respectively; the intensity for two rainfall events on July 9 and 14 of 1999 was 12.12 mm/hour; the intensity for one event on August 30 of 2000 was 13.63 mm/hour. Sparse vegetation at the site is predominantly *Larrea tridentata* (creosote bush). The Amargosa Desert is in the Basin and Range physiographic province. Sediments at the ADRS are mainly fluvial and alluvial deposits that are more than 170 meters (m) thick

(Nichols, 1987). Particle size analyses indicated the surface soil (0.75 to 1 m thick) was made of 79.8% sand, 14.1% silt, and 6.1% clay, as determined by sieve and hydrometer method (Andraski, 1996). The ADRS was chosen for our investigation because it and the Nevada Test Site (NTS) are located in the same physiographic province and have very similar climate and sediments. Therefore, conclusions from this study can be applied to both ecosystems and waste management.

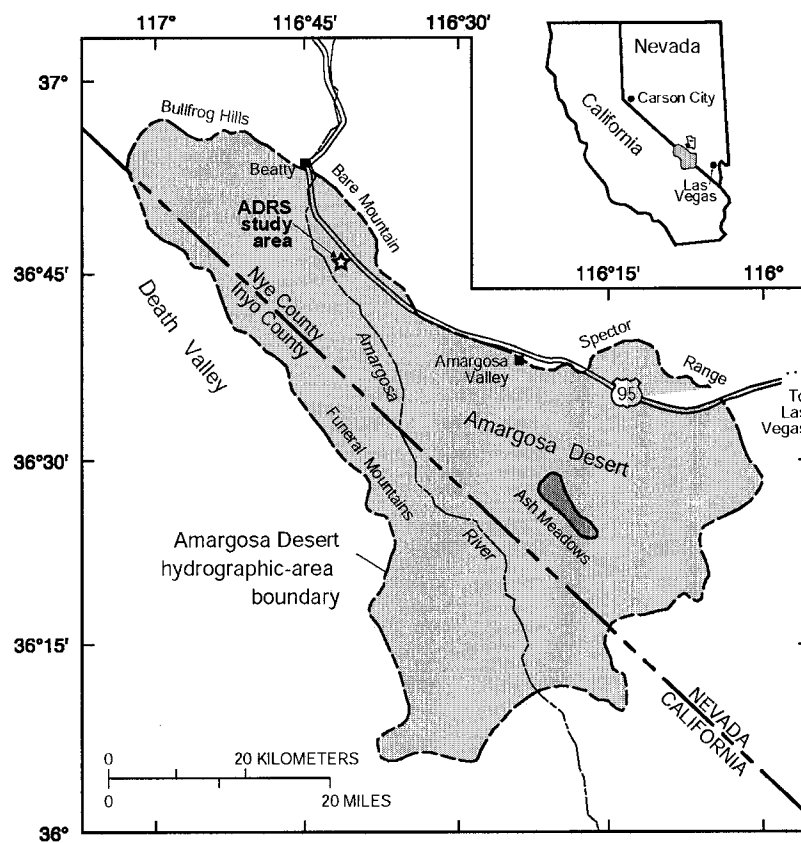


Figure 3.1. Location map of the ADRS (modified from the ADRS website).

3.3.2. Collection of Undisturbed Cores

Undisturbed soil cores were collected by using a retrieve split core sampler at ground surface (AMS (American Falls, ID)), directly below where tension infiltrometer measurements were made. However, some measurements did not have corresponding soil cores, because the core retrieve failed. The tension infiltrometer measurements were performed at matric heads equal to -5 , -10 and -15 cm H_2O . Most surface soils at ADRS are loamy sand, sand, and sandy loam that are very dry and coarse, thus a casing was used to collect the soil cores and to limit disturbing effects on the soil structure. Samples were contained in 6 inch brass liners with the outer 2.54 cm ends removed. Two 0.54 inch diameter holes were drilled about 1 inch from the both sides of the remaining 4 inch liner. After the split core sampler was advanced to the proper depth, the soil around the sampler was excavated to the bottom of the sampler, and the sampler was carefully retrieved. The outer (removable) 2.54 cm-sections of liner were carefully removed, yielding an undisturbed 10 cm long core. Both ends of the core were capped. The cores were stored, and transported back to laboratory. Root channels and gravel were visible at both ends of some soil cores. Totally 8 undisturbed soil cores with 4 from the soil under canopy and another 4 from the soil of intercanopy, were collected in the field.

3.3.3. Experimental Setup

The experimental setup was a combination of those methods described in Wierenga and Manz (1973), Wilson et al. (1998), and Ersahin et al. (2002) (Figure 3.2). The tension infiltrometer was used to determine the flow rate of the column under the saturation. Two tensiometers were installed at the two pre-drilled holes using compression fittings. To maintain a unit potential gradient along the column, soil water pressure inside of the

column and in the vacuum chamber was monitored. During the experiments, the inflow water flux and the pressure in the vacuum chamber were adjusted until the inlet and outlet matric heads were equal. The outlet tube used to connect the core and the fraction collector (ISCO, Lincoln, NE), set inside of the vacuum chamber was kept at same level on the bottom of the soil core. A precision pump (FMI Lab Pump, Model QG 50) was used to maintain a constant inflow during the duration of experiments.

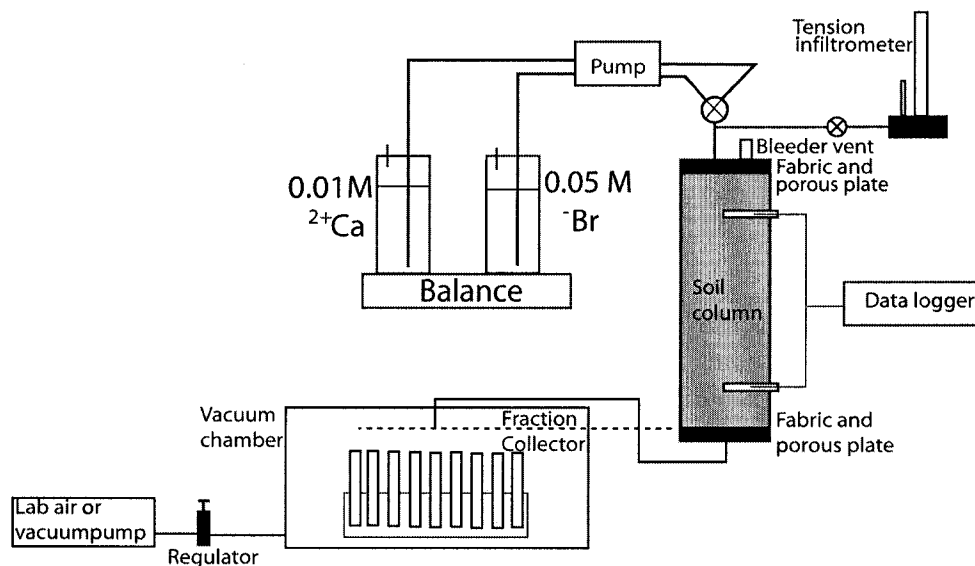


Figure 3.2. Schematic of the experimental setup used in this study (modified from Wilson et al., 1998 and Ersahin et al., 2002).

A series of four transport experiments was performed on each of five intact soil cores and a repacked sand column, all under steady-state flow conditions. The primary goal was to obtain Br breakthrough curves (BTC) at matric heads of 0, -2, -5 and -10 cm. Miscible displacement experiments were performed using the method of van Genuchten and Wierenga (1977). Each soil core was saturated with 0.01 M $CaSO_4$ and 0.03% thymol

solution for two days. The thymol was used to prevent microorganism developing during the experiment. Upon saturation, the inlet at the top of the assembled soil core was connected to a tension infiltrometer, and the outlet at the bottom was connected to a vacuum chamber. Saturated hydraulic conductivity of the assembled soil core was determined with the tension infiltrometer using zero tension. By comparing the saturated hydraulic conductivity made in the field and in the laboratory, only the soil cores with the close agreement of saturated hydraulic conductivity were used for the Br displacement experiment. As a result, three soil cores collected from the soil under canopy were excluded, because their saturated hydraulic conductivity from laboratory is much smaller than these derived from the field measurements with the tension infiltrometer. In this way, it was assured that effects of disturbance on the soil cores used for displacement experiments were limited. After the saturated hydraulic conductivity was measured, the top outlet of the assembled soil core was connected to the FMI (Fluid Metering, Inc.) precision pump, and the flow rate was set to that recorded when the tension was set with the infiltrometer. The input solution was then switched to the tracer solution of 0.05 M KBr in 0.01 M CaSO₄. After approximately 0.7 pore volumes of tracer solution were introduced into the column, the tracer solution was switched to the leaching solution. Approximately 3 pore volumes of 0.01 M CaSO₄ was used to leach the tracer from the column. The effluent was analyzed for bromide using a Br electrode (Abdall and Lear, 1975). To test the experimental system and to observe the effects of soil structure on the Br transport, a column with repacked sand was used to perform the Br displacement experiment with exactly same procedures used for the soil core collected in the field.

Following the experiment under saturated conditions, the column was leached with 4 pore volumes of 0.01 M CaSO₄ leaching solution to minimize the background effect of bromide on the next experiment. The water potential in the core was reset for subsequent experiments at different tensions. By applying -2 cm matric head to the bottom of the column, and adjusting the pump rate until the pressure readings in the column were equal, the procedures for the experiment under saturated conditions were repeated. Similarly, the experiment was repeated with the same column under -5 and -10 cm matric heads.

At conclusion of the experiments, the soil core was detached from the system, and dried in oven for 48 hours to obtain bulk density and final water content.

3.4. Modeling Approaches

Measured Br BTCs were evaluated using the convection–dispersion equation (CDE) as a mechanism to identify the presence or absence of physical nonequilibrium (Toride et al., 1999). The CDE used to describe one-dimensional transport of a sorbing solute under steady-state fluid flow conditions through homogeneous porous media is provided in Wierenga and van Genuchten (1988):

$$R \frac{\partial C}{\partial t} = D \frac{\partial^2 C}{\partial^2 X} - v \frac{\partial C}{\partial X} \quad (3.1)$$

Where C is the solution-phase solute concentration, t is time, D is the hydrodynamic dispersion coefficient, X is the distance from solute application, and v is the average pore water velocity which is defined as q/θ , where q is the Darcian fluid flux velocity, and θ is the volumetric water content. R is the retardation factor, which is defined as $1+\rho K_d/\theta$, where K_d is a distribution coefficient and ρ is the soil bulk density.

Equation (3.1) does not appropriately describe solute transport under conditions where water and solute movement along preferential pathways and nonuniform mixing with the soil matrix, which have generally been described as transport-related nonequilibrium. van Genuchten and Wierenga (1976) modified the CDE to explicitly differentiate two soil water regions: the mobile region where all convective–dispersive transport occurs, and the immobile region where diffusive transport is responsible for the exchange of solute between the mobile and immobile regions. The governing differential equations for the transport-related nonequilibrium are given as:

$$\theta_m R_m \frac{\partial C_m}{\partial t} + \theta_{im} R_{im} \frac{\partial C_{im}}{\partial t} = \theta_m D_m \frac{\partial^2 C_m}{\partial X^2} - \theta_m v_m \frac{\partial C_m}{\partial X} \quad (3.2)$$

$$\theta_{im} R_{im} \frac{\partial C_{im}}{\partial t} = \alpha (C_m - C_{im}) \quad (3.3)$$

Following parameters are also defined:

$$\beta = \frac{\theta_m + \rho f K_d}{\theta + \rho k} \quad \omega = \frac{\alpha L}{\theta_m v_m} \quad \varepsilon = D_m / v \quad \alpha = \frac{\omega q}{L} \quad (3.4)$$

where θ_m and θ_{im} are the mobile and immobile water content ($\theta_m + \theta_{im} = \theta$), C_m and C_{im} are solute concentrations in the mobile and immobile regions, f is the fraction of sorption sites that equilibrate with the mobile region, v_m is the average mobile phase pore water velocity, D_m is the mobile phase dispersion coefficient, ε is dispersivity, α is the first-order mass transfer coefficient between the two regions, L is the length of the column, and R_m and R_{im} are two retardation factors for adsorption in the mobile and immobile regions, respectively. If sorption sites in the soil are distributed in the same ratio as the mobile and immobile water contents, R_m and R_{im} become identical ($R = R_m = R_{im}$) (Nkedi-Kizza et al., 1983). The variable β is a partitioning coefficient describing the

fraction of solute present in the mobile region, and the parameter ω is a dimensionless rate coefficient describing mass transfer between the mobile and immobile regions (Toride et al., 1999). For nonsorbing solutes $K_d=0$, β reduces to the fraction of mobile water (θ_m/θ). Values of β and ω can be used to evaluate potential contributions from the transport-related nonequilibrium (Langner et al., 1999). Physical equilibrium conditions are approached when β approaches unity. Similarly, if ω increases, the rate of convergence of C_m and C_{im} increases. When $\omega \rightarrow \infty$, $C_m = C_{im}$, solutes in each region mix instantaneously, and the nonequilibrium status again reduces to the equilibrium status. Previous studies indicated that optimized values of ω 100 indicate absence of nonequilibrium conditions (Valocchi, 1985; Bahr and Rubin, 1987; Langner et al., 1999).

To distinguish between equilibrium and nonequilibrium conditions, measured Br BTCs from miscible displacement experiments were analyzed using both one-region and two-region models (Toride et al, 1999). Model parameter L was obtained from direct measurement. The initial average pore water velocity v was estimated based on the field measurements with the tension infiltrometer. The steady status water flux density, q was calculated for each experiment from the effluent flow rate. The data from the Br displacement experiments were quantitatively evaluated using the computer program CXTFIT2 (Toride et al., 1999). The relative concentrations (C/C_0) of Br used to represent the results, where C is Br concentration in effluent solution, and C_0 is Br concentration in the stock solution. Both the one-region model and the two-region (physical nonequilibrium) models were used to analyze the experimental data. Equilibrium transport conditions (absence of preferential flow) were assumed if the coefficient of determination (r^2) using the two-region model was equal to the r^2 for the one-region

model, and one or both of the optimized nonequilibrium parameters β and ω were 1 or 100 (upper limit for ω in CXTFIT2), respectively. Conversely, nonequilibrium conditions (preferential flow) were assumed if higher r^2 values were obtained with the two-region model at the case of $\beta < 1$ and $\omega < 100$ (Langner et al., 1999).

3.5. Results and Discussion

3.5.1. Infiltration Data Analysis

The fieldwork was conducted from May 4 to May 8, 2003. The site chosen for this study is a typical undisturbed spot at the ADRS. The tension infiltrometer measurements were performed at a bare ground site and at a site close to plants (dominantly creosote). Generally, the bare ground site is covered with sparse gravels and the particle size is coarser than the surface sediments close to the plants, because the plants trapped the dusts and falling leaves. Initial thought was that physical hydraulic properties could be very different between the bare site and the site close to plants. Five and six measurements at matric heads -5 , -10 , and -15 cm were done in the bare ground surface and in the surface close to the plants with a 20 cm disk tension infiltrometer (Soilmeasurement.com), respectively. Measured flow rates (cm^3/hr) are listed in Table 3.1.

Wooding (1968) proposed the following algebraic approximation of steady-state unconfined infiltration rates into soil from a circular source of radius r (cm)

$$Q = \pi r^2 K \left[1 + \frac{4}{\pi r \mu} \right] \quad (3.5)$$

where Q is the volume of water entering the soil per unit time (cm^3/hr), K (cm/hr) is the hydraulic conductivity, and μ is a parameter (1/cm) that is an inverse of macropore

capillary length (λ , cm). It is assumed that the unsaturated hydraulic conductivity of soil varies with matric potential h (cm) as proposed by Gardner (1958).

Table 3.1. In-situ measured water flow rates (cm^3/hour) with tension infiltrometer at the ADRS.

Matric											
head (cm)	Tree 1	Tree 2	Tree 3	Tree 4	Tree 5	Tree 6	Bare 1	Bare 2	Bare 3	Bare 4	Bare 5
-15	147.3	31.7	54.1	100.7	42.0	15.9	91.4	39.2	93.2	99.8	47.6
-10	-	279.7	271.3	554.8	141.7	117.5	467.1	96.0	607.9	638.7	251.7
-5	733.8	998.6	834.5	1228.9	313.3	983.7	1530.1	1589.7	2974.4	1519.8	863.4

Notes: Tree 3 corresponds soil core ID 5611; Bare 1 corresponds soil core ID 5711 and 5721; Bare 4 corresponds soil ID 5541 and 5551. Original design for collecting soil cores was to take one soil core each measurement, but only 8 soil cores were retrieved. Four of these soil cores were collected from bare soil surface (intercanopy) and other four soil cores were collected from the soil surface close to plants (undercanopy).

$$K(h) = K_{sat} \exp(\mu h) \quad (3.6)$$

where K_{sat} is the saturated hydraulic conductivity (cm/hr). For combining unsaturated soil at two different matric heads (h_1 and h_2), and solving for μ , it results

$$Q(h_1) = \pi r^2 K_{sat} \exp(\mu h_1) \left[1 + \frac{4}{\pi r \alpha} \right] \quad (3.7)$$

$$Q(h_2) = \pi r^2 K_{sat} \exp(\mu h_2) \left[1 + \frac{4}{\pi r \alpha} \right] \quad (3.8)$$

$$\mu = \frac{\ln[Q(h_2)/Q(h_1)]}{h_2 - h_1} \quad (3.9)$$

Calculated μ and K_{sat} (cm/s) are listed in Table 3.2. Based on the values of μ , λ ($1/\mu$) and K_{sat} in Table 3.2, the hydraulic conductivities were calculated at the matric head -2 ,

-5, -10, and -15 cm, and were plotted with matric head for the bare soil and the soil close to the plants (Figures 3.3a and 3.3b).

The saturated hydraulic conductivity ranges from 4.6×10^{-4} to 5.2×10^{-3} cm/s and 2.3×10^{-3} to 1.1×10^{-2} cm/s for the soil under the canopy and the soil of inter-canopy (bare surface), respectively. Mean values are 2.43×10^{-3} cm/s with standard deviation 1.79×10^{-3} for the soil under the canopy, and 5.42×10^{-3} cm/s with standard deviation 3.41×10^{-3} for the soil from the intercanopy, respectively. Based on the standard deviation, the saturated hydraulic conductivity for the soil under canopy and the soil from the intercanopy is indistinguishable. This could be a result of small sample population for these field measurements. The saturated hydraulic conductivity is 2.2 to 7.9 and 3.9 to 6.4 times of the hydraulic conductivity at matric head -5 cm for the soil under the canopy, and the soil from intercanopy, respectively.

3.5.2. Br Transport Characteristics

Each core was dried in an oven at 110°C for 48 hours after the Br displacement experiment, then the bulk density (ρ_b) and porosity were calculated and listed in the Table 3.3. The pore water velocity was calculated, and the experimental conditions for the undisturbed soil cores were replicated in the laboratory with engineering sand. By comparing the estimated pore water velocity at matric heads (Table 3.3), the magnitude of the pore water velocity from the matric head -10 cm to 0 cm is increased by 7.7 times for the column with repacked sand, by 16.5 times for the soil under canopy (5611), and by 13.5 to 21.8 times for the soil from the intercanopy (5541, 5551, 5711, and 5721), respectively, even though their porosities are similar. This could be a result of different

structures among these columns. The column with repacked sand is approximately homogeneous, while undisturbed soil cores are structural soils.

Table 3.2. Calculated parameters with the data in Table 3.1.

Location	μ	λ	K_{sat} (cm/s)	K at -5 cm
Tree 1	0.16	6.25	8.06E-04	3.61E-04
Tree 2	0.34	3.33	3.61E-03	6.44E-04
Tree 3	0.27	3.7	1.97E-03	5.03E-04
Tree 4	0.25	4	2.51E-03	7.19E-04
Tree 5	0.2	5	4.63E-04	1.69E-04
Tree 6	0.41	2.43	5.23E-03	6.64E-04
Mean	0.27±0.09	4.12±1.34	2.43E-03±1.79E-03	5.10E-04±2.12E-04
Bare 1	0.28	3.57	3.81E-03	9.30E-04
Bare 2	0.37	2.7	6.65E-03	1.04E-03
Bare 3	0.35	2.86	1.08E-02	1.92E-03
Bare 4	0.27	3.7	3.57E-03	9.14E-04
Bare 5	0.29	3.45	2.26E-03	5.29E-04
Mean	0.31±0.04	3.26±0.45	5.42E-03±3.41E-03	1.07E-03±5.15E-04

All experimental data for the undisturbed soil cores and the column with packing sand under saturated conditions were first analyzed with the one-region model. The BTCs and the fitted curves were plotted against pore volumes in Figure 3.4. The label C/C_0 of Y axle represents observed and fitted Br concentrations normalized for the initial Br concentration. The coefficients of determination (r^2) (Table 3.3) for all the fitted curves in Figure 3.4 are larger than 0.98; illustrating the good match between the observed data and the calculated curves. The BTCs for the soil cores exhibit asymmetries and tailing, but

the BTC for the column with repacked sand is reasonably symmetrical and typical of equilibrium conditions, because of its homogeneous hydraulic properties. The nonuniformity in bromide transport in the undisturbed soil cores is possibly caused by the lateral mass exchange between intraaggregate and interaggregate spaces. Fitted dispersion coefficients (D) increased with the pore water velocity in all soil cores, but the dispersivity was not much affected by the velocity (Table 3.3).

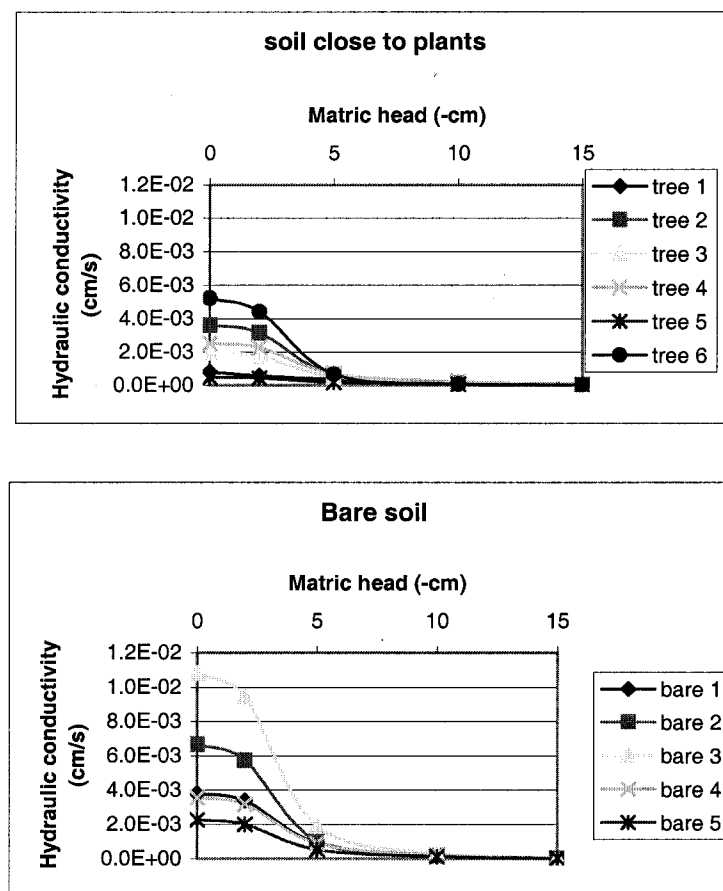


Figure 3.3. Calculated hydraulic conductivities based on the in-situ measurements; a. shows the hydraulic conductivity for soils close to plants, b. shows the hydraulic conductivity for the bare soils.

Dispersion was much smaller for the disturbed column than these for the undisturbed cores. The fitted pore water velocity was higher than those estimated for all soil cores, but it was very close to that measured in the disturbed column, because the pore water velocities for the disturbed was determined in the laboratory, while the pore water velocities for the undisturbed soil cores were estimated based on the field measurements with the tension infiltrometer, and the total porosity which is generally larger than effective porosity for the structural soils.

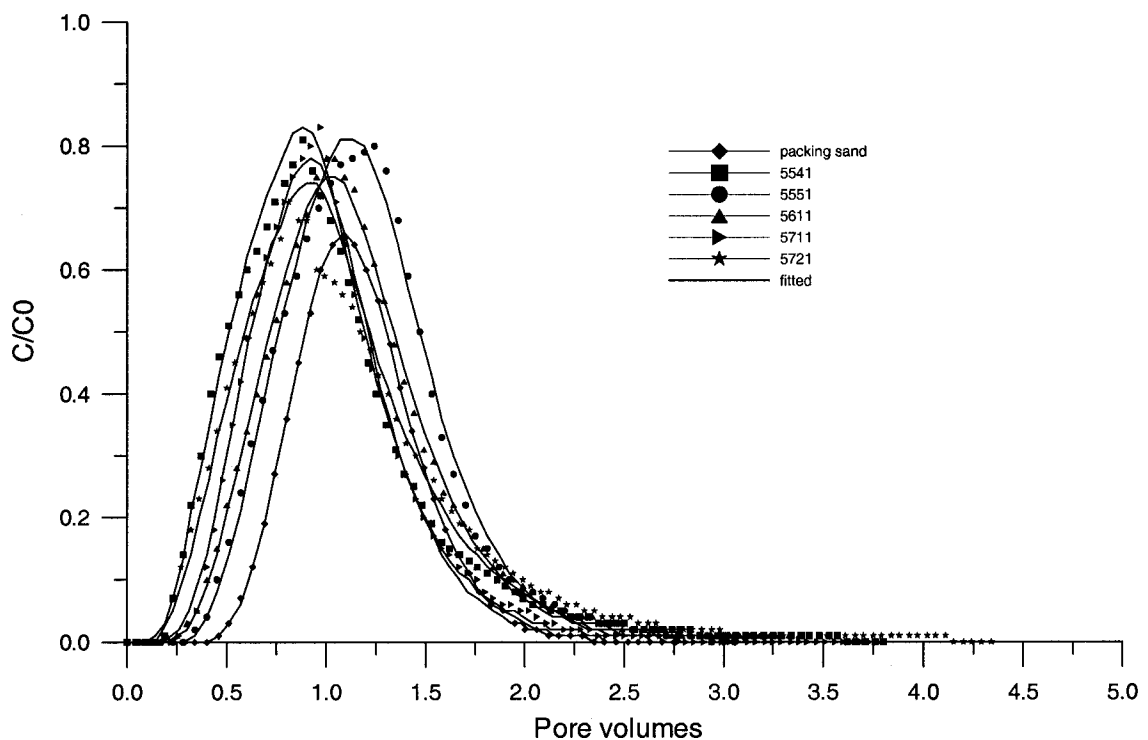


Figure 3.4. Observed data and fitted curves with the one-region model of CXTFIT2 at saturated conditions were plotted with pore volumes.

The values of dispersivity (ϵ) for the disturbed column were lower than those for the undisturbed soil cores (Table 3.3). This indicates that transport of bromide was dispersion

dominated in the undisturbed soil cores. The experimental BTCs for the undisturbed soil cores showed both early breakthrough and tailing as compared to the BTC for the disturbed column (Figure 3.4), which may indicate either a preferential flow or significant mass exchange between mobile and immobile regions in these soil cores, or both. High values of pore water velocity generally matched with high values of hydrodynamic dispersion coefficient D for the undisturbed soil cores (Table 3.3), indicating that the transport of Br in these soils is more a function of physical characteristics of the porous medium than diffusive characteristics of Br.

Table 3.3. Input parameters and fitted parameters with the one-region model.

Core ID	Matric head (cm)	Bulk density (ρ)	Calculated porosity	Tracer loaded (pore volume)	Estimated velocity v (cm/hr)	Fitted v (cm/hr)	Fitted D (cm ² /hr)	Dispersivity (ϵ)	Fitted T_2^* (hr)	r^2 *
PS-0	0	1.32	0.50	0.57	87.20	87.20	10.00	0.11	0.07	0.9990
PS-2	-2	1.32	0.50	0.74	34.31	41.00	23.77	0.58	0.20	0.9974
PS-5	-5	1.32	0.50	0.65	16.61	21.52	10.69	0.50	0.39	0.9990
PS-10	-10	1.32	0.50	0.65	11.30	17.71	9.71	0.55	0.57	0.9986
5541-0	0	1.52	0.43	0.74	28.26	56.60	100.00	1.77	0.26	0.9904
5541-2	-2	1.52	0.43	0.77	15.87	30.99	81.65	2.63	0.48	0.9955
5541-5	-5	1.52	0.43	0.73	6.52	15.39	56.48	3.67	1.10	0.9949
5541-10	-10	1.52	0.43	0.74	1.98	3.37	7.32	2.17	3.80	0.9939
5551-0	0	1.52	0.43	0.74	28.26	37.30	28.75	0.77	0.26	0.9947
5551-2	-2	1.52	0.43	0.73	17.19	22.70	17.58	0.77	0.43	0.9947
5551-5	-5	1.52	0.43	0.73	7.49	11.34	10.75	0.95	0.96	0.9984
5551-10	-10	1.52	0.43	0.72	2.09	3.13	2.92	0.93	3.45	0.9971
5611-0	0	1.41	0.47	0.70	15.17	21.50	22.80	1.06	0.46	0.9974
5611-2	-2	1.41	0.47	0.68	8.15	12.70	21.60	1.70	0.84	0.9986
5611-5	-5	1.41	0.47	0.66	3.87	5.45	7.76	1.42	1.72	0.9974
5611-10	-10	1.41	0.47	0.63	0.92	1.21	1.64	1.36	7.00	0.9933
5711-0	0	1.33	0.50	0.64	26.77	43.22	43.28	1.00	0.24	0.9947
5711-2	-2	1.33	0.50	0.64	16.38	23.55	20.10	0.85	0.39	0.9968
5711-5	-5	1.33	0.50	0.62	6.64	10.80	11.97	1.11	0.94	0.9992
5711-10	-10	1.33	0.50	0.61	1.52	2.17	2.23	1.03	4.16	0.9982
5721-0	0	1.43	0.46	0.72	27.53	47.91	100.00	2.09	0.26	0.9806
5721-2	-2	1.43	0.46	0.72	16.81	26.66	42.79	1.61	0.43	0.9989
5721-5	-5	1.43	0.46	0.72	7.21	10.37	10.98	1.06	0.99	0.9965
5721-10	-10	1.43	0.46	0.74	1.26	1.84	1.59	0.86	5.58	0.9974

* T_2 duration for loading Br tracer; r^2 regression coefficient.

In contrast to the high dispersion values for the undisturbed soil cores, little dispersion occurred in the disturbed column (Table 3.3). The low dispersion values in the disturbed column suggest that mass transport is more a function of convective flow than dispersive flow. The experimental BTCs for the disturbed column showed little tailing and no early breakthrough (Figure 3.4), indicating a more uniform solute front and lack of the conditions favoring a preferential transport as compared to those in the undisturbed soil cores.

The experimental data for the undisturbed soil cores and the disturbed column at the matric heads -2 cm and -5 cm were evaluated with the one-region model. The observed data and fitted curves were plotted with pore volumes in Figures 3.5 and 3.6. The BTCs for the undisturbed soil cores in Figure 3.5 are similar to those in Figure 3.4, but several differences can be noticed. First, the appearance of tracers for the soil cores 5541 and 5711 were delayed slightly. Second, the shapes of the BTCs for all the undisturbed soil cores were symmetrical than those in Figure 3.4. The BTCs for the undisturbed cores in Figure 3.6 are similar to those in Figure 3.4, not in Figure 3.5, which was not expected. The dispersion coefficient decreases at the matric heads -2 and -5 cm, because of much slower pore water velocity, versus those at saturation.

The experimental data for the undisturbed soil cores and the disturbed column at the matric head -10 cm were analyzed with the one-region model and all the data fit well to the calculated curves with r^2 greater than 0.98. The data and fitted curves were plotted with pore volumes in Figure 3.7. The shape of all BTCs for the undisturbed soil cores are very close to the shape of the BTC for the disturbed column in Figure 3.7, which is nearly symmetrical, little tailing and no early breakthrough, indicating a more uniform solute

front and lack of the conditions favoring the preferential transport as compared to those in Figures 3.4, 3.5, and 3.6.

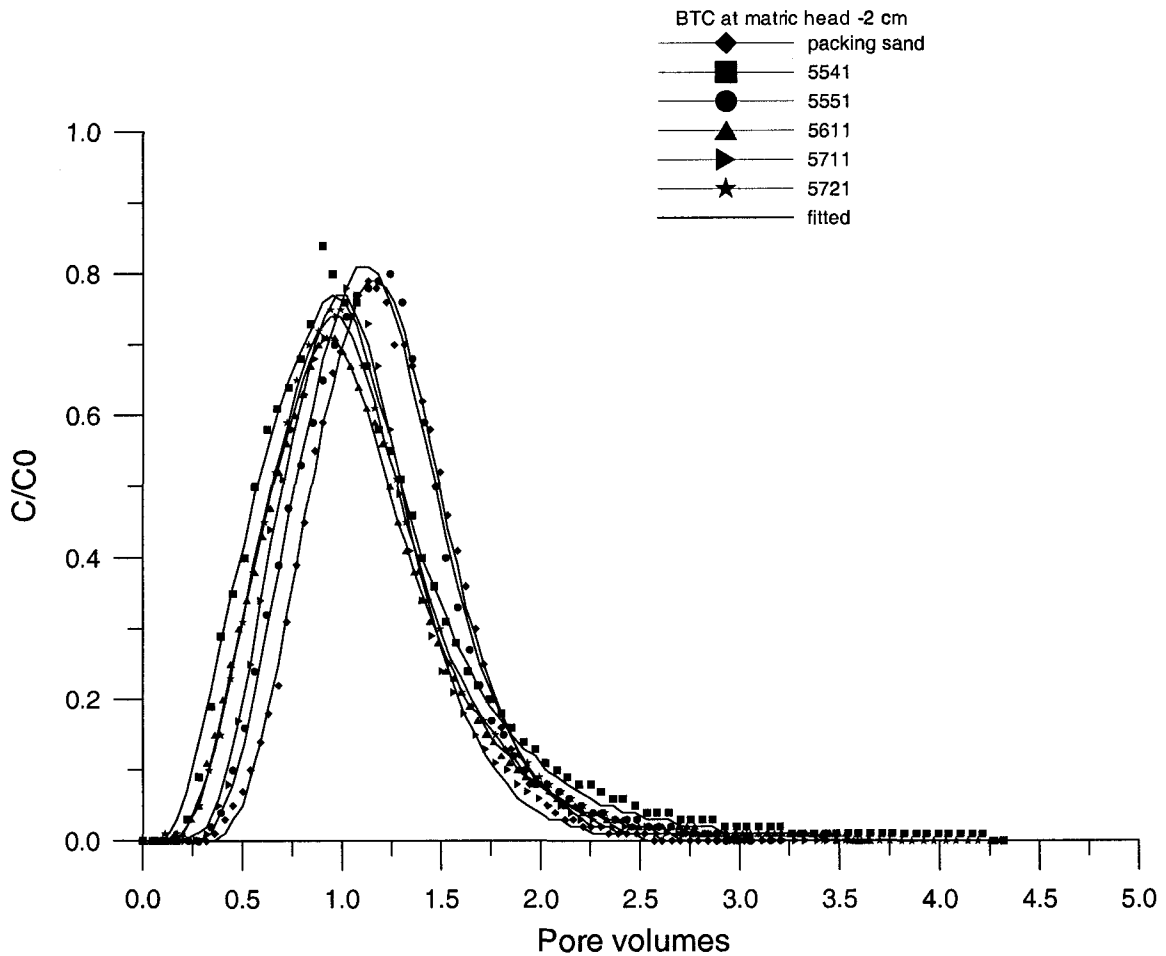


Figure 3.5. Observed data and fitted curves with the one-region model of CXTFIT2 at the matric head of -2 cm were plotted with pore volumes.

All the experimental data were also analyzed with the two-region (mobile-immobile) transport model given by Equations (3.2 & 3.3). Agreement between observed and calculated curves of the experiments for 5541, 5711, and 5721 at the saturation condition, and 5541 at the matric head of -5 cm are slightly better than these obtained with Equation

(3.1). The data and fitted curves were plotted against pore volumes in Figure 3.8. The fitted parameters including dispersion coefficient (D), mobile water fraction (β), and mass transfer coefficient (ω) are listed in Table 3.4. Based on the criteria for absence or presence of preferential flow (Langner et al., 1999), the preferential flow occurred in three undisturbed soil cores (5541, 5711, and 5721) at the saturation condition, and one soil core (5541) at the matric head of -5 cm. No preferential flow was simulated in other data sets.

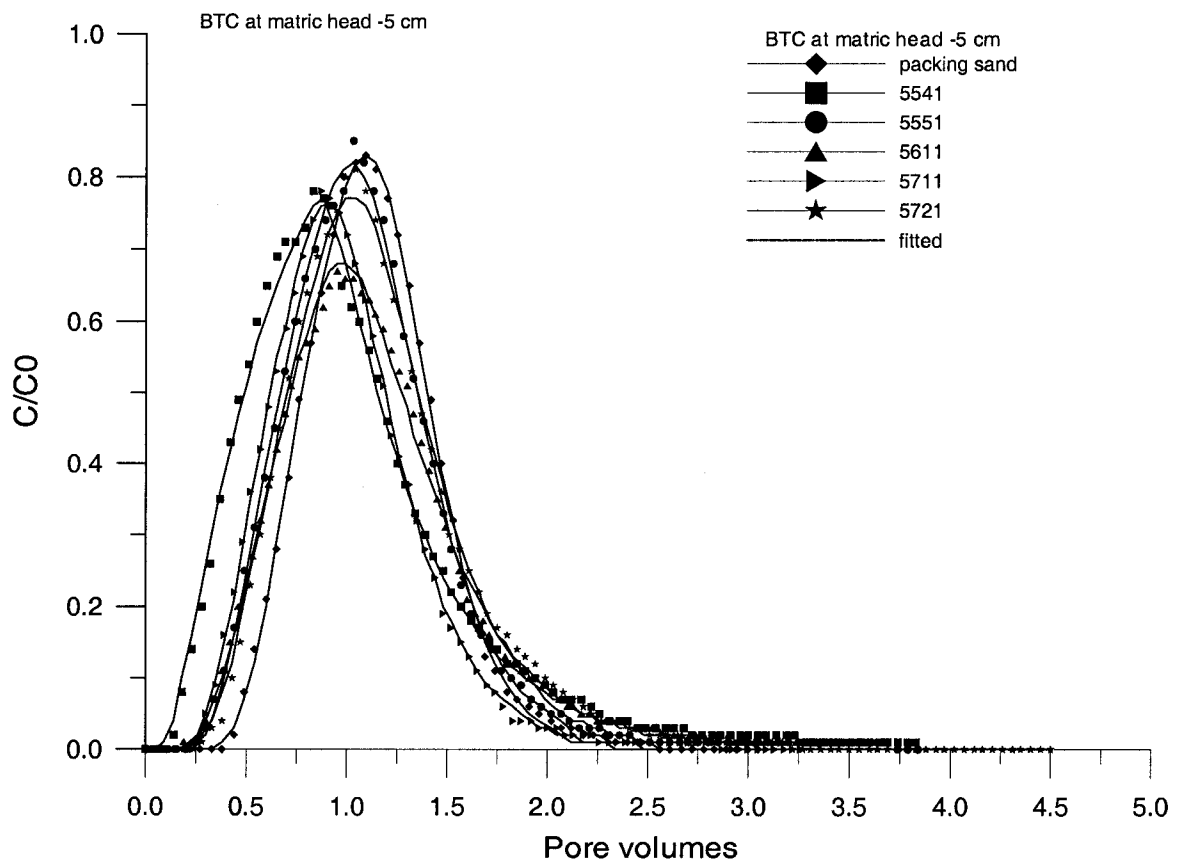


Figure 3.6. Observed data and fitted curves with the one-region model of CXTFIT2 at the matric head of -5 cm were plotted with pore volumes.

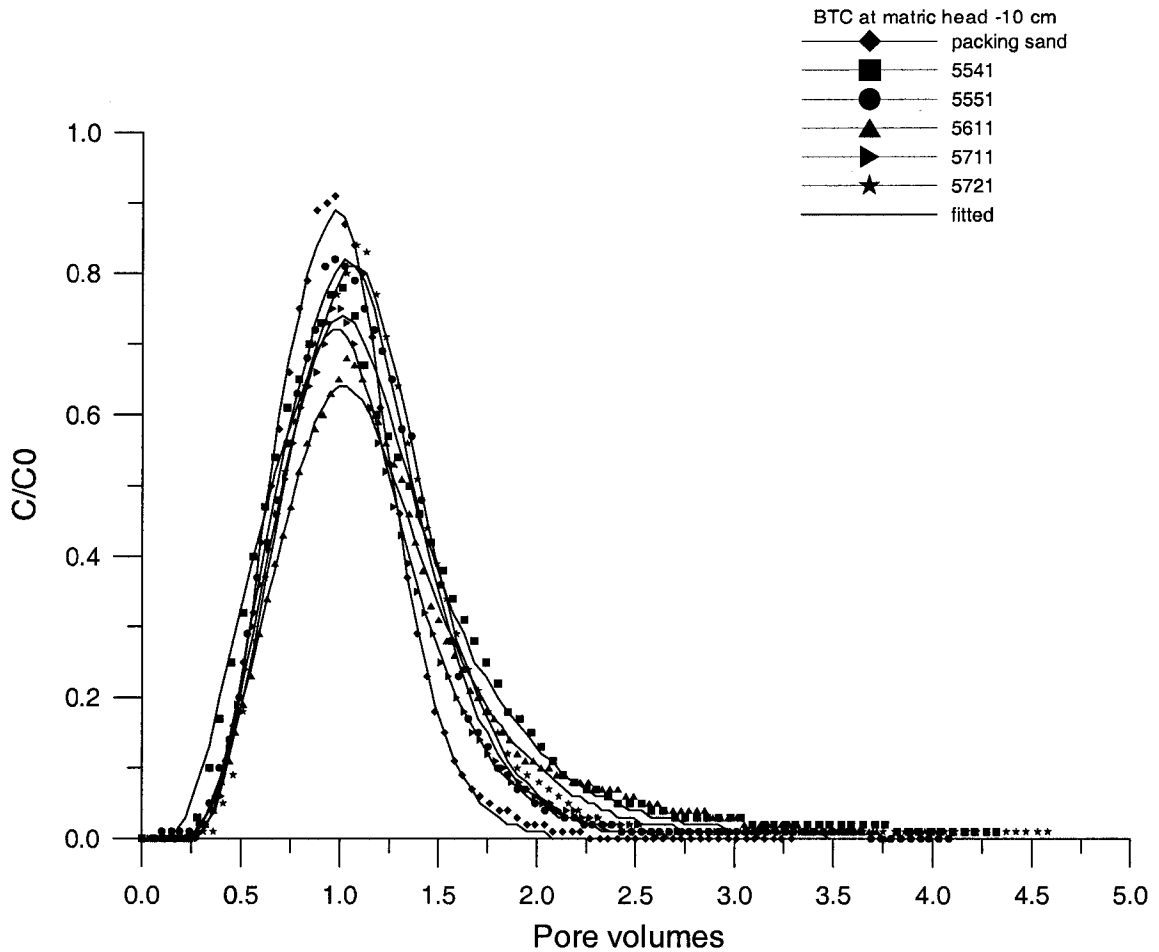


Figure 3.7. Observed data and fitted curves with the one-region model of CXTFIT2 at the matric head of -10 cm were plotted with pore volumes.

The two-region model-fitted values of mobile water fraction (β) under saturated conditions were 0.18, 0.23, and 0.21 for 5541, 5711, and 5721, respectively (Table 3.4). These small β values indicated the large immobile water content, which could be due to higher pore water velocity of macropores. The mobile mass fraction (β) value was 0.65 for 5541 at the matric head of -5 cm, which reflects a decrease in the immobile water contents with decrease in the matric head.

Table 3.4. Fitted parameters with the two-region model.

Laboratory ID	D (cm ² /hr)	β	ω	r^2	α (1/hour)
5541-0	70.93	0.18	0.030	0.9973	1.14
5541-5	25.66	0.65	0.006	0.9963	0.05
5711-0	27.57	0.23	0.008	0.9958	0.33
5721-0	89.92	0.21	0.008	0.9965	0.32

Note: The number after the laboratory ID is matric head in cm.

Preferential flow was not observed in any experimental data at matric head less than – 5 cm. Previous studies indicate that mobile water regimes become more important at the matric heads above -3 cm or –5 cm (Ersahin et al., 2002; Langner et al., 1999).

Nonequilibrium conditions often occurred in matric heads of 0 and -1 cm (Seyfried and Rao, 1987), but nonequilibrium conditions were not found at matric head of -10 cm.

Observed field data with a disc infiltrometer indicated that flow changed from gravity-dominated to capillary-dominated, when matric head at the infiltrometer base changed from -3 to -6 cm (Angulo-Jaramillo et al., 1996). Therefore, the lack of a preferential flow in conducted experiments under the matric head of –5 cm in this study is consistent with results reported above. The parameter (ω) is related to a rate coefficient α (hour⁻¹), which controls rate of diffusive mass exchange between mobile and immobile regions (van Genuchten, 1981; Parker and Toride, 1984). The rate coefficient values for 5541 decreased sharply when soil matric head decreased to -5 cm. This was attributed to the effect of pore water velocity and mobile water content on α , where the increasing pore water flux resulted in an increase in α values and increase in mobile water content resulted in a decrease in α values. A strong correlation between soil water potential and

values of α was found by Casey et al. (1998), which suggested that pressure head also has an effect on α .

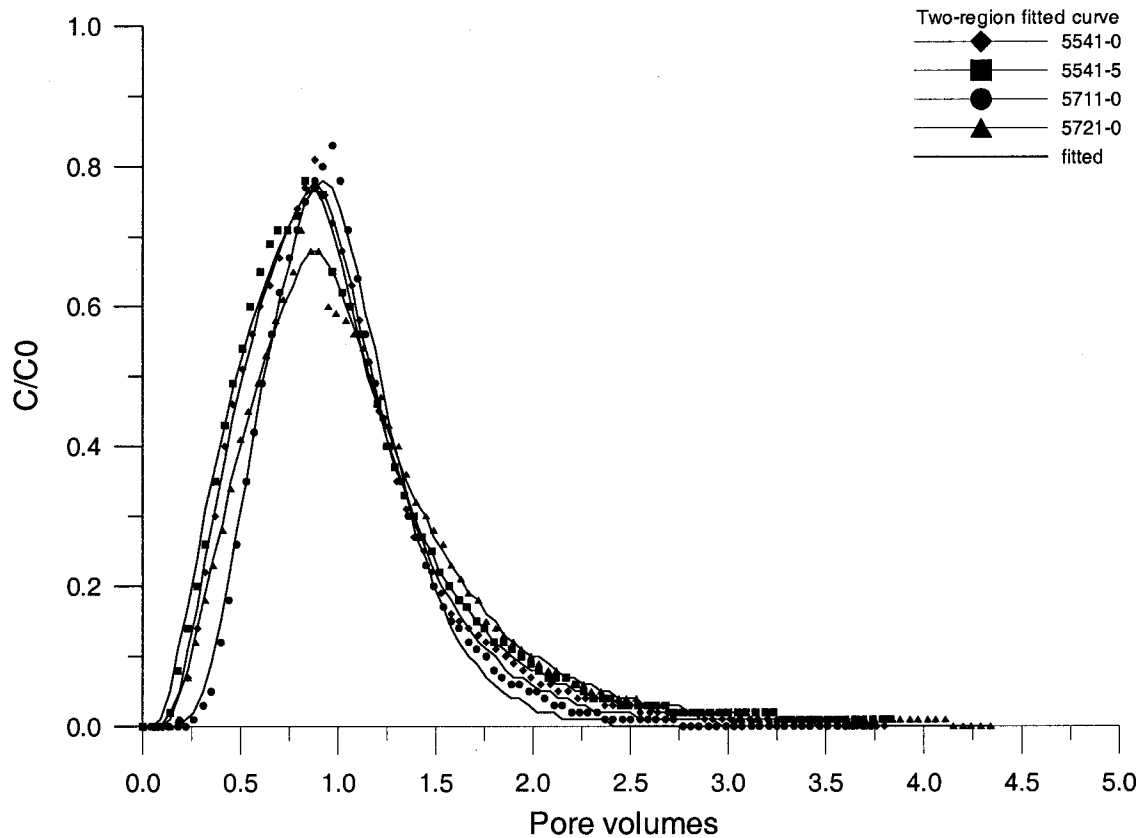


Figure 3.8. Observed data and fitted curves with the two-region model of CXTFIT2 were plotted with pore volumes.

3.5.3. Discussion

Transport of water and/or contaminants through thick vadose zones is directly related to climate and hydraulic properties of the vadose zone. Typically arid vadose zones are considered very suitable for waste disposal sites because of very low water availability for infiltration. However, intrinsic hydraulic properties in areas with

thick alluvial sequences are favorable for transmitting water and/or contaminants to a greater depth. In-situ measurements with tension infiltrometer at ADRS indicate that surface soils have the ability to transmit water up to 38.9 cm per hour for the bare surface soils and 18.8 cm per hour for the surface soils under plant canopy. Laboratory measurements indicated that the field soils at ADRS have the ability to conduct the water flux up to 23.0 cm per hour (Andraski, 1996). These potential water fluxes are extremely high. Therefore, the ability of the vadose zone to transmit water and/or contaminants is mainly dependent on the climate. It is apparent that these high fluxes would not occur for most surface soils at ADRS under present climate. However, these high water fluxes are more likely to occur in ephemeral washes that collect runoff from larger contributing areas. Previous studies with chloride-mass balance and water-balance modeling show that, despite minimal or nonexistent percolation of precipitation below a depth of 10 m at ADRS for at least the last 6,000 (Fouty, 1989) to 16,000 years (Prudic, 1994), the potential for infrequent percolation of precipitation below a depth of 2 m does occur under present climatic conditions in bare soil (Nichols, 1987), which indicates that the native vegetation plays an important role in removing available water. Episodic, deep drying during periods of below average precipitation limited the potential for deep percolation under natural, vegetated conditions (Gee et al., 1994; Andraski, 1997; Dong et al., 2003). Therefore, the lack of plants can increase the risk for deep water percolation.

The coarse soil texture of the surface soil at ADRS leads to low water retention which reduces limited water resources available for plants. The coarse soil texture is also less capable of holding the nutrients that are needed for plant growth. Therefore, higher

precipitation will lead to a greater loss of soil nutrients. This may indicate that the desert ecosystem is vulnerable and difficult to be recovered. However, desert plants are expected to use water more efficiently due to the ongoing rise in CO₂ content of atmosphere (Grunzweig et al., 2003; Eklundh and Olsson, 2003). A dynamic relationship among the soil physical properties, climate, and CO₂ content of atmosphere thus controls the desert ecosystem.

Paleoclimate studies indicated that the high-stand water in Death Valley occurred at 26 ka, 18 ka, and 12 ka, and was mainly contributed by surface water from the Amargosa River (Anderson and Wells, 2003). Major wetlands formed by paleo-spring discharge in southern Nevada were present during periods of 16.4-26.3 ka, 13.9-13.5 ka, and 11-9.5 ka (Quade et al., 2003); thus, the age of the latest wet climate event is only about 10 ka. Based on plant macrofossils of the Yucca Mountain region, Thompson et al. (1999) concluded that at the LGM (18 ka), the annual temperature was 5.2°C cooler than modern annual temperature and the precipitation was 2.35 times greater than modern precipitation. Given the proximity of ADRS to Yucca Mountain, a similar climate change is assumed for ADRS and the Yucca Mountain. If wetter climate patterns occur in the next 10 ka, the annual precipitation at ADRS could be as high as 253.8 mm, high precipitation intensity could be about 40 mm per hour which is more than most water fluxes measured in the field at the matric head -5 cm. The fitted pore water velocity at the matric head -5 cm is up to 15.4 cm/hour (Table 3.3). Based on assumptions, potential evapotranspiration calculated with the Hargreaves model was subtracted (Hargreaves and Samani, 1982) from the precipitation to obtain minimum net water for infiltration during rainfalls with high intensities. These values were up to 10.9 mm and 25.5 mm for the

modern climate and the LGM conditions, respectively. Therefore, the surface soils at ADRS could experience local high water fluxes during highly intensive rainfall events under present climate conditions, and could have higher water fluxes in past or future wet climates.

Experimentally measured BTCs for structured soils often exhibit asymmetries and tailing that are not consistent with the CDE, but the CDE does provide a reasonably accurate description of nonreactive solute transport in uniformly packed columns (Skaggs et al., 2002). The Br effluent data from the undisturbed soil columns exhibited asymmetries and tailing (Figures 3.4, 3.5, and 3.6) as compared to the Br effluent data from the packed column with sand. Because the Br is nonreactive, these asymmetries and tailing are attributed by macroscopic heterogeneities. However, the effluent data from the undisturbed columns were reasonably well described with the CDE, and only slight improvements on the fit for the effluent data for 5541, 5711, and 5721 at saturated conditions, and 5541 at the matric head -5 cm with the two-region model were observed. This is largely a result of coarse particles in these undisturbed soil columns.

The fitted dispersion coefficient is an increasing function of the pore water velocity in the undisturbed soil column, but not in the column with the packing sand (Table 3.3). The undisturbed columns are expected to have original soil structures that lead to spatial variations in local bulk densities, water contents and resultant flow variability. This purely explains the Br early appearance in the undisturbed soil cores (Figure 3.4, 3.5, 3.6, and 3.7) as compared to the column with repacked sand. These phenomena became insignificant with a decrease in matric head in each undisturbed column.

The Br effluent data for cores 5541, 5711, and 5721 at saturation condition, and 5541 at the matric head -5 were better fitted to the two-region model (Figure 3.8). This indicated that a preferential flow occurred in these cores. Those three cores were collected from bare ground surface of ADRS. The field measurements with the tension infiltrometer (Figure 3.3) exhibited large spatial variability of soil hydraulic properties of the interspace at ADRS, which could be results of different sediment bedding, grain size distribution, and clay content in both lateral and vertical directions. It is known that textural differences can promote the development of preferential flow (Glass et al., 1988, 1989; Hillel and Baker, 1988; Ritsema et al., 1993, 1998; DiCarlo et al., 1999; Bauters et al., 2000; Sililo and Tellam, 2000). In addition, macropores formed by root channels (Devitt and Smith, 2002), cracks, and animal burrows may be an important conduit for the preferential water flow and solute movement. Decayed roots were often found in the undisturbed cores used for this study. Preferential flow was not observed in cores 5551 and 5611. This could be a result of spatial variability of soil structures, or the cores used for our experiments are not big enough to capture the macropores in all scales. The preferential flow was only observed in core 5541 at the matric head -5 cm, not in cores 5711 and 5721. This may be attributed by the fact that the grain size of the surface soils at ADRS is very coarse with coarse fragments (Andraski, 1996), or the preferential flow is generally significant when the soils are nearly saturated (Luxmoore, 1981). There was no preferential flow observed for all undisturbed soil cores at the matric head -10 cm, because the matric head is one of most important factors to affect the preferential flow. Previous studies suggested preferential flow occurs predominantly at the matric

head larger than -10 cm, or through soil pores with an effective radius greater than 150 μm (Langner et al., 1999; Elrick and French, 1966; and Seyfried and Rao, 1987).

The preferential flow can contribute an important fraction of solute movement to significant depths in the vadose zone when near saturation. Under present climate conditions at ADRS, the surface soils are dry for most of the year; thus, preferential flow may not be a major mechanism for solute movement in the vadose zones of ADRS. However, precipitation with high intensities occurring in winter seasons could promote deep recharge of water through surface soils of ADRS. In that case, the contribution of preferential flow to the acceleration of the soil water percolation and solute transport could occur. It is likely that the preferential flow would occur in ephemeral washes that collect runoff from larger contributing areas under present climate conditions. This conclusion was supported by a recent study that indicated that deep percolation and groundwater recharge occur beneath areas of irrigation and ephemeral channels (Stonstrom et al., 2003). However, higher water infiltration and preferential flow through the surface soil could also occur during wetter climates, like the past pluvial periods or potentially in the future, if wetter climate returns to the desert.

3.6. Conclusions and Further Work

Water fluxes from the in-situ measurements with tension infiltrometer, and Br dispersion coefficients obtained from displacement experiments in undisturbed soil cores were quite high. These high water fluxes are mainly results of coarse soil textures and possibly from the preferential flow, which was supported by the effluent data for the undisturbed cores of 5541, 5711, and 5721. Four undisturbed soil cores collected from

the bare ground sites at ADRS used in this study should be representative of soil types. Effluent data from these four cores show a close fit between calculated and experimental BTCs. One undisturbed soil core from the plant canopy area exhibits similar transport characteristics to the cores from the interspace, which may not be typical for the soils under plant canopy, because the field measurements with the tension infiltrometer indicated larger variation in hydraulic properties for the soils under canopy. Fine particle sizes and more root channels for the soil under canopy are more favorable for producing a preferential flow when enough water is available. It can be expected that large soil cores would better capture more information on the water movement and solute transport in structured soils. Multiple tracers could also be used to identify the contributions of the preferential flow and matrix diffusion in structured soils.

Acknowledgement

This project was funded by the Department of Energy under sponsored project (DE-RP08-OONV13813), Geological Society of America Student Grant # 6870-01, 2002, and UNLV Graduate Student Association Grant, 2002. The authors appreciate the efforts of Dennis Weber who supported this work. The authors wish to acknowledge USGS ADRS Research Team, especially Brian Andraski for letting me work at the ADRS and to use their data. Many thanks to John Goreham for his assistance on experiments, and to Feng Pan and Suxia Wu for their assistance on field work and collecting samples.

References

- Abdall, N.A., and Lear, B., 1975. Determination of inorganic bromide in soils and plant tissues with a bromide selective-ion electrode. *Commun. Soil Sci. Plant Anal.* 6, 489–494.
- Anderson, D.E., and Wells, S.G., 2003. Latest Pleistocene lake highstands in Death Valley, California, in Enzel, Y., Wells, S.G., and Lancaster, N., eds., *Paleoenvironments and paleohydrology of the Mojave and southern Great Basin Deserts*: Boulder, Colorado, Geological Society of America Special Paper 368, 115-128.
- Andraski, B.J., 1996. Properties and variability of soil and trench fill at an arid waste-burial site. *Soil. Sci. Soc. Am. J.* 60, 54-66.
- Andraski, B.J., 1997. Soil-water movement under natural-site and waste-site conditions-- A multiple-year field study in the Mojave Desert, Nevada: *Water Resources Research* 33, 1901-1916.
- Andraski, B.J., and Stonestrom, D.A., 1999. Overview of research on water, gas, and radionuclide transport at the Amargosa Desert Research site, Nevada, in Morganwalp, D.W., and Buxton, H.T., eds., *U.S. Geological Survey Toxic Substances Hydrology Program--Proceedings of the Technical Meeting, Charleston, South Carolina, March 8-12, 1999--Volume 3 of 3--Subsurface Contamination from Point Sources*: U.S. Geological Survey Water-Resources Investigations Report 99-4018-C, 459-466.

- Andraski, B.J., Prudic, D.E., and Nichols, W.D., 1995. Waste burial in arid environments--Application of information from a field laboratory in the Mojave Desert, southern Nevada: U.S. Geological Survey Fact Sheet FS-179-95, 4 p.
- Angulo-Jaramillo, R., Gaudet J.-P., Thony J.-L., and Vauclin M., 1996. Measurement of hydraulic properties and mobile water content of a field soil. *Soil Sci. Soc. Am. J.* 60, 710-715.
- Bahr, J.M., and Rubin, J., 1987. Direct comparison of kinetic and local equilibrium formulations for solute transport affected by surface reactions. *Water Resour. Res.* 23, 438-452.
- BassiriRad, H., Reynolds, J.F., Virginia, R.A., and Brunelle, M.H. 1998. Growth and root NO_3^- and PO_4^{3-} uptake capacity of three desert species in response to atmospheric CO_2 enrichment. *Australian Journal of Plant Physiology* 24, 353-358.
- Bauters, T.W.J., DiCarlo, D.A., Steenhuis, T.S., and Parlange, J.-Y. 2000. Soil water content dependent wetting front characteristics in sands. *J. Hydrol.* 231-232, 244-254.
- Casey, F.X.M., Logsdon, S.D., Horton, R., and Jaynes, D.B. 1998. Measurement of field soil hydraulic and solute transport parameters. *Soil Sci. Soc. Am. J.* 62, 1172-1178.
- Devitt, D.A., and Smith, S.D., 2002. Root channel macropores enhance downward movement of water in a Mojave Desert ecosystem. *Journal of Arid Environments* 50, 99-108.
- DiCarlo, D.A., Bauters, T.W.J., Darnault, J.G., Steenhuis, T.S., and Parlange, J.-Y. 1999. Lateral expansion of preferential flow paths in sands. *Water Resour. Res.* 35, 427-434.
- Dong, W., Yu, Z., and Weber, D., 2003. Simulations on water variation in arid regions. *J. Hydrol.* 275, 165-181.

- Eklundh, L., and Olsson, L. 2003. Vegetation index trends for the African Sahel 1982-1999. *Geophysical Research Letters* 30, 10.1029/2002GL016772.
- Elrick, D.E., and French, L.K., 1966. Miscible displacement patterns on disturbed and undisturbed soil cores. *Soil Sci. Soc. Am. Proc.* 30, 153-155.
- Ersahin, S., Papendick, R.I., Smith, J. L., Keller, C.K., and Manoranjan, V.S., 2002. Macropore transport of bromide as influenced by soil structure differences. *Geoderma* 108, 207-203.
- Fouty, S.C., 1989. Chloride mass balance as a method for determining long-term groundwater recharge rates and geomorphic surface stability in arid and semi-arid regions Whisky Flat and Beatty, Nevada. M.S. Thesis. Univ. of Arizona, Tucson.
- Gardner, W.R., 1958. Some steady state solutions of unsaturated moisture flow equations with application to evaporation from a water table. *Soil Sci.* 85, 228-232.
- Gee, G.W., Wierenga, P.J., Andraski, B.J., Young, M.H., Fayer, M.J., and Rockhold, M.L., 1994. Variations in water balance and recharge potential at three western desert sites: *Soil. Sci. Soc. Am. J.* 58, 63-72.
- Glass, R.J., Steenhuis, T.S., and Parlange, J.-Y. 1988. Wetting front instability as a rapid and far-reaching hydrologic process in the vadose zone. *J. Contain. Hydrol.* 3, 207-226.
- Glass, R.J., Steenhuis, T.S., and Parlange, J.-Y. 1989. Mechanism for finger persistence in homogenous, unsaturated, porous media: Theory and verification. *Soil Sci.* 148, 60-70.

- Graham, E.A., and Nobel, P.S. 1996. Long-term effects of a doubled atmospheric CO₂ concentration on the CAM species *Agave deserti*. *Journal of Experimental Botany* 47, 61-69.
- Grunzweig, J.M., Lin, T., Rotenberg, E., Schwartz, A., and Yakir, D. 2003. Carbon sequestration in arid-land forest. *Global Change Biology* 9, 791-799.
- Hamerlynck, E.P., Huxman, T.E., Charlet, T.N., and Smith, S.D., 2002. Effects of elevated CO₂ (FACE) on the functional ecology of the drought-deciduous Mojave Desert shrub. *Lycium andersonii*. *Environmental and Experimental Botany* 48, 93-106.
- Hargreaves, G.H., and Samani, Z.A., 1982. Estimation of evapotranspiration by present plant cover for the Western Great Basin, *Transactions of the American Geophysical Union* 68, 1299.
- Hillel, D., and Baker, R.S., 1988. A descriptive theory of fingering during infiltration into layered soils. *Soil Sci.* 146, 51-56.
- Huxman, T.E., and Smith, S.D. 2001. Photosynthesis in an invasive grass and native forb at elevated CO₂ during an El Niño year in the Mojave Desert. *Oecologia* 128, 193-201.
- Idso, S.B. 1986. Industrial age leading to the greening of the Earth? *Nature* 320, 22.
- Johnson, M.J., Mayers, C.J., and Andraski, B.J., 2002. Selected micrometeorological and soil-moisture data at Amargosa Desert Research Site in Nye County near Beatty, Nevada, 1998-2000: U.S. Geological Survey Open-File Report 02-348.

- Langner, H.W., Gaber, H.M., Wraith, J.M., Huwe, B., and Inskeep, W.P., 1999.
Preferential flow through intact soil cores: effects of matric head. *Soil Sci. Soc. Am. J.* 63, 1591–1598.
- Luxmoore, R.J., 1981. Micro-, meso-, and macroporosity of soil. *Soil Sci. Soc. Am. J.* 45, 671-672.
- Mayes, M.A., Jardine, P.M., Mehlhorn, T.L., Bjornstad, B.N., and Ladd, J.L., 2003.
Transport of multiple tracers in variably saturated humid region structured soils and semi-arid region laminated sediments. *J. Hydrol.*, 275, 141-161.
- Naumburg, E., Housman, D.C., Huxman, T.E., Charlet, T.N., Loik, M.E., and Smith, S.D., 2003. Photosynthetic responses of Mojave Desert shrubs to free air CO₂ enrichment are greatest during wet years. *Global Change Biology* 9, 276-285.
- Nichols, W.D., 1987. Geohydrology of the unsaturated zone at the burial site for low-level radioactive waste near Beatty, Nye County, Nevada: U.S. Geological Survey Water-Supply Paper 2312, 57 p.
- Nichols, W.D., 1990. The significance of climate in southern Nevada for the shallow burial of low-level radioactive wastes: LaGrange, Ill., American Nuclear Society, Topical on Nuclear Waste Isolation in the Unsaturated Zone, Proceedings, Las Vegas, Nev., September 1989, 93-98.
- Nikedi-Kizza, p., Biggar, J.W., van Genuchten, M.Th., Wierenga, P.J., Selim, H.M., Davidson, J.M., and Nielsen, D.R., 1983. Modeling tritium and chloride ³⁶ transport through an aggregated oxisol. *Water Resour. Res.* 19, 691–700.

- Parker, J.C., and van Genuchten, M.Th., 1984. Determining transport parameters from laboratory and field tracer experiments. In: Bulletin 84-3, Virginia Agric. Exp. St., Blacksburg.
- Prudic, D.E., 1994. Estimates of percolation rates and ages of water in unsaturated sediments at two Mojave Desert sites, California-Nevada: U.S. Geological Survey Water-Resources Investigations Report 94-4160, 19 p.
- Quade, J., Forester, R.M., and Whelan, J.F., 2003. Late Quaternary paleohydrologic and paleotemperature change in southern Nevada, in Enzel, Y., Wells, S.G., and Lancaster, N., eds., *Paleoenvironments and paleohydrology of the Mojave and southern Great Basin Deserts*: Boulder, Colorado, Geological Society of America Special Paper 368, 165-188.
- Reith, C.C., and Thompson, B.M., 1992. *Desert as dumps? The disposal of hazardous materials in arid ecosystems*. Univ. of New Mexico Press, Albuquerque.
- Ritsema, C.J., Dekker, L.W., Hendrickx, J.M.H., and Hamminga, W. 1993. Preferential flow mechanism in a water repellent sandy soil. *Water Resour. Res.* 29, 2183-2193.
- Ritsema, C.J., Dekker, L.W., Nieber, J.L., and Steenhuis, T.S. 1998. Modeling and field evidence of finger formation and finger recurrence in a water repellent sandy soil. *Water Resour. Res.* 34, 555-567.
- Scanlon, B.R., 1991. Evaluation of moisture flux from chloride data in desert soils. *J. Hydrol.* 128, 137-156.
- Seyfried, M.S., and Rao, P.S.C., 1987. Solute transport in undisturbed columns of an aggregated tropical soil: Preferential flow effects. *Soil Sci. Soc. Am. J.* 51, 1434-1444.

- Sililo, O.T.N., and Tellam, J.H., 2000. Fingering in unsaturated zone flow: A qualitative review with laboratory experiments on heterogeneous systems. *Ground Water* 38, 864-871.
- Singh, P., and Kanwar R.S., 1991. Preferential solute transport through macropores in large undisturbed saturated soil columns. *J. Environ. Qual.* 20, 295-300.
- Stokstad, E., 2003. Unsuspected underground nitrates pose a puzzle for desert ecology. *Science* 302, 969.
- Stonestrom, D.A., Prudic, D.E., Laczniaik, R.L., Akstin, K.C., Boyd, R.A., and Henkelman, K.K., 2003. Estimates of deep percolation beneath native vegetation, irrigated fields, and the Amargosa River channel, Amargosa Desert, Nye County, Nevada: U.S. Geological Survey Open-File Report 03-104.
- Thompson, R.S., Anderson, K.H., and Patrick J. Bartlein, P.J., 1999. Quantitative paleoclimatic reconstructions from late Pleistocene plant macrofossils of the yucca mountain region. U.S. Geological Survey Open-File Report 99-338.
- Toride, N., Leij, F.J., and van Genuchten, M.Th., 1999. The CXTFIT code for estimating transport parameters from laboratory or field tracer experiments. Riverside, CA: USDA-ARS, Version 2.1. Res. Report no. 137. U.S. Salinity Lab..
- Valocchi, A.J., 1985. Validity of the local equilibrium assumption for modeling sorbing solute transport through homogeneous soils. *Water Resour. Res.* 21, 808-820.
- van Genuchten, M.Th., and Wierenga P.J., 1976. Mass transfer studies in sorbing porous media: I. Analytical solutions. *Soil Sci. Soc. Am. J.* 40, 473-480.

- van Genuchten, M.Th., 1981. Non-equilibrium transport parameters from miscible displacement experiments. Res. Rep. no. 119, US Salinity Lab., USDA, ARS, Riverside, CA.
- van Genuchten, M.Th., and Wierenga, P.J., 1977. Mass transfer in sorbing porous media: II. Experimental evaluation with tritium ($^3\text{H}_2\text{O}$). *Soil Sci. Soc. Am. J.* 41, 272–278.
- Walvoord, M.A., Phillips, F.M., Stonestrom, D.A., Evans, R.D., Hartsough, P.C., Newman, B.D., and Striegl, R.G., 2003. A reservoir of nitrate beneath desert soils: *Science*, 302, 1021-1024.
- Walvoord, M. A., 2002. A unifying conceptual model to describe water, vapor, and solute transport in deep arid vadose zones, Ph.D. thesis, N.M. Inst. of Mining and Technol., Socorro.
- Wierenga, P.J., and van Genuchten, M.Th., 1988. Solute transport through small and large unsaturated soil columns. Journal Article 1303. Agric. Exp. Stn., New Mexico State University, Las Cruces, New Mexico 88003.
- Wierenga, R.J., and Manz , B.P., 1973. A multichannel syringe pump for steady-state flow in soil columns. *Soil Sci. Soc. Am. Proc.* 37, 133–135.
- Wilson, G.V., Yunsheng, L., Selim, H.M., Essington, M.E., and Tyler, D.D. 1998. Tillage and cover crop effects on saturated and unsaturated transport of fluometuron. *Soil Sci. Soc. Am. J.* 62, 46-55.
- Winograd, I.J., 1981. Radioactive waste disposal in thick unsaturated zones. *Science*, 212, 1457-1463.

Wood, J.L., and Andraski, B.J., 1995. Selected meteorological data for an arid site near Beatty, Nye County, Nevada, calendar years 1990-91: U.S. Geological Survey Open-File Report 94-489, 49.

Wooding, R.A., 1968. Steady infiltration from a shallow circular pond. *Water Resour. Res.* 4, 1259-1273.

CHAPTER 4

SIMULATION OF PALEOLAKE EXTENTS IN OWENS VALLEY

4.1. Abstract

Quantitative paleoclimate information is necessary for the realistic estimation of groundwater recharge and prediction of future climate change. A physically based catchment-lake model was developed to extract quantitative paleoclimate information over the past 18 ka from lake records in the Owens River Valley, California, a hydrologically closed basin including Owens Lake, China Lake, Panamint Lake, and Death Valley. Since the lake serves as an integrator that reflects climatic and hydrologic conditions for the entire catchment, it is sensitive to regional as well as local climatic fluctuations. Shoreline terraces, beach deposits, lake sediments, and fossil data in this chain of lakes document several cycles of pluvial events in the late Quaternary. Studies have shown that these pluvial events were triggered by the global climate change. A catchment-lake model was used to reconstruct the observed paleolake levels for Owens Lake and Searles Lake at key times in the past (18 ka, 15 ka, 12 ka, 9 ka, and 6 ka). The initial model inputs were prepared based on modern regional spatial and temporal climate data, boundary conditions from the General Circulation Model, and fossil proxy data. The inputs subsequently were systematically varied in order to produce the observed lake levels. In this way, a large number of possible paleoclimatic combinations can quickly

narrow the possible range of paleoclimatic combinations that could have produced the paleolake level and extent. Finally, a quantitative time-series of paleoclimate information for key times was obtained.

4.2. Introduction

Yucca Mountain (YM), Nevada, was selected as the first long-term geological repositories for high-level radioactive wastes in the United States in 2002. Understanding long-term groundwater flux at the repository is fundamental for predicting future groundwater flow and transport in the region. The time for the safe isolation of radioactive wastes from public requires up to hundreds of thousands of years. Therefore, in addition to characterizing present-day site hydrology, the knowledge of long-term hydrologic variability is needed. YM is composed of a sequence of welded and non-welded tuffs. The present-day arid climate and a thick unsaturated zone (UZ) (the present water table is about 400 to 600 m below land surface) comprise of two major positive attributes that may limit the releases of radioactive material into the environment (Winograd, 1981). However, the region was strongly influenced by wetter, cooler climate conditions during the Quaternary period (Spaulding, 1985; Quade et al., 1995), and nearly 100 closed basins in the western United States contained lakes during the late Pleistocene (Benson and Thompson, 1987). A variety of paleoclimatic proxy data have offered qualitative information on past climate, but quantitative data are often needed for studying long-term hydrologic processes. Although atmospheric general circulation models (GCMs) have been utilized in attempts to estimate quantitative paleoclimate information at a global scale (Kutzbach, 1987; COHMAP Members, 1988; Street-Perrott,

1991), their resolution is not fine enough for the investigation of localized climate change (Kutzbach, 1987; Dickinson et al., 1989) that is very critical for the analysis of regional groundwater recharge and transport.

Paleoprecipitation proxies have been extracted from a variety of sources such as tree rings, ice cores, and marine and continental sediments (e.g., Stuiver et al., 1995; Spaulding, 1985; Shackleton, 1967). Excepting ice core records, most of these records can only provide indirect and qualitative estimates of paleoprecipitation. However, lake levels in closed basins are the most sensitive indicators of the water balance between precipitation and evapotranspiration in the watershed (Street-Perrott and Harrison, 1985). Lakes fluctuate in volume at both seasonal and interannual time scales in response to variations in the water balance over the lakes and their catchments. These volume fluctuations are reflected in the lake level fluctuations in closed basin lakes, and in the rate change of overflow in open lakes.

The distinctive tectonic setting and geomorphic characteristic of the southern Great Basin create many hydrologically closed basins that were filled with water during pluvial lake periods (e.g., Smith and Street-Perrott, 1983; Street-Perrott and Harrison, 1985; Phillips et al., 1994; Bischoff et al., 1997; Menking et al., 1997; Benson, 1999; Lowenstein et al., 1999; Bischoff and Cummins, 2001). Although variations in wind velocities, relative humidity, temperature, and other climatic variables that influence evaporation rates are factors in determining lake sizes, the change in precipitation is the most important factor (Smith, 1991). Studies on the lakes in Owens River system, California, have shown that lake levels primarily record annual precipitation amounts and almost quantitatively document changes in precipitation within their catchments, thus

these lakes are sometimes termed as - “natural rain gauges” (Smith and Bischoff, 1997) that can be used to extract quantitative paleoprecipitation for the catchment area of the Owens River and its neighboring regions including Yucca Mountain.

Studies on the lakes in the Owens River system have shown that their water levels primarily record annual precipitation amounts within their catchment, but the interpretation on paleoclimatic changes is generally limited to either wetter or drier climate, and offers little specific data about the nature of the climate change. The reason for this is that lake level in a particular basin is a complicated function of intrabasin and extrabasin climate and basin topography (Benson and Thompson, 1987). In order to extract quantitative paleoclimatic proxies from these lake records, one of the best approaches is through numerical modeling.

A variety of models have been used to simulate the paleorecord of closed basin lakes in arid and semiarid areas (e.g., Kutzbach, 1980; Benson, 1981; Benson, 1986; Hostetler and Bartlein, 1990; Hostetler and Benson, 1990; Hostetler et al., 1993, 1994). Physically-based lake models, which explicitly represent the physical processes governing the energy and water balances of the lake, offer a more robust way to predict climate induced changes in water volume, level, and outflow of the lakes. A suitable lake model for paleolake level studies should require a minimum of site-specific parameters (Hostetler and Giorgi, 1993). In this study, a coupled catchment-lake model was developed and used to quantitatively estimate paleoclimate information, especially annual mean precipitation and temperature in southwestern Great Basin since the last glacial maximum (LGM).

4.3. Owens River System

The Owens River system, California, located at the western margins of the Great Basin, is a hydrologically closed basin that consists of a chain of lakes including Mono Lake, Owens Lake, China Lake, Searles Lake, Panamint Lake, and Death Valley Lake (Figure 4.1). Excepting Mono Lake, the floors of these lakes are now occupied by playa lakes or salt flats. The valley is bound on the west by the Sierra Nevada, on the northeast by the Inyo and White Mountains, and on the southeast by the Coso Range. Presently, Owens River drains an area of about 8,550 km², but due to a strong rain shadow effect, most of the runoff is derived from about 16% of the catchment area, which lies on the eastern slope of the Sierra Nevada (Lee, 1912). Modern climate at the floor of the Owens River system is semi-arid with about 15 cm of annual precipitation. Thus, precipitation that falls directly on the surface of the basins in the Owens River system is an insignificant contribution to the lake water budget, which could also be true for the lakes in the paleo-Owens River system (Jannik et al., 1991). Street-Perrott and Harrison (1985) termed such lakes as “amplifier” lakes, describing a simple relationship among basin runoff, lake evaporation, and lake area (Smith and Bischoff, 1997).

Owens Lake, at the base of high mountains, is the first to respond to the increasing amounts of regional precipitation. Until 1912, the Owens Lake, which was about 10 m deep and 290 km² in area before agricultural irrigation in the area became extensive, was a terminal lake of the Owens River. All of the river’s water was diverted to Los Angeles in 1912, and subsequently, the Owens Lake desiccated. Searles Lake was third in a chain of five permanent lakes receiving water from the Owens River during the late Pleistocene, and Mono Lake was separated from the Owens River system to the south by

a high-altitude sill in the late Wisconsin (Benson and Thompson, 1987). During the LGM, Owens Lake, China Lake, and Searles Lake overflowed and the Panamint Valley was a terminal lake of the Owens River hydrological system. Lake stages at Searles Lake are sensitive to climatic changes because of the storage capacities of the upper lakes in the series. Inflow to Searles Lake depends on the overflow from the other lakes and therefore it is first lake affected by a decreasing inflow in the lake system.

Studies of lacustrine outcrops, cores, and landforms have allowed the reconstruction of the past histories of lakes in the Owens River system and its downstream basins (Smith and Street-Perrott, 1983; Smith and Bischoff, 1997). Geomorphic and sedimentary evidence, including staircases of abandoned shorelines and abrupt changes of facies in sediments, records fluctuations of the paleolake levels. Smith and Street-Perrott (1983) provided a chronology of Late Wisconsin to present lake level fluctuations for Searles Lake (Figure 4.2).

Benson et al. (1997) identified two hiatuses at 2.25 and 9.2 m based on the ^{14}C data of Core OL84B from Owens Lake. These two hiatuses represent two desiccation events that occurred at ~15.3-13.5 and ~6.1-4.3 ka (all ages used in the text of this study are on ^{14}C time scale before present (B.P.)) in Owens Lake. The $\delta^{18}\text{O}$ data of sediments between the two hiatuses show four abrupt dry/wet oscillations that correspond the four dry/wet oscillations in the North Atlantic region (Benson et al., 1997). Relatively wet intervals precede each of the dry events. An extreme overflow occurred at about 12 ka, which resulted in the lowest $\delta^{18}\text{O}$ (-13 ‰) of lake carbonate (Benson, 1999).

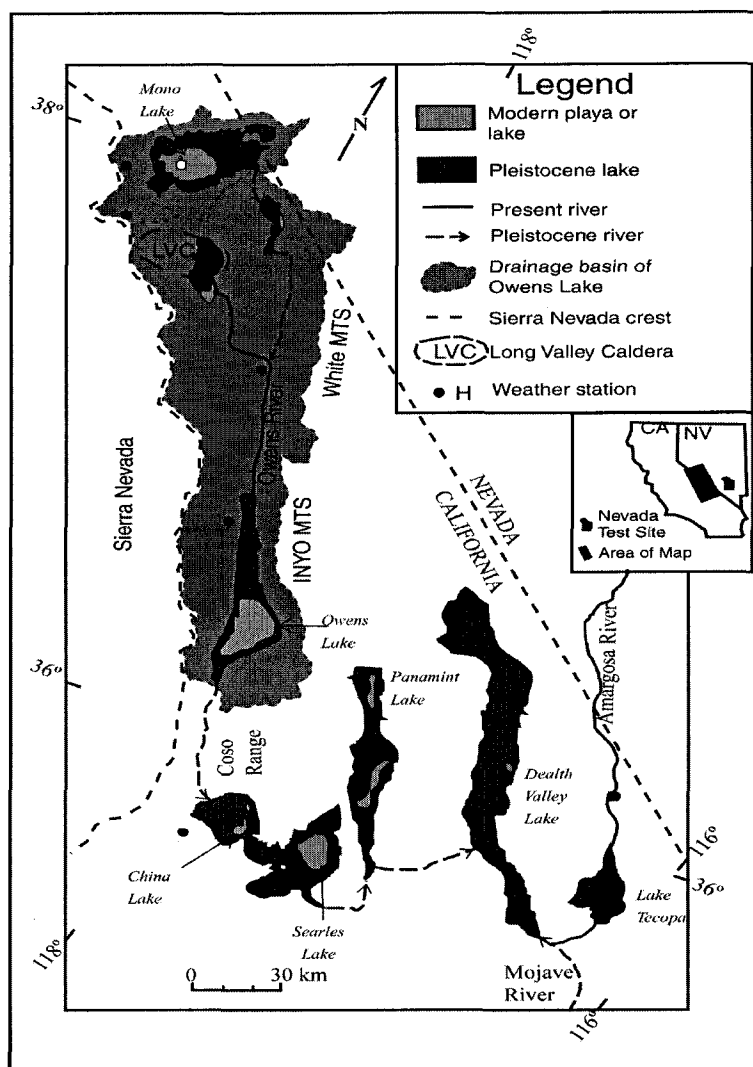


Figure 4.1. Location map of Owens River system (Modified from Smith and Bischoff, 1997).

Based on the ostracode assemblage from Owens Lake, Forester (2001) derived more details on lake level changes of the Owens Lake from 25 ka to 4 ka while Li et al. (2000) provided detailed information on climate for the past 1000 years. $\delta^{18}\text{O}$ was plotted with age (Benson et al., 2002) for past 20 ka in Figure 4.2.

In summary, the detailed paleolake records in the Owens River system offer a good opportunity to extract quantitative paleoclimate information in the southwestern Great Basin.

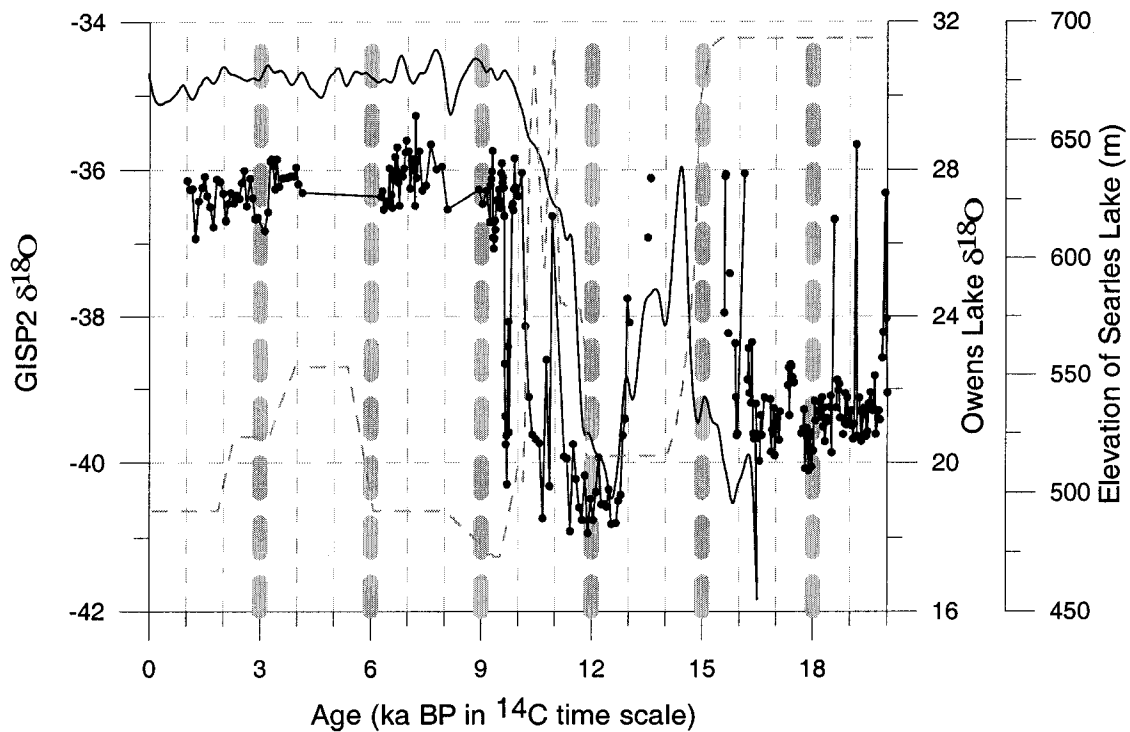


Figure 4.2. $\delta^{18}\text{O}$ for core OL84B (solid line with dot) (Benson et al., 1997), $\delta^{18}\text{O}$ from GISP2 (solid line) (Stuiver et al., 1995), and elevation of lake surface for Searles Lake (dashed line) (Smith and Street-Perrott, 1983) in the last 20 ka.

4.4. Description of Model and Modeling Strategies

The surface area of a closed-basin lake under natural conditions is strictly dependent on the dynamic equilibrium between precipitation and evapotranspiration over its entire catchment (Halley, 1715). Any changes in this equilibrium result in a change in terminal lake depth, which directly influences its area, and the cumulative lake area in the drainage

basin (Benson and Paillet, 1989). The mean annual water balance of a lake is governed by the equation (Street-Perrott and Harrison, 1985)

$$\Delta V = A_L(P_L - E_L) + (R - D) + (G_I - G_O) \quad (4.1)$$

where ΔV is the net change in volume of the lake, P_L is precipitation on the lake, E_L is evaporation from the lake, A_L is the area of the lake, R and D are runoff from the catchment and the surface discharge from the lake respectively, and G_I and G_O are groundwater flows into and out of the lake respectively. For a closed basin lake, G_I and G_O can be assumed negligible, and D is zero (Street-Perrott and Harrison, 1985), so Equation (1) reduces to the following form for equilibrium conditions

$$R = A_L(E_L - P_L) \quad (4.2)$$

If the runoff from the drainage basin can be represented by

$$R = A_B(P_B - E_B) \quad (4.3)$$

where A_B represents area of the catchment, P_B is the precipitation over the catchment, and E_B is the evapotranspiration over the catchment, then

$$A_B(P_B - E_B) = A_L(E_L - P_L) \quad (4.4)$$

This simple expression shows that the equilibrium area of a closed lake under natural conditions is strictly dependent on the precipitation and evaporation over its catchment and water surface. In the Owens River system, based on paleolake records, values for A_L and A_B for those paleolakes can be measured quite accurately using a digital elevation model (DEM). Remaining components in Equation (4.4) are precipitation and evaporation over the drainage basin. The evaporation mainly depends on temperature, thus the purpose for this study is to develop a coupled catchment-lake model to resolve these two unknown variables in the Equation (4.4).

Besides temperature, the evaporation value also depends on many other climatic factors including solar radiation, wind speed, and cloud cover. With the exception of temperature, other relevant factors are difficult to reconstruct from geologic data. Many studies assume that paleo-values for the evaporation can be satisfactorily estimated from empirical relationships between modern data on evaporation and air temperature. However, a change in evaporation rates could result from higher wind velocities, higher relative humidities and lower solar radiation values, and greater amounts of precipitation on the lake surface (Smith and Street-Perrott, 1983). Therefore, it is desirable to have a model that considers all of these factors. Hostetler and Bartlein (1990) developed a one-dimensional surface energy-balance lake model, where the vertical heat transfer was simulated by eddy diffusion and convective mixing. Several studies using this model have successfully simulated the modern and paleolake level change both in humid and arid regions (Vassiljev, 1997; Hostetler and Benson, 1990; Hostetler et al., 1994). Orndorff (1994) developed a surface hydrologic model (OSHM) that has been successfully applied to the Owens River system to test the proxy estimates of the LGM against the paleolake records. The OSHM has three modules: the snow module that computes mean monthly snowfall, snowmelt, snowpack, ice accumulation, ice transport, and icemelt for each grid cell based on the input of temperature, precipitation, and elevation of that cell, the runoff module that calculates mean annual runoff from available water (rain, snowmelt, and icemelt), and the lake module that computes lake extent from the results of basin-wide mean annual runoff calculated by the runoff module and lake evaporation. In the OSHM, empirical relationships between modern data on evaporation and air temperature are used to calculate the evaporation for the pluvial lakes in the

Owens River system during the LGM, which may not represent the actual situation as discussed above. In this study, the lake module in the OSHM was modified with the addition of Hostetler's lake model and used to simulate evaporation over the lake surface. The paleoclimatic evaluation strategy is first to model the lake extent under current climatic conditions with the coupled catchment-lake model developed in this study. The input parameters under current climatic conditions are then systematically varied in order to reconstruct lake extent based on lake records under paleoclimatic conditions. The modeling strategy is essentially an inverse approach to inferring paleoclimatic conditions based on past lake extent. The advantage of this modeling strategy is that a large number of possible paleoclimatic combinations can be quickly narrowed to a possible range of temperature/precipitation combinations that could have produced a particular paleolake extent.

A simulation on lake extent begins with dry closed basins. Each basin's runoff volume is added to the current lake volume at each time step. The lake volume is compared to the basin threshold volume, which corresponds to a lake level equal to the controlling elevation of the lowest basin outlet. Overflow occurs into the basin on the other side of the outlet when the lake volume exceeds the threshold volume. The model also checks for lake merging during overflow, which occurs when two lakes with a common active outlet overflow, thus inundating the active outlet. If two lakes merge, the downstream basin becomes a part of the upstream basin, and the remaining outlets of both basins are sorted to determine the new active outlet for the complex basin (Orndorff, 1994). Lake evaporation is then calculated using the eddy diffusion and convective mixing (Hostetler and Bartlein, 1990), and the lake level is adjusted accordingly

(Orndorff, 1994). The simulation runs in one year time step until the cumulative lake volume equilibrates or the run time exceeds a specified end time. Benson and Paillet (1989) state that “the proper gage of lake response to change in the hydrologic balance is neither lake depth (level) nor lake volume but instead lake surface area”, thus this study focused on lake surface area for a comparison of simulated lake extent and derived lake extent based on geologic evidence.

4.5. Calibration of Catchment-Lake Model

The catchment-lake model used in this study was developed by coupling a distribution hydrology model (Orndorff, 1994) and an energy-balance lake model (Hostetler and Bartlein, 1990). Both of these models were independently calibrated with observed data (Orndorff, 1994; Hostetler and Bartlein, 1990; Hostetler, 1991), thus they are valid when used independently. However, the catchment-lake model developed for this study has to be calibrated before applying it to simulate paleolake levels. Mono Lake is presently the only lake with standing water in Owens Valley. The three major streams (Rush, Lee Vining, and Mill Creeks) that delivery water to Mono Lake originate in the high Sierra Nevada (Benson et al., 1990), so the hydrological characteristics of Mono Lake and Owens Lake are similar. Observed data including climate data, hydrological data and lake level data are available for the Mono Lake drainage basin since 1857 (Mono Basin Environmental Impact Report, 1993). The data on measured temperature profiles and lake evaporation are also available for some periods of time (MacIntyre et al., 1999). The calibration was done with input data including modern precipitation and temperature matrix data for the Mono Lake drainage basin from the LCM (Stamm, 1991),

solar radiation data from the Desert Rock, vapor pressure, wind speed, and cloudiness data from stations close to the Mono Lake. The Desert Rock is located at about 150 km southeast of Mono Lake. The simulated monthly runoff for the Mono Lake drainage basin in this study is compatible with the observed (Figure 4.3) and the annual runoff is about 1% less than the observed. The simulated lake surface area is 227 km², which is 0.5% less than the average of the observed lake surface area from 1940 to 1989 (Mono Basin Environmental Impact Report, 1993).

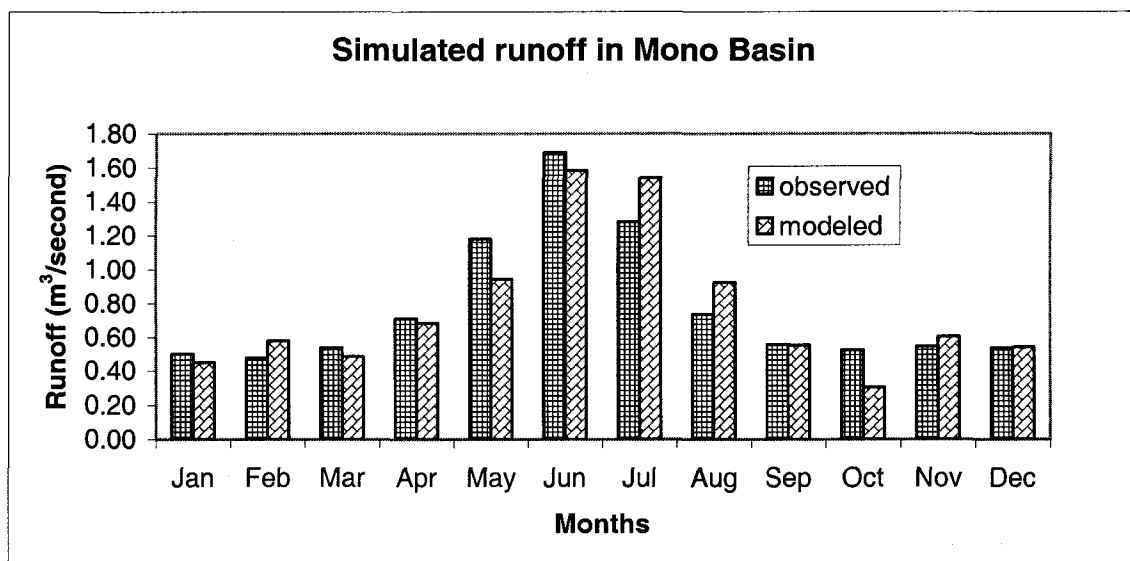


Figure 4.3. A comparison of observed runoff and simulated runoff in Mono Lake drainage basin.

The lake temperature profile simulated by the model agreed very well with measured temperature profile (Figure 4.4a). Furthermore, the simulated evaporation also compares well with the observed evaporation data through the grand pan, but slight higher than the evaporation estimated from water budget method (Figure 4.4b). These comparisons

indicated that the overall ability of the coupled catchment-lake model developed here to reproduce observed basin-wide mean annual runoff, mean lake surface area, temperature profile and evaporation of lake water in modern Mono Lake drainage basin.

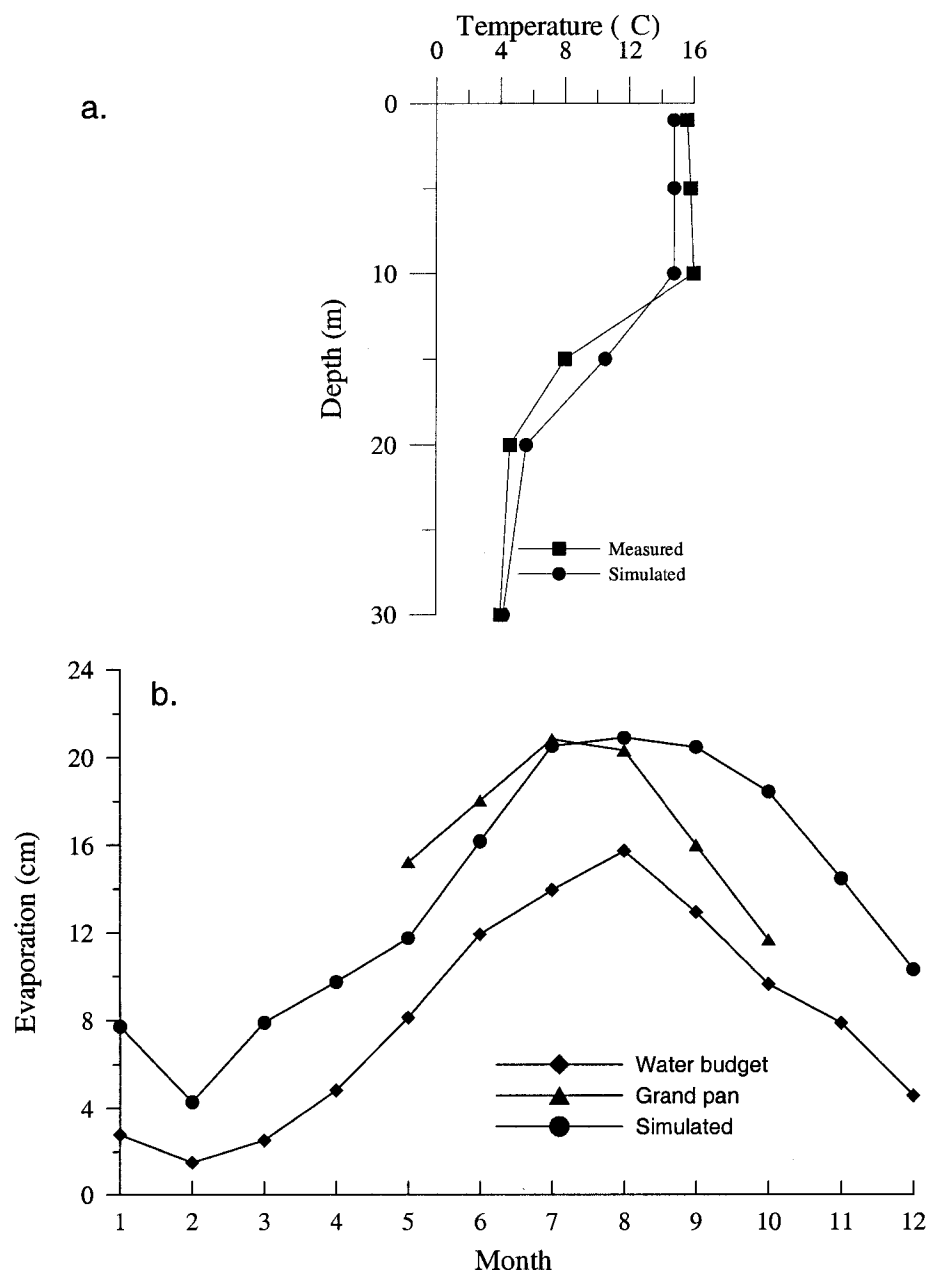


Figure 4.4. a. A plot of simulated and measured temperature profile (MacIntyre et al., 1999) in Mono Lake; b. Simulated evaporation and observed evaporation for Mono Lake.

4.6. Input Parameters

A number of input parameters are required for the coupled catchment-lake model. Coarse grid cell (5 km x 5 km) used in the OSHM missed some small snow cover and stream networks, and did a poor job representing some basin shapes (Orndorff, 1994). In this study, the fine resolution (1 km x 1 km) data was used to obtain better results. The topographic data used in this model is from the global 30 arc-second elevation data set (GTOPO30) (<http://edc.usgs.gov/products/elevation/gtopo30.html>). The GTOPO30 has a horizontal grid spacing of 30 arc seconds (approximately 1 kilometer). Observed solar radiation, cloud cover, wind speed, atmospheric pressure from near weather stations, and modern monthly temperature and precipitation matrix from the LCM (Stamm, 1991) that are based on boundary conditions including terrain, wind field, and radiation balance were used to drive the newly developed catchment-lake model and to reproduce the historical lake level of the Owens Lake. Precipitation and temperature matrix data at 18 ka, 15 ka, 12 ka, 9 ka, and 6 ka were prepared based on the proxy data in Table 4.1 by applying the appropriate perturbation (simple additive change for temperature, and multiplicative change for precipitation) to the modern monthly precipitation and temperature matrix data from the LCM. For example, climate at the LGM might be hypothesized to be 5° colder and 50% wetter than the present based on proxy data in Table 4.1. The input climate matrix at the LGM could be prepared for temperature by subtracting 5°C from the modern temperature matrix, and for precipitation by multiplying 1.5 times the modern precipitation matrix. Other climate parameters including cloud cover (Figure 4.5a), solar radiation (Figures 4.5b, c), and wind speed (Figure 4.6) were from historic records for modern conditions, and from the Community Climate Model

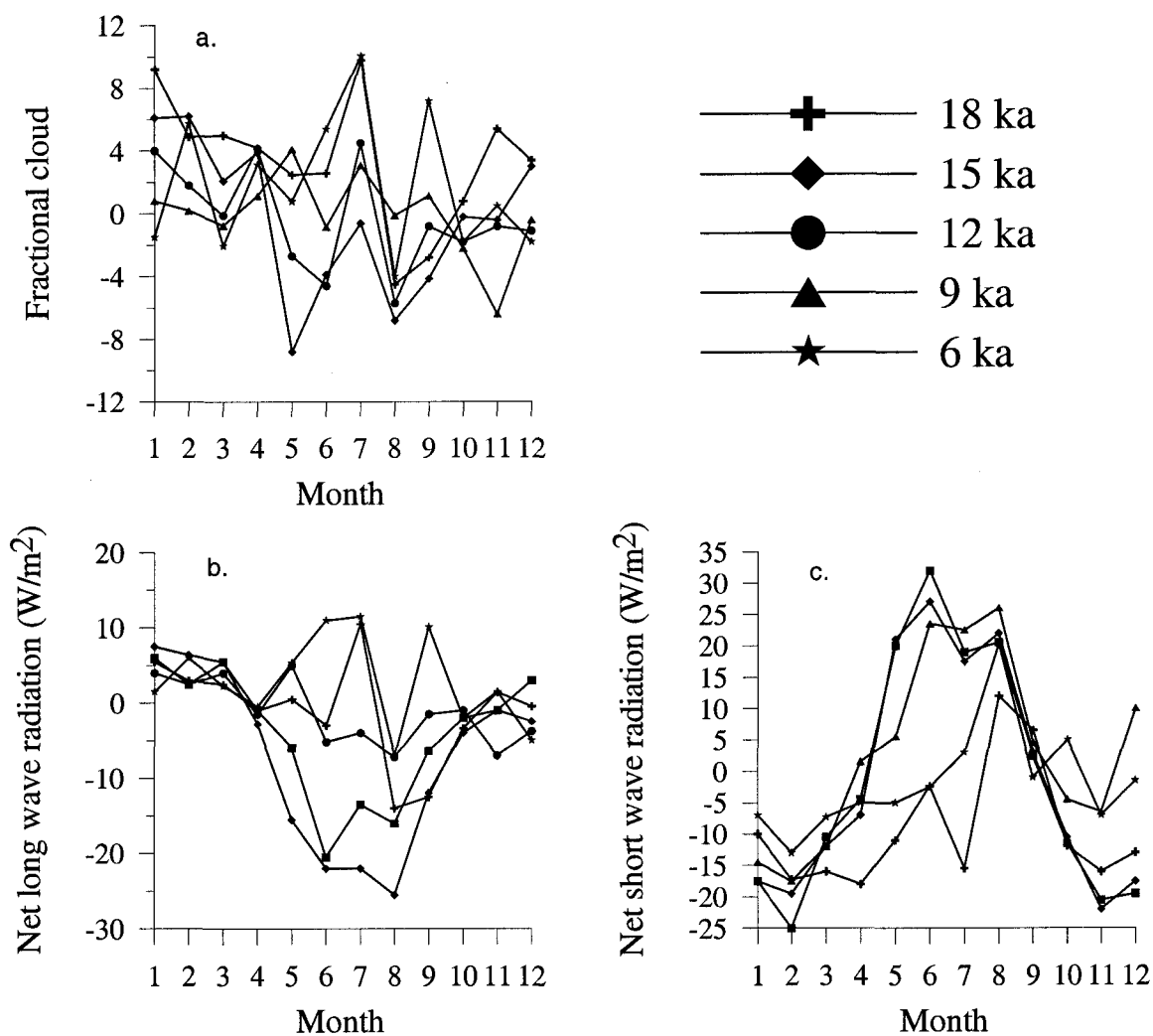


Figure 4.5. Inputs of cloud cover, solar radiation for the simulations at 18 ka, 15 ka, 12 ka, 9 ka, and 6 ka (Bartlein et al., 1998).

(CCM0) (Kutzbach and Guetter, 1986) and the results of paleoclimate simulation of North America (Bartlein et al., 1998) for paleoclimatic simulation. However, the single monthly value for these parameters was used for the whole area. The reason for this is: first, there are no fine resolution data available for these parameters in the study area; second, previous study indicated that precipitation and temperature are the two primary factors controlling glacial extent (Plummer and Phillips, 2003).

Because Owens Lake, China Lake, and Searles Lake overflowed and the Panamint Valley was a terminal of the Owens River hydrological system at the LGM, and most observation data are available for Owens Lake and Searles Lake, the comparison between the simulated results and the observation data in this study focused on Owens Lake and Searles Lake.

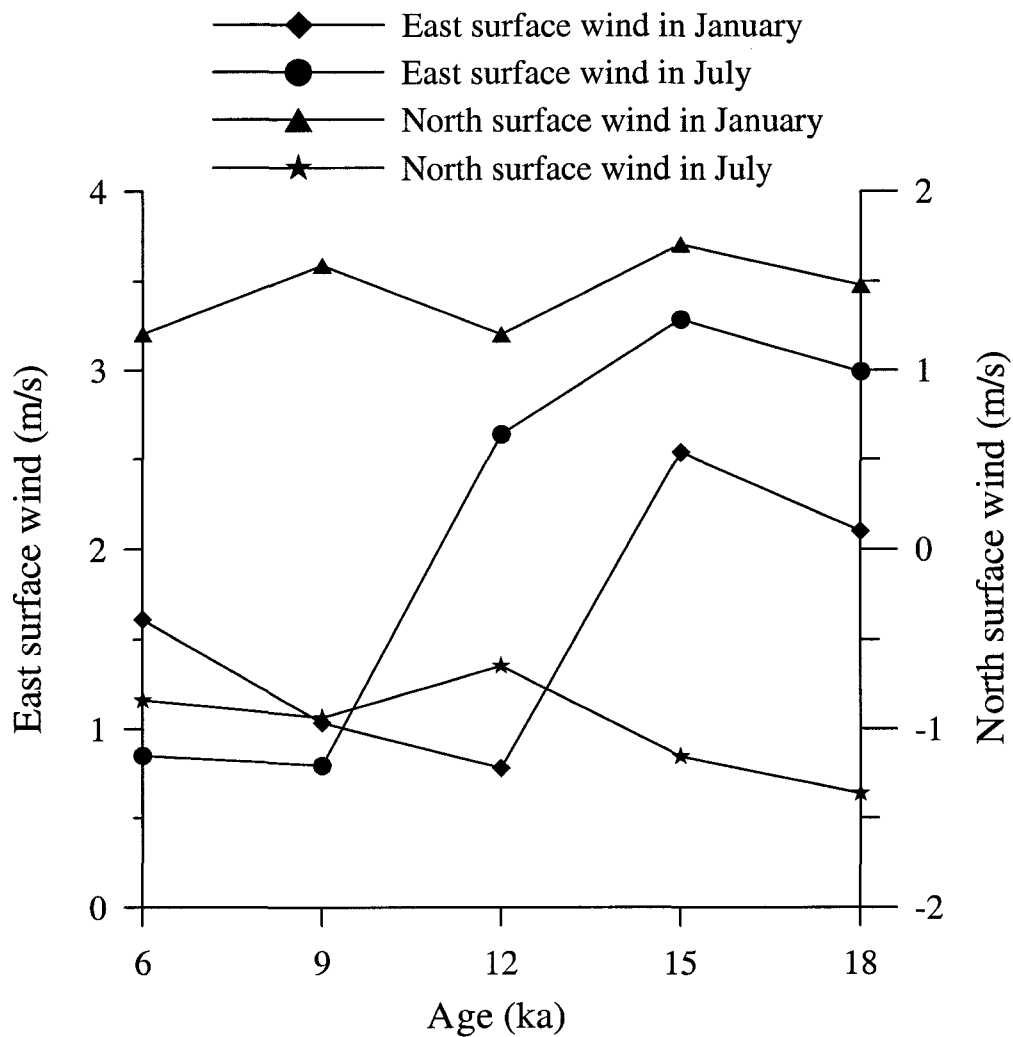


Figure 4.6. Inputs of wind speed for the simulations at 18 ka, 15 ka, 12 ka, 9 ka, and 6 ka (Kutzbach and Guetter, 1986).

4.7. Results

4.7.1. Simulation on Modern Lakes

Mean annual runoff, computed for modern climate from the runoff module is input to the lake model to simulate modern lake extent in the Owens Valley. The resulting lakes along with hillshed and stream network that were derived from the DEM are shown in Figure 4.7a. The lake system converges in 80 years (the lake system reaches its steady-state). There is no lake mergence occurring. The results from modern simulation accurately portray Mono Lake, Lake Crowley (in the Long Valley basin), Black Lake (in Adobe Basin), and Owens Lake. Simulated Mono Lake has a surface area of 227 km² that is about 0.5% less as compared to the average 228 km² of the observed lake surface area from 1940 to 1989 (Mono Basin Environmental Impact Report, 1993). Simulated Owens Lake has a surface area of 289 km² that is about 0.3% less as compared to an observed pre-diversion surface area of 290 km² (Smith and Street-Perrott, 1983).

4.7.2. Simulations on Lakes at Last Glacial Maximum (LGM)

Simulations on lakes at the LGM in the Owens Valley were done with modern temperature and precipitation matrices perturbed based on proxy-based LGM temperature and precipitation departures (Table 4.1), other climate parameters including solar radiation, cloud cover, and wind speed from CCM0 (Kutzbach and Guetter, 1986) and the results of paleoclimate simulation of North America (Bartlein et al., 1998) that were fixed. By varying combinations of temperature and precipitation with appropriate

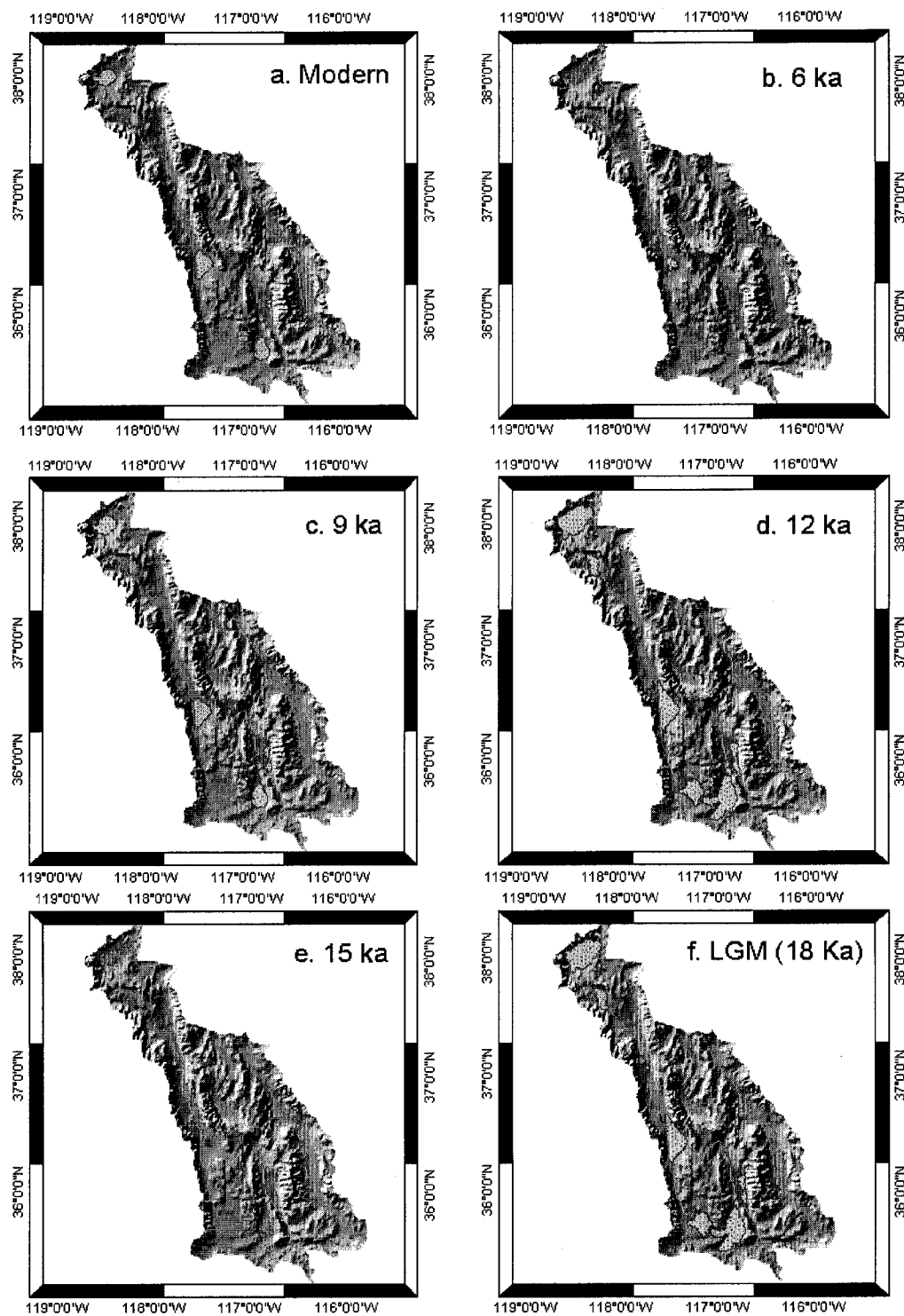


Figure 4.7. Simulated lake extents (dotted area) in the last 18 ka, and hillshaded (Gray scale) and stream network (solid lines) derived from DEM data.

perturbation until the derived lake extent at the LGM from field evidence was reproduced, the final combination with temperature 5.5°C cooler than modern temperature, and 1.25 times of modern precipitation was obtained. Simulated final lake extents with hillshed and stream network are shown in Figure 4.7f. Owens Lake overflows, and has a lake surface area of 692 km². China Lake and Searles Lake coalesce and have an area of 949 km². Searles Lake also overflows and a small lake with an area of 144 km² is formed in Panamint Valley. These results are very compatible with observed lake extent in Owens Valley at the LGM. Smith and Street-Perrott (1983) reported that both Owens Lake and Searles Lake overflow and have a lake surface area of 694 and 994 km², respectively.

Table 4.1. Proxy data in the southwest United States in the last 18 ka

Time	Temperature (°C)	Precipitation	Source
Late Wisconsin	-6.25 annual	+37 cm winter	Dohrenwend (1984)
	-3.0 annual	+68% annual	Mifflin and Wheat (1979)
	-5.5 annual	+27.5% annual	Merrill and Pewe (1977)
	-6.5 annual	+65% winter, -45% summer	Spaulding (1985)
	-6.0 summer	Summer precipitation 10% of annual	Betancourt (1990)
	-6.7 annual	+32% annual	Cole (1990)
	+1.0 winter, -1.0 summer	+57% winter, +56% summer	Leffler and Cochran (1989)
	-3.0 Jan, -3.0 Jul	+19 mm Jan, -31 mm Jul	Spaulding and Graumlich (1986)
18 ka	-3.29 annual	-0.29 mm/day annual	Thompson et al, 1994
	-3.17 Jan, -3.01 Jul	+0.25 mm/day Jan, -0.84 mm/day Jul	
20.5 to 18 ka	-7.5 annual	2.40x	Thompson et al., 1999
14 to 11.5 ka	-6.7 annual	2.58x	Thompson et al., 1999
12 ka	-2.52 annual	-0.18 mm/day annual	Thompson et al, 1994
	-3.01 Jan, -0.63 Jul	-0.27 mm/day Jan, -0.15 mm/day Jul	
9 ka	+0.43 annual	+0.30 mm/day annual	Thompson et al, 1994
	-0.09 Jan, +2.15 Jul	+0.80 mm/day Jan, -0.27 mm/day Jul	
6 ka	+0.69 annual	-0.03 mm/day annual	Thompson et al, 1994
	+0.30 Jan, +0.68 Jul	-0.16 mm/day Jan, +0.07 mm/day Jul	

4.7.3. Simulations on Lakes at 15 ka

The techniques used to prepare input data for simulations on lakes in Owens Valley at 15 ka are the same as these at the LGM. Based on ^{14}C dating and sedimentary features, Benson et al. (1997) reported a desiccation event occurred at Owens Lake at 15 ka. Because Owens Lake is an upstream lake of Searles Lake, and Searles Lake received most of its inflow from the overflow of Owens Lake, Searles Lake could also desiccate at 15 ka. This is supported by the field evidence that indicates that Searles Lake was at its low water level with an elevation of 510 m. Therefore, the simulation on the lake extent in Owens Valley at 15 ka is to find a combination of precipitation and temperature that can create a dry Owens Lake and Searles Lake. After multiple runs, a combination with temperature 1.8°C cooler than modern temperature and precipitation 20% less than modern precipitation could produce a dry Owens Lake and Searles Lake (Figure 4.7e). The results from this simulation also indicated that a significant decline on the water level in Mono Lake. This is consistent with possible hiatuses in cores from the Mono Lake basin (Newton, 1991) and major declines on the levels in Mono Lake and Lake Lahontan (Benson et al., 1998; Benson et al., 1996).

4.7.4. Simulations on Lakes at 12 ka

The $\delta^{18}\text{O}$ data from Core OL84B drilled in Owens Lake indicated the lowest values of $\delta^{18}\text{O}$ at 12 ka for the last 15 ka (Figure 4.2) (Benson et al., 1997). This represents the highest ratio of overflow to flow into Owens Lake (Benson et al., 1997), which implies that Searles Lake probably also received its highest inflow at 12 ka for the last 18 ka. The field evidence indicated that the water level of Searles Lake started to increase at 12 ka and reached its highest level at 11 ka (Figure 4.2) (Smith and Street-Perrott, 1983). It can

be expected that the overflow from Searles Lake might finally reach its highest level, and the largest lake might be formed in Panamint Valley in the last 18 ka. Based on multiple runs, a combination of temperature 4.5°C cooler than modern temperature and 1.8 times of modern precipitation could reproduce a lake system with the highest lake level in Panamint Valley (Figure 4.7d) since the LGM. However, the lake level of Panamint Lake was still not high enough to cause overflow.

4.7.5. Simulations on Lakes at 9 ka

$\delta^{18}\text{O}$ values of Owens Lake at 9 ka are around 27 ‰, indicating Owens Lake was at its hydrological closure at this time (Benson et al., 1996). A dry event was recognized based on the presence of prismatic cracking that suggests the existence of soil formed during subaerial exposure of lake sediments at about 9 ka (Benson et al., 1997). In the meantime, Searles Lake was at its lowest water level since the LGM (Smith and Street-Perrott, 1983). A combination of temperature 0.5°C warmer than modern temperature and 1.2 times of modern precipitation could reproduce a lake system in Owens Valley at 9 ka (Figure 4.7c).

4.7.6. Simulations on Lakes at 6 ka

Owens Lake experienced a second desiccation event between 6.1-4.3 ka (Benson et al., 1997), while Searles Lake was at a water levels that were about the same as today (Smith and Street-Perrott, 1983). Thus the lakes at 6 ka might have shallower water levels than modern lakes in Owens Valley. Based on this evidence, a combination of temperature 1.2°C warmer than modern temperature and 0.9 times of modern precipitation could produce a lake system in Owens Valley at 6 ka (Figure 4.7b).

4.8. Sensitivity Analysis

Sensitivity analysis was only performed for the simulation of lakes in Owens Valley at the LGM (18 ka), because more evidence for paleolake levels are available. Based on the proxy data at the LGM in Table 4.1, a combination of the lowest temperature (7.5°C cooler than modern temperature) and the maximum precipitation (2.4 times modern precipitation) was used to prepare the input data for simulation on the lake extent. The results from simulation based on this combination indicate that all basins including Death Valley in Owens River system are full of water, which was not the case in the last 18 ka. Another combination of the highest temperature (3.0°C cooler than modern temperature) and the lowest precipitation (1.2 times modern precipitation) was used to simulate lake extent in Owens Valley. The results from this simulation indicate that Searles Lake is not full and no lake was formed in Panamint Valley. The results from these two extreme cases of the combination are in conflict with the geological evidence. First, Panamint Lake did not overflow, and there was no full lake in Death Valley in the last 18 ka (Smith and Street-Perrott, 1983). Second, Mono Lake was separated from the Owens River system to the south by a high-altitude sill in the late Wisconsin (Benson and Thompson, 1987). Third, Searles Lake was full and overflowed into Panamint Valley where a small lake was formed at the LGM (Smith and Street-Perrott, 1983). Therefore, the coupled catchment-lake model developed in this study is very sensitive to a change of both temperature and precipitation, and it can be used to infer paleoclimatic conditions based on past lake extents.

4.9. Discussion

The coupled catchment-lake model developed in this study has several advantages for paleoclimatic interpretation of paleolake extents. By using physically based models to examine the climatic conditions that could produce a particular lake extent at a specific time, a quantitative estimate on temperature and precipitation as compared to field evidence was obtained. This approach allows a direct consideration of the effects of changes in both precipitation and temperature, as well as numerous climate variables including cloud cover, solar radiation, and wind speed. Simulated lake surface areas and the elevation of lake surfaces for major lakes in Owens Valley in the last 18 ka are listed in Table 4.2.

Table 4.2. Simulated lake extent and elevation of lake levels in Owens Valley in the last 18 ka

Age (ka)	Mono Lake		Owens Lake		Searles Lake		Panamint Lake	
	Elevation (m)	Area (km ²)						
18	2040	461	1145	692	688	949	340	144
15	1952	3	1070	30	475	2	310	3
12	2120	689	1145	692	688	949	350	349
9	1978	270	1100	302	525	252	325	94
6	1949	2	1075	96	490	4	315	5
0	1958	227	1097	289	515	225	320	30

The combinations of temperature (Figure 4.8a) and precipitation (Figure 4.8b) that could produce observed lake extent in Owens Valley in the last 18 ka were obtained from the simulations above. Reconstructed temperature and precipitation based on pollen in Owens Lake core OL84B are plotted in Figure 8. Simulated combination of temperature and precipitation at the LGM (18 ka) is 5.5°C cooler than modern temperature, and 1.25 times of modern precipitation. This result is close to some proxy data (Merrill and Pewe, 1977) in Table 4.1, but different from other proxy data in Table 4.1. This could be the result that the proxy-based estimates of LGM climate are representative of the area where the fossil assemblage or glacial feature was founded. A mixed conifer forest from Kings Canyon that includes red fir, western juniper, incense cedar, sugar pine, ponderosa pine, California nutmeg, and single-needle pinon pine (Cole, 1983) indicated a colder climate than today with near-modern precipitation levels in the southern Sierra Nevada at 18 ka.

The 9.2 m hiatus found in Owens Lake core OL84B was dated at 15.5 to 13.5 ka (Benson et al., 1997). Simulation indicated lake extent at 15 ka is the smallest in the last 18 ka. The combination of precipitation and temperature that produced this smallest lake extent is the lowest precipitation in the last 18 ka, and about 1.8°C cooler than modern temperature. The lake extent at 12 ka in Owens Valley is largest in the last 18 ka. Simulated combination of precipitation and temperature at 12 ka is 4.5 °C cooler than modern temperature, and 1.8 times of modern precipitation. This result is consistent with the pollen data from core OL84B (Figures 4.8a,b) (Mensing, 2001). The pollen data indicated that a mean annual precipitation of 308-370 mm and a >80% increase in effective moisture, and 4 to 5°C cooler than the present mean temperature in Owens Valley starting from 13.5 ka. A very wet climate in the western Great Basin at this time is

also supported by the $\delta^{18}\text{O}$ data from Owens Lake (Benson et al., 1996) and Mono Lake (Benson et al., 1998), and ages of tufa from Searles Lake (Lin et al., 1998) and Lake Lahontan (Benson, 1993) that indicate high lake stands from 14 to 13.5 ka. However, the climate in Sierra Nevada shifted from cool, wet conditions to possibly a more seasonal climate with cool, wet winters and warmer summers (Mensing, 2001; Smith and Anderson, 1992), but still wetter and cooler than today (Spaulding, 1985) after 12 ka. Simulated lake extent in Owens Valley at 9 ka indicates a significant decrease in lake extent from 12 ka.

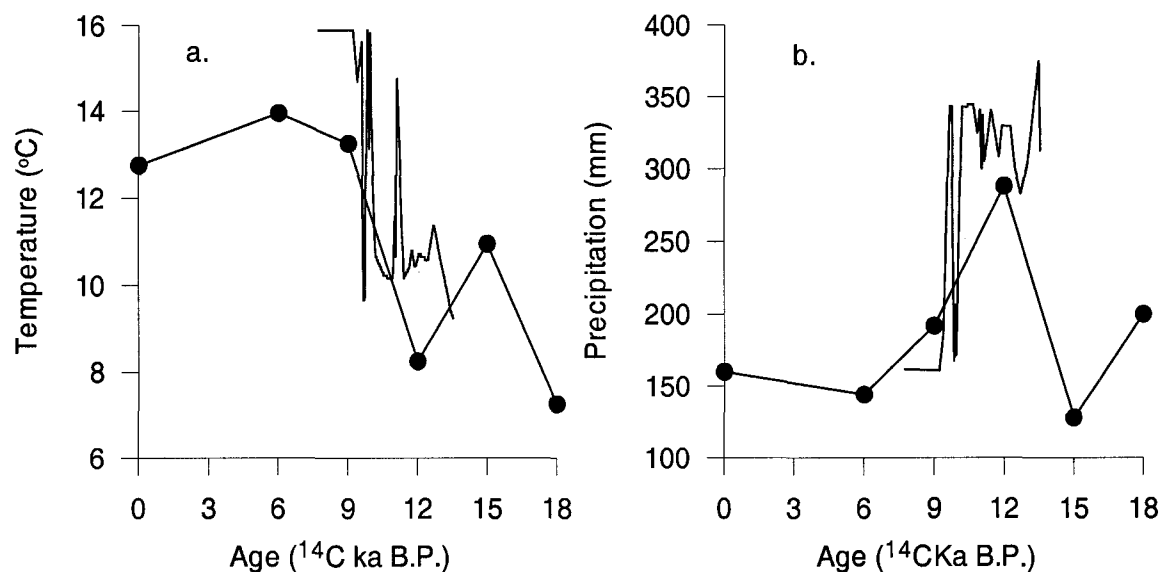


Figure 4.8. a. Simulated temperature (solid line with dots) and estimated temperature based on pollen (solid line) (Mensing, 2001) in Owens Lake; b. Simulated precipitation (solid line with dots) and estimated precipitation based on pollen (solid line) (Mensing, 2001) in Owens Lake.

The last deglaciation was interrupted by a worldwide cooling event, the Younger Dryas (YD) from 11 to 10 ka. Studies from western North America have identified late-glacial climatic oscillations roughly synchronous with the YD interval (Stuiver et al., 1995). The pollen data from core OL84B indicates a series of abrupt climatic oscillations between 10.8 to 9.5 ka, but it is not sufficient to clearly define the YD for a direct comparison with other sites (Mensing, 2001). Summer insolation reached the maximum between 9 to 8 ka, resulting in higher summer temperatures and probably increased seasonality (Grigg and Whitlock, 1998). Low lake levels (Benson et al., 1997) and the increased dominance of desert shrubs (Mensing, 2001) indicate the beginning of warm, dry Holocene conditions. The results from our simulations indicate 0.5°C warmer than modern temperature, and 1.2 times of modern precipitation could produce the observed lake extent at 9 ka, which is generally in agreement with high isolation and increased desert shrubs. A second hiatus found in core OL84B indicates that Owens Lake was probably dry at 6 ka (Benson et al., 1997), and quantitative analysis of the pollen record from Sierra Nevada suggests temperatures 1.4-2.1°C warmer than today (Adam and West, 1983). The lake level of Searles Lake was also low at 6 ka (Smith and Street-Perrott, 1983). Simulated lake extent with a combination of temperature 1.2°C warmer than modern temperature, and 0.9 times of modern precipitation is consistent with geologic evidence.

The climate in Owens Valley after 6 ka was probably similar to modern climate conditions. However, a slight increase in precipitation and decrease in temperature could happen, because the historic lake level of Owens Lake was higher than those at 6 ka. An increased frequency of modern extreme storm events in Mojave River watershed in late

Holocene was concluded based on lake deposits in the Silver Lake playa, CA (Enzel et al., 1989). The relatively high lake level of Searles Lake from 5 to 3 ka could be a result of an increased frequency of modern extreme storm events and summer monsoon circulation (Bush, 2001).

4.10. Conclusions and Future Work

The coupled catchment-lake model developed in this study is capable of accurately simulating lake extent as a function of modern climate and paleoclimate. This model can be used to quantitatively estimate paleoclimate, especially annual precipitation and temperature against field evidence in a catchment-lake watershed hydrologic system. The simulations on lake extent at 18 ka, 15 ka, 12 ka, 9 ka, 6 ka, and modern climate conditions are very compatible with observed or derived data. The annual precipitation and temperature in Owens Valley for these times are generally in agreement with the proxy data that are derived from Owens Valley and localities near Owens Valley. The accuracy of quantitative estimates in paleotemperature and paleoprecipitation in Owens Valley in this study is completely dependent on the accuracy of the field observations, especially the elevation of paleo-shorelines and their chronology for the lakes. Therefore, numeric values for the temperature and precipitation at 18 ka, 15 ka, 12 ka, 9 ka, and 6 ka are only effective for the geologic evidence used in this study. However, these numeric values of paleotemperature and paleoprecipitation can be adjusted based on new geologic evidence. The two advantages of the coupled catchment-lake model are: (1) Based on the proxy data, the possible range of temperature/precipitation combinations that could produce a particular paleolake extent can be obtained by narrowing a large number of

possible paleoclimatic combinations; (2) The model developed in this study is a physically based model that requires a minimum of site-specific parameters (Hostetler and Giorgi, 1993), thus it can be applied to any lake system if input parameters are available.

Simulations performed in this study did not consider that the seasonal distribution of precipitation and temperature in the last 18 ka that might be different from modern climatic conditions. The reason for this is that information on the seasonal distribution of precipitation and temperature in the past are seldom available. However, the lake levels of the Mediterranean region were significantly affected by the seasonal distribution of temperature (Prentic et al., 1992). Therefore, it is very important to consider the seasonal distribution of paleoclimate into the simulation on the paleolake extent in Owens Valley with the accumulation of more data on the seasonal distribution of paleoprecipitation and paleotemperature in future studies. When the simulations on lake extent were performed, an initially dry lake was assumed, which is not true for most situations, thus the model could be improved if the simulation on the lake extents in the last 18 ka is continuously run with starting a high lake level at 18 ka to a historic lake level. A time-series result of temperature and precipitation from the continuous simulation is more useful than the discrete results of temperature and precipitation in this study. However, in order to reach this goal, besides improving computation efficiency of the model, faster computers are needed.

Acknowledgements

This project was funded by the Department of Energy under Sponsored Project (DE-RP08-OONV13813). The authors wish to acknowledge S. W. Hostetler for providing me the source code of his lake model. Many thanks to K.M. Menking for her assistance on running the lake model.

References

- Adam, D.P., and West, G.J., 1983. Temperature and precipitation estimates through the last glacial cycle from Clear Lake, California, pollen data. *Science* 219, 168-170.
- Bartlein, P.J., Anderson, K.H., Anderson, P.M., Edwards, M.E., Mock, C.J., Thompson, R.S., Webb, R.S., Webb, T. III, and Whitlock, C., 1998. Paleoclimate simulations for North America over the past 21,000 years; features of the simulated climate and comparisons with paleoenvironmental data. *Quaternary Science Reviews* 17, 549-585.
- Benson, L., 1981. Paleoclimatic significance of lake-level fluctuations in the Lahontan Basin. *Quat. Res.* 16, 390-403.
- Benson, L., 1986. [Monograph] The sensitivity of evaporation rate to climate change; results of an energy-balance approach. *Water-Resources Investigations - U. S. Geological Survey, Report: WRI 86-4148*, 40p.
- Benson, L.V., and Thompson, R.S., 1987. The physical record of lakes in the Great Basin, in Ruddiman, W.F. and H.E. Wright, Jr., eds., *North America and adjacent*

- oceans during the last deglaciation, Boulder, Colorado, Geological Society of America, The geology of North America, K-3, 241-260.
- Benson, L.V., and Paillet, F.L., 1989, The use of total lake-surface area as an indicator of climatic change: examples from the Lahontan Basin. *Quat. Res.* 32, 262-275.
- Benson, L.V., Currey, D., Dorn, R., Lajoie, K. R., Oviatt, C.G., Robinson, S.W., Smith, G. I., and Stine, S., 1990. Chronology of expression and contraction of four Great Basin lake systems during the past 35,000 years. *Palaeogeography, Palaeoclimatology, Palaeoecology* 78, 241-286.
- Benson, L., 1993. Factors affecting ^{14}C ages of lacustrine carbonates: Timing and duration of the last highstand lake in the Lahontan Basin. *Quat. Res.* 39, 163-174.
- Benson, L.V., Burdett, J.W., Kashgarian, M., Lund, S.P., Phillips, F.M., and Rye, R.O., 1996. Climatic and hydrologic oscillations in the Owens Lake Basin and adjacent Sierra Nevada, California. *Science* 274,746-749.
- Benson, L., Burdett, J., Lund, S., Kashgarian, M., and Mensing, S., 1997. Nearly synchronous climate change in the Northern Hemisphere during the last glacial termination. *Nature* 388, 263-265.
- Benson, L.V., Lund, S.P., Burdett, J.W., Kashgarian, M., Rose, T.P., Smoot, J.P., and Schwartz, M., 1998. Correlation of late-Pleistocene lake-level oscillations in Mono Lake, California, with North Atlantic climate events. *Quat. Res.* 49, 1-10.
- Benson, L., 1999. Records of millennial-scale climate change from the Great Basin of the Western United States. *Geophysical Monograph* 112, 203-225.
- Benson, L.V., and Paillet, F.L., 2002. HIBAL: a hydrologic-isotopic-balance model for application to paleolake systems. *Quaternary Science Reviews* 21, 1521-1539.

- Betancourt, J.L., 1990. Late Quaternary biogeography of the Colorado Plateau, in
Betancourt, J.L., T.R. Van Devender, and P.S. Martin, eds., *Packrat Middens: the
Last 40,000 Years of Biotic Change*. The University of Arizona Press, Tucson, p.
259-292.
- Bischoff, J.L., Menking, K.M., Fitts, J.P., and Fitzpatrick, J.A., 1997. Climatic
oscillations 10,000-155,000 B.P. at Owens Lake, California reflected in glacial rock
flour abundance and lake salinity in Core OL-92. *Quat. Res. (New York)* 48, 313-
325.
- Bischoff, J.L., and Cummins, K., 2001. Wisconsin glaciation of the Sierra Nevada
(79,000-15,000 yr B.P.) as recorded by rock flour in sediments of Owens Lake,
California. *Quat. Res. (New York)* 55, 14-24.
- Bush, A.B.G., 2001. Pacific sea surface temperature forcing dominates orbital forcing of
the early Holocene monsoon. *Quat. Res.* 55, 25-32.
- COHMAP Members, 1988. Climatic changes of the last 18000 years: observations and
model simulations. *Science* 241, 1043-1052.
- Cole, K.L., 1983. Late Pleistocene vegetation of Kings Canyon, Sierra Nevada,
California. *Quat. Res.* 19, 117-129.
- Cole, K.L., 1990. Late Quaternary vegetation gradients through the Grand Canyon, in
Betancourt, J.L., T.R. Van Devender, and P.S. Martin, eds., *Packrat Middens: the
Last 40,000 Years of Biotic Change*. The University of Arizona Press, Tucson, p.
240-258.
- Dickinson, R.E., Errico, R.M., Giorgi, F., and Bates, G.T., 1989: A regional climate
model for western United States. *Clim. Change* 15, 383-422.

- Dohrenwend, J.C., 1984. Nivation landforms in the western Great Basin and their paleoclimatic significance. *Quat. Res.* 22, 275-288.
- Enzel, Y., Cayan, D.R., Anderson, R.Y., and Wells, S.G., 1989. Atmospheric circulation during Holocene lake stands in the Mojave Desert: evidence of regional climate change. *Nature* 341, 44-47.
- Forester, R.M., 2001. An ostracode record of Holocene climate change from Owens Lake, California. Open-File Report - U. S. Geological Survey, Report: OF 01-0202, pp.7-8.
- Grigg, L.D., and Whitlock, C., 1998. Late-glacial vegetation and climate change in Western Oregon. *Quat. Res.* 49, 287-298.
- Halley, E., 1715. On the cause of the saltness of the ocean, and of the several lakes that emit no rivers. *Philosophical Transactions of the Royal Society of London* 6, 169.
- Hostetler, S.W., and Bartlein, P.J., 1990. Simulation of lake evaporation with application to modeling lake level variations of Harney-Malheur Lake, Oregon. *Water Resour. Res.* 26, 2603-2612.
- Hostetler, S.W., and Benson, L.V., 1990. Paleoclimatic implications of the high stand of Lake Lahontan derived from models of evaporation and lake level. *Climate Dynamics* 4, 207-212.
- Hostetler, S.W., 1991. Modeling the late-Pleistocene paleohydrology of the Great Basin in Kelmelis, John A; Snow, K Mitchell eds. *Proceedings of the U.S. Geological Survey global change research forum, Herndon, Virginia.* U. S. Geological Survey Circular, Report: C 1086, pp.90.

- Hostetler, S.W., and Giorgi, F., 1993. Use of output from high-resolution atmospheric models in landscape-scale hydrologic models; an assessment. *Water Resour. Res.* 29, 1685-1695.
- Hostetler, S.W., Bates, G.T., and Giorgi, F., 1993. Interactive coupling of a lake thermal model with a regional climate model. *J. Geophys. Res., D, Atmospheres* 98, 5045-5057.
- Hostetler, S.W., Giorgi, F., Bates, G.T., and Bartlein, P.J., 1994. Lake-atmosphere feedbacks associated with paleolakes Bonneville and Lahontan. *Science* 263, 665-668.
- Jannik, N.O., Phillips, P.M., Smith, G.I., and Elmore, D., 1991. A ^{36}C 1 chronology of lacustrine sedimentation in the Pleistocene Owens River system. *Geological Society of America Bulletin* 103, 1146-1159.
- Kutzbach, J.E., 1980. Estimates of past climate at Paleolake Chad, North Africa, based on a hydrological and energy-balance model. *Quat. Res.* 14, 210-223.
- Kutzbach, J.E., and H.E. Wright, 1985. Simulation of the climate of 18,000 yr B.P.; results for the North American/North Atlantic/European sector. *Quaternary Science Reviews* 4, 147-187.
- Kutzbach, J.E., and Guetter, P.J., 1986. The influence of changing orbital parameters and surface boundary conditions on climate simulations for the past 18,000 years. *J. Atmos. Sci.* 43, 1726-1759.
- Kutzbach, J.E., 1987. Model simulations of the climatic patterns during the deglaciation of North America, in Ruddiman, W.F. and H.E. Wright, Jr., eds., *North America and*

- adjacent oceans during the last deglaciation, Boulder, Colorado, Geological Society of America, *The Geology of North America K-3*, 425-446.
- Lee, C.H., 1912. An intensive study of the water resources of a part of Owens Valley, California. U.S. Geological Survey Water-Supply Paper 294.
- Leffler, P.M., and Cochran, G.F., 1989. Utilizing the historical climate record to construct an analogue of past (wetter) climatic regimes in the southwest Great Basin. *Proceedings of the Topical Meeting on Nuclear Waste Isolation in the Unsaturated Zone, Focus 1989*, American Nuclear Society, Inc., La Grange Park, Illinois, 73-77.
- Li, H-C, Bischoff, J.L., Ku, T-L., Lund, S.P., and Stott, L.D., 2000. Climate variability in east-central California during the past 1000 years reflected by high-resolution geochemical and isotopic records from Owens Lake sediments. *Quat. Res. (New York)* 54, 189-197.
- Lin, J.C., Broecker, W.S., Hemming, S.R., Hajdas, I., Anderson, R.R., Smith, G.I., Kelley, M., and Bonani, G., 1998. A reassessment of U-Th and ^{14}C ages for late-glacial high-frequency hydrological events at Searles Lake, California. *Quat. Res.* 49, 11-23.
- Lowenstein, T.K., Li, J., Brown, C.B., Roberts, S.M., Ku, T.-L., Luo, S., and Yang, W., 1999. 200 k.y. paleoclimate record from Death Valley salt core: *Geology* 27, 3-6.
- MacIntyre, S., Flynn, K.M., Jellison, R., and Romero, J., 1999. Boundary mixing and nutrient fluxes in Mono Lake, California. *Limnol. Oceanogr.* 44, 512-529.
- Menking, K.M., Bischoff, J.L., Fitzpatrick, J.A., Burdette, J.W., and Rye, R.O., 1997. Climatic/Hydrologic oscillations since 155,000 yr B.P. at Owens Lake, California,

- reflected in abundance and stable isotope composition of sediment carbonate, *Quat. Res.* 48, 58-68.
- Mensing, S.A., 2001. Late-glacial and early Holocene vegetation and climate change near Owens Lake, eastern California. *Quat. Res.* 55, 57-65.
- Merrill, R.K., and Pewe, T.L., 1977. Late Cenozoic geology of the White Mountains, Arizona. State of Arizona Bureau of Geology and Mineral Technology Special Paper No. 1, Tempe, Arizona, 65 p.
- Mifflin, M.D., and Wheat, M.M., 1979. Pluvial lakes and estimated pluvial climates of Nevada. Nevada Bureau of Mines and Geology Bulletin 94, 57 p.
- Newton, M.S., 1991. Holocene stratigraphy and magnetostratigraphy of Owens and Mono Lakes, eastern California. Thesis, Univ. S. California.
- Orndorff, R.L., 1994. Development of a surface hydrologic model and its application to modern and last glacial conditions within the great basin. Dissertation, Kent State University.
- Phillips, F.M., Campbell, A.R., Smith, G.I., and Bischoff, J.L., 1994. Intersadial climatic cycles: A link between western North America and Greenland? *Geology* 22, 1115-1118.
- Plummer, M. A., and Phillips, F.M., 2003. A 2-D numerical model of snow/ice energy balance and ice flow for paleoclimatic interpretation of glacial geomorphic features. *Quaternary Science Reviews* 22, 1389-1406.
- Prentice, I.C., Guiot, J., and Harrison, S.P., 1992. Mediterranean vegetation, lake levels and palaeoclimate at the Last Glacial Maximum. *Nature* 360, 658-660.

- Quade, J., Mifflin, M.D., Pratt, W.L., McCoy, W., and Burckle, L., 1995. Fossil spring deposits in the southern Great Basin and their implications for changes in water-table levels near Yucca Mountain, Nevada during Quaternary time. *Geological Society of America Bulletin* 107, 213-230.
- Shackleton, N.J., 1967. Oxygen isotope analyses and Pleistocene temperatures re-addressed. *Nature* 215, 15-17.
- Smith, G.I., and Bischoff, J.L., 1997. Core OL-92 from Owens Lake: Project rationale, geologic setting, drilling procedures, and summary. In "An 800,000-year paleoclimatic record from core OL-92, Owens Lake, Southern California" edited by Smith, G.I. and Bischoff, J.L. Special Paper 317, the Geological Society of America, Boulder, pp. 165.
- Smith, G.I., and F.A. Street-Perrott, 1983, Pluvial lakes of the western United States, in S.C. Porter, ed., *The Late Pleistocene*. University of Minnesota Press, Minneapolis, Minnesota, p. 53-70.
- Smith, G.I., 1984. Paleohydrologic regimes in the southwestern Great Basin, 0-3.2 my ago, compared with other long records of "global" climate. *Quat. Res.* 22, 1-17.
- Smith, G.I., 1991. Continental paleoclimatic records and their significance, in Chapter 2, *Quaternary paleoclimates* (Smiley, T.L., et al.), in Morrison R.B. ed., *Quaternary nonglacial geology: Conterminous U.S.*, Boulder, Colorado, The Geological Society of America, *The Geology of North America K-2*: 35-41.
- Smith, S.J., and Anderson, R.S., 1992. Late Wisconsin paleoecologic records from Swamp Lake, Yosemite National Park, California. *Quat. Res.* 38, 91-102.

- Spaulding, W.G., 1985. Vegetation and climates of the last 45,000 years in the vicinity of the Nevada Test Site, south-central Nevada. U.S. Geological Survey Professional Paper 1329, 83 p.
- Spaulding, W.G., and Graumlich, L.J., 1986. The last pluvial climate episodes in the deserts of southwestern North America. *Nature* 320, 441-444.
- Stamm, J.F., 1991. Modeling local paleoclimates and validation in the southwest United States, Ph.D. dissertation, Kent State University, Kent, Ohio, 211 p.
- Street-Perrott, F.A., and Harrison, S.P., 1985. Lake levels and climate reconstruction, in A.D. Hecht, ed., *Paleoclimate Analysis and Modeling*. John Wiley and Sons, New York, p. 291-340.
- Street-Perrott, F.A., 1991. General circulation (GCM) modelling of palaeoclimates: a critique. *The Holocene* 1, 74-80.
- Stuiver, M., Grootes, P.M., and Brasiunas, T.E., 1995. The GISP2 $\delta^{18}\text{O}$ climate record of the past 16,500 years and the role of the sun, ocean, and volcanoes. *Quat. Res.* 44, 341-354.
- Thompson, R.S., Benson, L.V., and Hattori, E.M., 1986. A revised chronology for the last Pleistocene lake cycle in the central Lahontan Basin. *Quat. Res.* 25, 1-9.
- Thompson, R.S., Whitlock, C., Bartlein, P.J., Harrison, S.P., and Spaulding, W.G., 1994. Climatic changes in the western United States since 18,000 yr B.P., in Wright et al, eds., *Global Climates since the Last Glacial Maximum*. University of Minnesota Press, 468-513.

- Thompson, R.S., Anderson, K.H., and Patrick J. Bartlein, P.J., 1999. Quantitative paleoclimatic reconstructions from late Pleistocene plant macrofossils of the yucca mountain region. U.S. Geological Survey Open-File Report 99-338.
- Vassiljev, J., 1997. simulating the palaeorecord of northern European lakes using a coupled lake-catchment model. Dissertation, Lund University.
- Winograd, I.J., 1981. Radioactive waste disposal in thick unsaturated zones. *Science* 212, 1457-1463.

CHAPTER 5

SIMULATION OF CHLORIDE TRANSPORT

5.1. Introduction

Thick vadose zones in arid regions have been considered suitable for waste disposal sites (Winograd, 1981; Scanlon, 1991) because low effective precipitation rates result in low rates of water movement. Flow and transport in arid regions have been extensively studied in the last four decades for that purpose (e.g., Winograd, 1981; Tyler et al., 1992; Gee et al., 1994; Tyler et al., 1996; Andraski, 1997). The time scales over which the unsaturated zone responds to the surface boundary conditions are much longer in arid regions than in humid regions (Allison and Hughes, 1983; Phillips, 1994; Scanlon et al., 1997), which allows thick vadose zones to serve as long-term records of flow and transport. Because of very low water fluxes, on the order of a few millimeters or less annually, the ability to determine water fluxes using physical techniques (e.g., lysimeters, time domain reflectometry (TDR), remote sensing, tensiometers, thermocouple psychrometers, and electromagnetic induction (EMI)) in arid areas is limited. However, methods using tracers (e.g., Cl^- , ^3H , and ^{36}Cl) have advantages in quantifying the correlation between long-term net water flux variation and climate in arid regions (Allison et al., 1994). Among available tracer techniques, chloride mass balance (CMB) is the simplest, least expensive, and most universal for recharge estimation. Low water fluxes and water content in arid vadose zones significantly reduce the effects of diffusion

thus resulting in excellent preservation of tracers in the infiltrating water (Phillips, 1994; Allison et al., 1994). Edmunds and Walton (1980) first recognized that paleoclimate could be reconstructed from vadose zone chemistry. Cook et al. (1992) reported that the unsaturated chloride profiles from Cyprus and northern Senegal record the past 400 yr climate changes. The variations in chloride are well correlated with changes in recorded rainfall and lake levels. Recent studies have shown that thick unsaturated zones can be used to infer climatic changes over longer glacial time scales of 10 to 100 ka (Tyler et al., 1996; Ginn and Murphy, 1997). However, due to dispersion and diffusion, the paleoclimatic input signals are often smoothed out, which ultimately limits the usefulness of data for a paleoclimatic reconstruction. Chloride bulges (peaks) and reduction below the bulges in deep profiles have been attributed to the non-piston-type flow (Nativ et al., 1995; Sharma and Hughes, 1985), to the diffusion of chloride to groundwater (Cook et al., 1989), and to changes in recharge due to paleoclimatic variations (Stone, 1992).

Chloride transport in the vadose zones of arid regions not only represents a spatially uniform input to the soil water-groundwater systems, but also offers a natural experiment on the solute transport that is very important for engineering designs of a potential repository. Therefore, the extraction of the natural chloride transport in the vadose zone is important on both continental paleoclimatic study and natural solute transport.

The CMB is based on the following assumptions (Scanlon, 1991): downward piston-type flow, atmospheric fallout as the only source of chloride, mean annual precipitation and chloride concentration of precipitation constant through time, and steady-state chloride flux equal to the chloride accession rate in rainfall. However, the temporal changes in the fallout of chloride during pre-historic records are little known, and the

assumption of piston-type flow has been questioned at many sites. Furthermore, previous studies have shown that the climate changed many times since the LGM. The steady flow assumption is violated when precipitation or chloride mass deposition varies over time, and a nonuniform profile is formed. Previous studies concluded that climate changes in the late Quaternary might be responsible for the nonuniform chloride “bulge” (Scanlon, 1991; Phillips, 1994). Therefore, in order to model chloride transport in vadose zones since the LGM, all assumptions above have to be clarified.

In this study, a modified version of the HYDRUS-1D computer code was used (Simunek et al., 1998; Scanlon et al., 2003) to forward model the vertical chloride transport in the vadose zone of ADRS (Amargosa Desert Research Site, United States Geological Survey), southern Nevada since the LGM. This modified HYDRUS-1D has been demonstrated capable of simulating water movement and solute transport in desert vadose zones (Scanlon et al., 2003) because it coupled liquid water, water vapor, and energy and solute transport. By using variable boundary conditions including time-varying precipitation, temperature, and chloride deposition, in this modified HYDRUS-1D, the unclear assumptions in the CMB can be avoided. The variable boundary conditions were obtained based on the paleoprecipitation and paleotemperature from a coupled catchment-lake model (Chapter 4), and chloride deposition rate in Greenland ice core (Mayewski et al., 1994). Finally, the chloride transport through the unsaturated zone of ADRS was simulated. By comparing the simulated results to the actual measured chloride profile, the independent estimate of paleoprecipitation and/or chloride deposition rates were evaluated. In this way, chloride profile variations in the unsaturated zone were quantitatively evaluated against the variations of paleoprecipitation.

5.2. Site Description

The USGS initialized studies of unsaturated zone hydrology at a site in the Amargosa Desert near Beatty, Nevada, in 1976. The site is located about 20 km east of Death Valley Nation Park (Figure 5.1) (Andraski and Stonestrom, 1999). Basic data on soil hydraulic properties, climate, and soil-water movement for both undisturbed and disturbed conditions have been accumulated and are available for public use. Average annual precipitation and annual pan evaporation at the ADRS is about 108 millimeters (mm) and 1900 mm respectively (Johnson et al., 2002). Mean annual temperature is 18.4°C (Stonestrom et al., 2003). Seventy percent of the precipitation at ADRS occurs between October and April through frontal systems. Remaining summer rainfall is predominantly through localized and short-duration convective storms (Wood and Andraski, 1995). The site is covered with sparse vegetation predominantly *Larrea tridentata* (creosote bush). The Amargosa Desert is in the Basin and Range physiographic province. More than 170 meters (m) thick sediments at the ADRS are mainly fluvial and alluvial deposits (Nichols, 1987). The water table in the area ranges from about 85 to 115 m below land surface (Fischer, 1992). Particle size analyses indicated the surface soil (0.75 to 1 m thick) is made of 79.8% sand, 14.1% silt, and 6.1% clay, as determined by sieve and hydrometer method (Andraski, 1996).

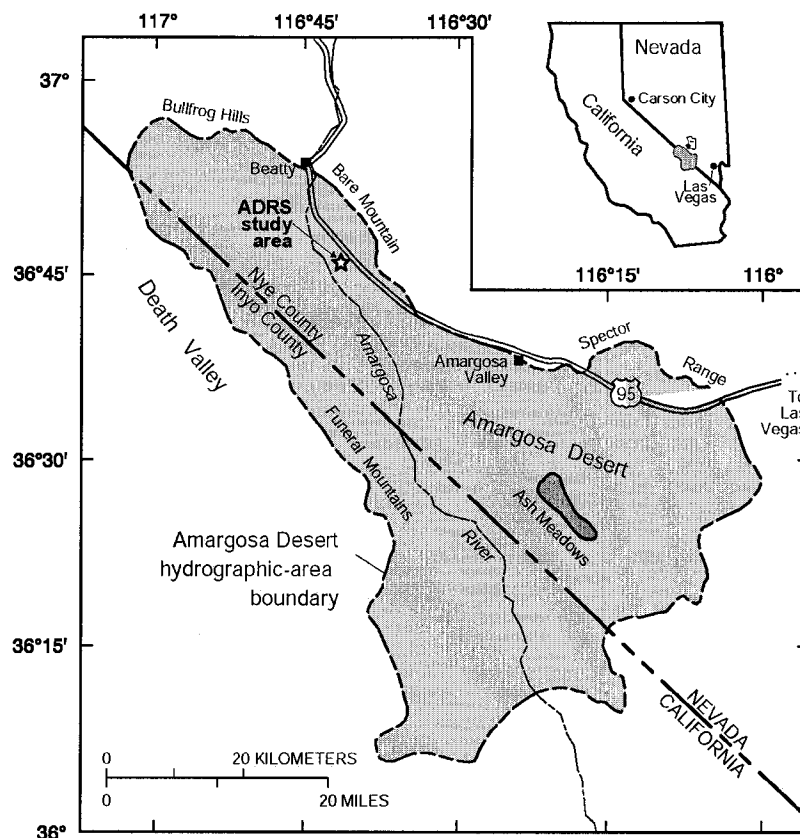


Figure 5.1. Location map of the ADRS (modified from Johnson et al., 2002).

Actual measured chloride profile and soil water content (Prudic, 1994) are plotted against depth in Figure 5.2. Chloride is less than 50 mg/L in surface soils (less than 0.5 m), and quickly reaches its peak of 9000 mg/L between 0.5 to 2.3 m. Chloride then decreases to less than 50 mg/L below a depth of 10 m. Groundwater chloride at the site is about 79 mg/L that is higher than chloride concentration of soils close to water table (Prudic, 1994). Soil water content is lower in soils less than 2.5 m, and reaches a constant value of water content below 2.5 m (Figure 5.2).

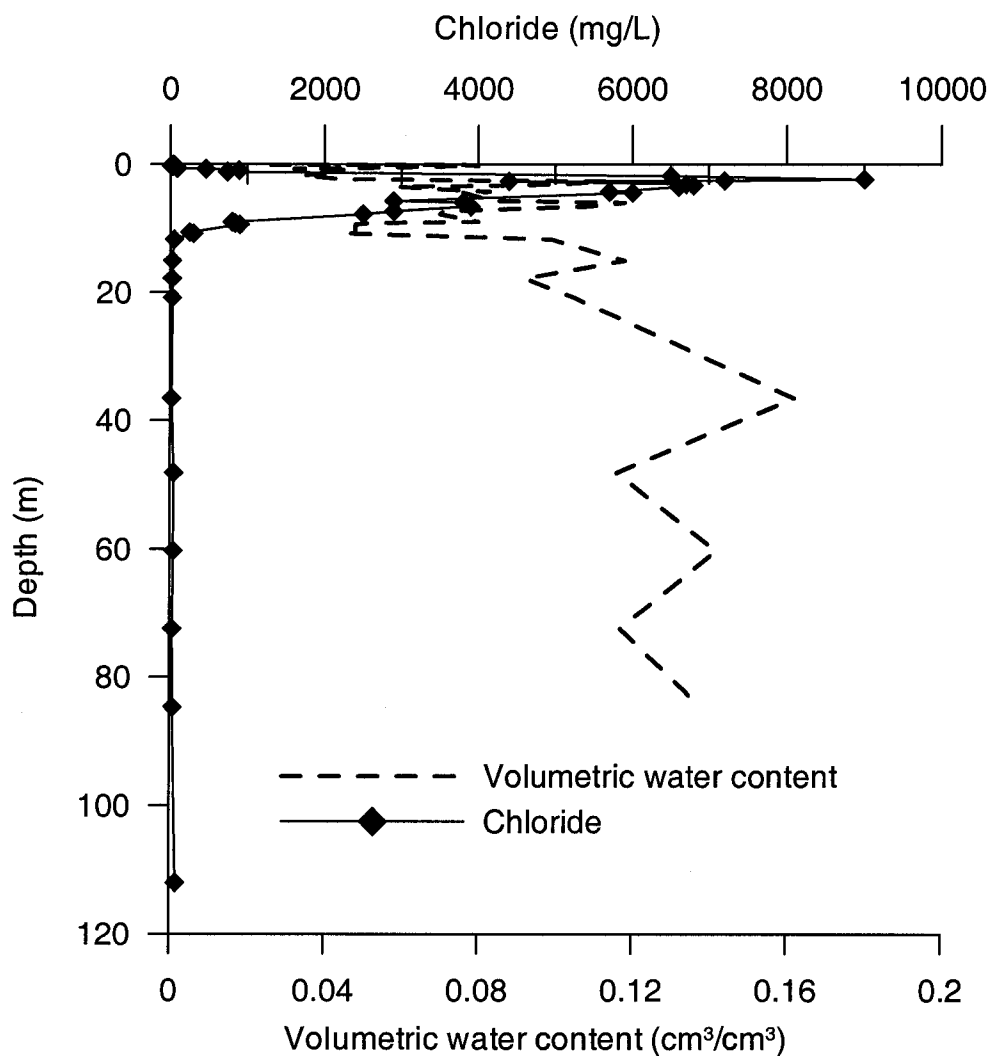


Figure 5.2. Measured chloride and soil water content profiles (Prudic, 1994).

5.3. Numerical Modeling

A modified version of the HYDRUS-1D computer code (Simunek et al., 1998, Scanlon et al., 2003) with variable boundary conditions was used in this study to forward model the chloride transport in vadose zones of ADRS since the LGM. Because basic equations for water flow and solute transport are provided in the manual of HYDRUS-1D (Simunek et al., 1998), details on equations for vapor flow are only given here (Scanlon et al., 2003). Vapor flux (q_v) can be described by Fick's law of diffusion:

$$q_v = q_{vh} + q_{vT} = -K_{vh} \frac{\partial h}{\partial z} - K_{vT} \frac{\partial T}{\partial z} = -\frac{D}{\rho_w} \rho_{vs} \frac{Mg}{RT} H_r \frac{\partial h}{\partial z} - \frac{D}{\rho_w} \eta H_r \frac{\partial \rho_{vs}}{\partial T} \frac{\partial T}{\partial z} \quad (5.1)$$

where q_{vh} , and q_{vT} , are isothermal vapor flux, and thermal vapor flux, respectively. K_{vh} and K_{vT} are isothermal vapor conductivity, thermal vapor conductivity, respectively. D is vapor diffusivity in soil, ρ_w is density of liquid water, ρ_{vs} is saturated vapor density, M is molecular weight of water (kg /mol), g is gravitational acceleration, R is gas constant, H_r is relative humidity, h is matric potential head, η is enhancement factor, and T is temperature (K). The vapor diffusivity in soil is described by

$$D = \tau \theta_a D_a = \frac{\theta_a^{7/3}}{\theta_s^2} \theta_a D_a; D_a = 2.12 \times 10^{-5} \left(\frac{T}{273.15} \right)^2 \quad (5.2)$$

where T is tortuosity given by Millington and Quirk (1961), θ_a is volumetric air content, D_a is diffusivity of water vapor in air, and θ_s is saturated water content. Enhancements for thermal vapor flux as a result of liquid islands and increased temperature gradients in the air phase relative to the average temperature gradient (Philip and de Vries, 1957) were included in this modified HYDRUS-1D (Scanlon et al., 2003). The following equation (Cass et al., 1984) was used to derive the enhancement factor (Campbell, 1985):

$$\eta = 9.5 + 3 \frac{\theta}{\theta_s} - 8.5 \exp(-) - \left(\left(1 + \frac{2.6}{\sqrt{f_e}} \right) \frac{\theta}{\theta_s} \right)^4 \quad (5.3)$$

where f_e is the mass fraction of clay in soil.

Modeling strategies used in this study were starting with downward water fluxes that were estimated from chloride concentrations beneath the bulge at the LGM (18 ka) (Scanlon et al., 2003). Variable upper boundary conditions that water and solute fluxes were set equal to precipitation and chloride deposition rate. The potential evaporation was calculated based on the Penman equation (Penman, 1948). The root zone was set as

2.3 m that is the depth of the chloride peak. The simulation was performed for the entire 110 m unsaturated zone. The lower boundary condition for the water flux is assigned zero pressure equal to the water table (Scanlon et al., 2003). The geothermal gradient was incorporated by specifying the temperature at the surface and in the groundwater. The surface temperature is set equal to air temperature. The grid cell size generally varies from 0.1 m at the surface to a maximum of 2 m within the profile and decreased to a minimum value of 0.05 m at the water table. Adaptive time stepping is used in HYDRUS-1D, and a minimum initial time step is generally set at 0.01 day. There was no limit on the maximum time step size.

5.4. Input Parameters

Input parameters (Table 5.1) for soil hydraulic properties at ADRS were prepared from the data provided by Prudic (1994), Andraski (1996), and Scanlon et al. (2003). Soil profile was set up as one layer (110 m) of homogenous sediment. Soil texture is set to loamy sand that represents the particle size less than 2 mm fraction after removing 22% gravel (Andraski, 1996).

The parameters related to chloride profile at ADRS were listed in Table 5.2. Atmospheric boundary file (atmosphere.in in HYDRUS-1D) for the last 18 ka was prepared based on paleoprecipitation and paleotemperature from our simulation on lake extent in Owens Valley. The potential evaporation was calculated based on paleotemperature with the Penman equation (Penman, 1948). The chloride concentration in precipitation at ADRS for the last 18 ka was obtained by adjusting the chloride concentration in the Greenland Ice Core (GISP2) (Mayewski et al., 1994) with

comparison of modern chloride precipitation at ADRS and Greenland. Four parameters including precipitation, temperature, potential evaporation, and chloride concentration of precipitation were plotted along with time in Figure 5.3.

Table 5.1. Hydraulic properties of representative soil at ADRS.

Texture	Percentage of			K_s (m/day)	θ_s (m^3/m^3)	θ_r (m^3/m^3)	α (1/m)	n
	Sand	Silt	Clay					
Loamy sand	80	14	6	0.43	0.29	0.026	2.6	1.42

Source: Andraski, 1996; Scanlon et al., 2003.

Table 5.2. The parameters related chloride profile used in this study.

Parameters	ADRS	Source
Precipitation (m/yr) (30-yr average)	0.108	Johnson et al., 2002
Temperature ($^{\circ}C$)	18.4	Stonestrom et al., 2003
Water table depth (m)	110	Prudic, 1994
Profile depth for water potential (m)	47.5	Prudic, 1994
Profile depth for chloride profile (m)	85	Prudic, 1994
Modern chloride precipitation (mg/L)	0.82	Prudic, 1994
Cl peak (mg/L)	9,000	Prudic, 1994
Cl peak depth (m)	2.3	Prudic, 1994
Cl base (mg/L)	20	Prudic, 1994
CMB age at the base of the chloride bulge (ka)	16	Prudic, 1994
CMB age at the base of the chloride profile (ka)	18	Prudic, 1994
Matric potential (root sink) (m)	-500	Scanlon et al., 2003
Root sink depth (m)	2.3	Scanlon et al., 2003
Geothermal gradient ($^{\circ}C/km$)	40	Scanlon et al., 2003

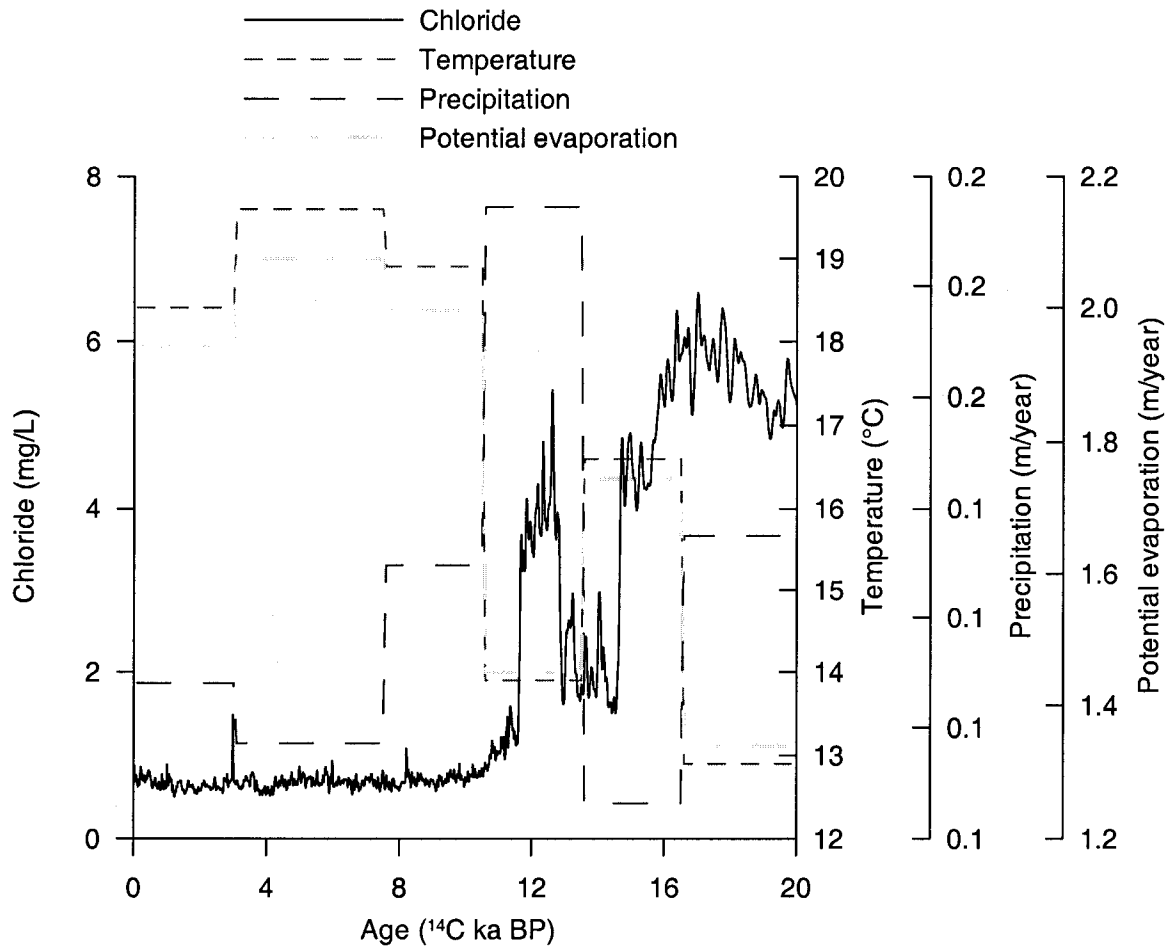


Figure 5.3. The data used to prepare atmospheric boundary input file for HYDRUS-1D.

5.5. Results

Simulated and measured chloride concentrations were plotted with depth in Figure 5.4. Simulated and measured chloride shows good agreement. Simulated chloride concentrations below the peak at 10 to 20 m depth overestimate the measured values. Measured water potential and vapor density increase downward between the depths of 12 and 48 m, indicating that water movement both as liquid and vapor is upward (Prudic and Striegl, 1994). The simulation overestimating measured chloride profile from 10 to 20 m may be due to this upward water movement that was not well implemented in the model.

The estimated chloride age using CMB is 16 ka, based on assumptions of precipitation of 10 to 15 cm/year and chloride concentration in precipitation of 0.82 to 1.1 mg/L (Prudic, 1994). This estimated age is close to the age of the first desiccated event (15 ka) in Owens Lake after the LGM (Benson et al., 1997). Previous studies concluded that a reversal in the direction of water movement from downward to upward was attributed to changes from mesic vegetation during Pleistocene pluvial periods to xeric vegetation during Holocene arid conditions (Walvoord et al, 2002; van Devender, 1990). The chloride profile at ADRS did not show the latest pluvial event at 12 ka, because climate had more oscillation at this time, and high and low precipitation could offset each other, and resulted no indications in measured chloride profile. Low chloride concentrations beneath the chloride bulge at depths of 10 to 25 m represent higher water fluxes during the last pluvial event. Simulated final water flux at ADRS is ~0.016 mm/year upward at the base of the profile. This result is in the opposite direction and much lower than the downward CMB flux of 8.4 mm/yr (Prudic, 1994).

5.6. Uncertainty Analyses

Uncertainty analysis performed by Walvoord et al. (2002), Scanlon et al. (2003), and Scanlon (2000) addressed the effects of varying water table depths, saturated hydraulic conductivities, geothermal gradients, vapor diffusion enhancement, osmotic component of water potentials, and numerical modeling. Uncertainties of numerical modeling come from those related to conceptual models, hydraulic parameterization, and solute diffusion coefficients.

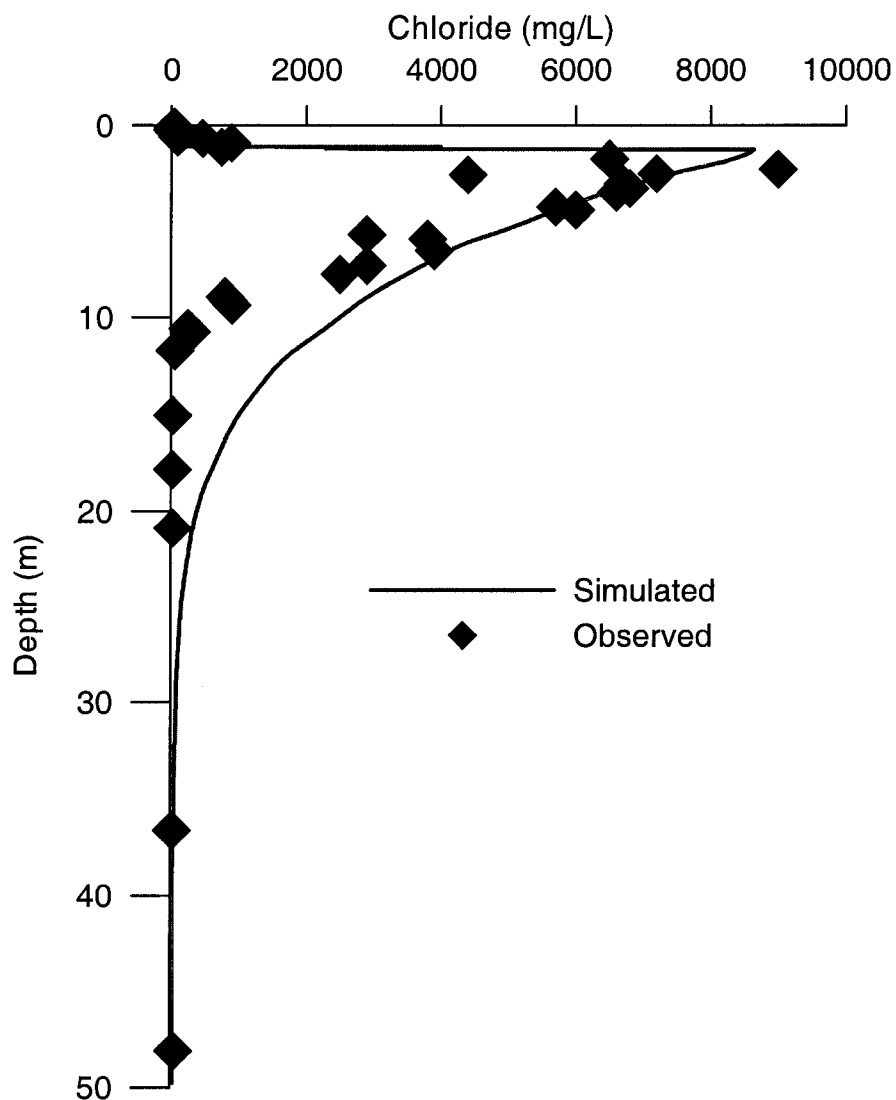


Figure 5.4. Simulated chloride and measured chloride profiles are plotted along with depth.

CMB age is significantly influenced by the chloride input. The CMB age previously estimated at the base of the ADRS site's chloride bulge is 28 ka (Phillips, 1994; Scanlon et al., 2003) with chloride input of $100 \text{ mg/m}^2/\text{yr}$, and 16 ka with a chloride input of $173 \text{ mg/m}^2/\text{yr}$ (Prudic, 1994; Scanlon et al., 2003). The chloride input of $173 \text{ mg/m}^2/\text{yr}$ is similar to the upper range of values suggested by Prudic (1994). Higher estimates on the

chloride input result a higher estimate of water flux during the Pleistocene. In this study, the chloride input was prepared based on quantitative paleoclimate information (Chapter 4) and chloride records in GISP2 (Mayewski et al., 1994). The average chloride input in the last 18 ka used in this study is $316 \text{ mg/ m}^2/\text{yr}$. However, the average chloride input is $646 \text{ mg/ m}^2/\text{yr}$ from 18 ka to 12 ka, and $228 \text{ mg/ m}^2/\text{yr}$ from 12 ka to present. The CMB age by using $228 \text{ mg/ m}^2/\text{yr}$ is 12 ka that is consistent with the last pluvial event in the ADRS area (Quade et al., 2003; Anderson and Wells, 2003). Therefore, variable chloride input used in this study is better than a single value of the chloride input used for thousands of years. Uncertainty of the chloride input used in this study could be from different magnitudes of climate change between the Greenland and the ADRS.

Scanlon et al. (2003) concluded that osmotically driven vapor fluxes are negligible at the ADRS. Since osmotic potentials also affect the simulated time required to reproduce the measured water potentials, ignoring osmotic potentials may result in overestimation of this time (Scanlon et al., 2003).

Assuming a fixed root depth of 2.3 m for the last 18 ka in this study may not be appropriate because water potential and chloride profiles in some settings indicate that roots may extend to greater depths (Scanlon et al., 2003). One layer of homogenous sediment profile was used in this study. By using three layers of soil profiles configuration, Scanlon et al. (2003) found that varying the porosity by ~25% resulted in the same amount of change in the simulated Cl concentrations. Simulated chloride profiles are also sensitive to residual water content, and the van Genuchten n parameter (Scanlon et al., 2003). Uncertainties related to chloride diffusion result primarily from

uncertainties in the calculation of effective diffusivities (D_e). Higher D_e values result in more diffuse chloride profiles with lower peaks (Scanlon et al., 2003).

5.7. Conclusions and Further Work

The measured chloride profile at ADRS was successfully simulated with the modified version of the HYDRUS-1D computer code (Simunek et al., 1998, Scanlon et al., 2003) by using variable boundary conditions. The paleoprecipitation and paleotemperature estimated from the simulations on lake extents in Owens Valley in the last 18 ka with a coupled catchment-lake model were tested and first evaluated. Simulated water flux at ADRS is ~ 0.016 mm/year upward at the base of the profile, which is consistent with the previous study (Scanlon et al., 2003). Because variable boundary conditions including time-varying precipitation, temperature, and chloride deposition were used to drive the modified HYDRUS-1D, the unclear assumptions in the CMB were avoided, and the resulted simulation on measured chloride profile was improved. However, many uncertainties such as varying water table depths, saturated hydraulic conductivities, geothermal gradients, vapor diffusion, hydraulic parameterization, and solute diffusion coefficients, may exist in our simulations. Therefore, it is very critical to perform the uncertain analysis in future studies.

Acknowledgement

This project was funded by the Department of Energy under Sponsored Project (DE-RP08-OONV13813), Geological Society of America Student Grant # 6870-01, 2002, and UNLV Graduate Student Association Grant, 2002. The authors wish to

acknowledge USGS ADRS Research Team, especially Brian Andraski for letting me work at the ADRS and to use their data. I gratefully acknowledge Bridget R. Scanlon for providing me the modified version of the HYDRUS-1D computer code.

References

- Allison, G.B., and Hughes, M.W., 1983. The use of natural tracers as indicators of soil-water movement in a temperate semi-arid region, *J. Hydrol.* 60, 157-173.
- Allison, G.B., Gee, G.W., and Tyler, S.W., 1994. Vadose-zone techniques for estimating groundwater recharge in and semiarid regions, *Soil Sci. Soc. Am. J.* 58, 6-14.
- Anderson, D.E., and Wells, S.G., 2003. Latest Pleistocene lake highstands in Death Valley, California, in Enzel, Y., Wells, S.G., and Lancaster, N., eds., *Paleoenvironments and paleohydrology of the Mojave and southern Great Basin Deserts: Boulder, Colorado, Geological Society of America Special Paper 368*, 115-128.
- Andraski, B.J., 1996. Properties and variability of soil and trench fill at an arid waste-burial site: *Soil. Sci. Soc. Am. J.* 60, 54-66.
- Andraski, B.J., 1997. Soil-water movement under natural-site and waste-site conditions-- A multiple-year field study in the Mojave Desert, Nevada. *Water Resour. Res.* 33, 1901-1916.
- Andraski, B.J., and Stonestrom, D.A., 1999. Overview of research on water, gas, and radionuclide transport at the Amargosa Desert Research site, Nevada, in Morganwalp, D.W., and Buxton, H.T., eds., *U.S. Geological Survey Toxic*

- Substances Hydrology Program--Proceedings of the Technical Meeting, Charleston, South Carolina, March 8-12, 1999--Volume 3 of 3--Subsurface Contamination from Point Sources: U.S. Geological Survey Water-Resources Investigations Report 99-4018-C, 459-466.
- Andraski, B.J., Prudic, D.E., and Nichols, W.D., 1995. Waste burial in arid environments--Application of information from a field laboratory in the Mojave Desert, southern Nevada: U.S. Geological Survey Fact Sheet FS-179-95, 4 p.
- Benson, L., Burdett, J., Lund S., Kashgarian, M., and Mensing, S., 1997. Nearly synchronous climate change in the Northern Hemisphere during the last glacial termination. *Nature* 388, 263-265.
- Campbell, G.S., 1985. *Soil Physics With BASIC: Transport Models for Soil-Plant Systems*, Elsevier Sci., New York.
- Cass, A., Campbell, G. S., and Jones, T. L., 1984. Enhancement of thermal water vapor diffusion in soil. *Soil Sci. Soc. Am. J.* 48, 25-32.
- Cook, P.G., Edmunds, W.M., and Gaye, C.B., 1992. Estimating paleorecharge and paleoclimate from unsaturated zone profiles. *Water Resour. Res.* 28, 2721-2731.
- Cook, P.G., Hughes, M.W., Walker, G.R., and Allison, G.B., 1989. The calibration of frequency-domain electromagnetic induction meters and their possible use in recharge studies. *J. Hydrol.* 107, 251-265.
- Dong, W., Yu, Z., and Weber, D., 2003. Simulations on water variation in arid regions. *J. Hydrol.* 275, 165-181.

- Edmunds, W. M., and Walton, N.G.R., 1980. A geochemical and isotopic approach to recharge evaluation in semi-arid zones, past and present. *Arid Zone Hydrology, Investigations with Isotopes Techniques*, pp.47-68. IAEA, Vienna.
- Fischer, J.M., 1992. Sediment properties and water movement through shallow unsaturated alluvium at an arid site for disposal of low-level radioactive waste near Beatty, Nye County, Nevada. U.S. Geological Survey Water-Resources Investigations Report 92-4032, 48 p.
- Fouty, S.C., 1989. Chloride mass balance as a method for determining long-term groundwater recharge rates and geomorphic surface stability in arid and semi-arid regions Whisky Flat and Beatty, Nevada. M.S. Thesis. Univ. of Arizona, Tucson.
- Gee, G.W., Wierenga, P.J., Andraski, B.J., Young, M.H., Fayer, M.J., and Rockhold, M.L., 1994. Variations in water balance and recharge potential at three western desert sites. *Soil. Sci. Soc. Am. J.* 58, 63-72.
- Ginn, T.R., and Murphy, E.M., 1997. A transient flux model for convective infiltration: Forward and inverse solutions for chloride mass balance studies. *Water Resour. Res.* 33, 2065-2097.
- Hargreaves, G.H., and Samani, Z.A., 1982. Estimation of evapotranspiration by present plant cover for the Western Great Basin, *Transactions of the American Geophysical Union* 68, no. 44, pp. 1299.
- Johnson, M.J., Mayers, C.J., and Andraski, B.J., 2002. Selected micrometeorological and soil-moisture data at Amargosa Desert Research Site in Nye County near Beatty, Nevada, 1998-2000: U.S. Geological Survey Open-File Report 02-348.

- Mayewski, P.A., Meeker, L.D., Whitlow, S., Twickler, M.S., Morrison, M.C., Bloomfield, P., Bond, G.C., Alley, R.B., Gow, A.J., Grootes, P.M., Meese, D.A., Ram, M., Taylor, K.C., and Wumkes, W., 1994. Changes in atmospheric circulation and ocean ice cover over the North Atlantic during the last 41,000 years. *Science* 263, 1747-1751.
- Millington, R. J., and J. P., 1961. Quirk, Permeability of porous solids, *Trans. Faraday Soc.* 57, 1200-1207.
- Nativ, R., Adar, E., Dahan, O., and Geyh, M., 1995. Water recharge and solute transport through the vadose zone of fractured chalk under desert conditions. *Water Resour. Res.* 31, 253-261.
- Nichols, W.D., 1987. Geohydrology of the unsaturated zone at the burial site for low-level radioactive waste near Beatty, Nye County, Nevada: U.S. Geological Survey Water-Supply Paper 2312, 57 p.
- Nichols, W.D., 1990. The significance of climate in southern Nevada for the shallow burial of low-level radioactive wastes: LaGrange, Ill., American Nuclear Society, Topical on Nuclear Waste Isolation in the Unsaturated Zone, Proceedings, Las Vegas, Nev., September 1989, 93-98.
- Penman, H.L. 1948: Natural evaporation from open water, bare soil and grass. *Proc. Roy. Soc. A*, 193, 120-45.
- Philip, J.R., and de Vries, D.A., 1957. Moisture movement in porous materials under temperature gradients, *Eos Trans. AGU* 38, 222-232.
- Phillips, F.M., 1994. Environmental tracers for water movement in desert soils: A regional assessment for the American South-west. *Soil. Sci. Soc. Am. J.* 58, 15-24.

- Prudic, D.E., 1994. Estimates of percolation rates and ages of water in unsaturated sediments at two Mojave Desert sites, California-Nevada: U.S. Geological Survey Water-Resources Investigations Report 94-4160, 19 p.
- Prudic, D.E., and Striegl, R.G., 1994. Water and carbon dioxide movement through unsaturated alluvium near an arid disposal site for low-level radioactive waste, Beatty, Nevada [abs.]: Eos, American Geophysical Union Transactions, 75, p. 161.
- Quade, J., Forester, R.M., and Whelan, J.F., 2003. Late Quaternary paleohydrologic and paleotemperature change in southern Nevada, in Enzel, Y., Wells, S.G., and Lancaster, N., eds., *Paleoenvironments and paleohydrology of the Mojave and southern Great Basin Deserts*: Boulder, Colorado, Geological Society of America Special Paper 368, 165-188.
- Scanlon, B.R., 1991. Evaluation of moisture flux from chloride data in desert soils. *J. Hydrol.* 128, 137-156.
- Scanlon, B.R., and Goldsmith, R.S., 1997. Field study of spatial variability in unsaturated flow beneath and adjacent to playas. *Water Resour. Res.* 33, 2239-2252.
- Scanlon, B. R., 2000. Uncertainties in estimating water fluxes and residence times using environmental tracers in an arid unsaturated zone. *Water Resour. Res.* 36, 395-409.
- Scanlon, B.R., Keese, K., Reedy, R.C., Simnuek, J., and Andraski, B.J., 2003. Variations in flow and transport in thick desert vadose zones in response to paleoclimatic forcing (0-90 kyr): Field measurements, modeling, and uncertainties. *Water Resour. Res.* 39, SBH 3-1-17.

- Sharma, M.L., and Hughes, M.W., 1985. Groundwater recharge estimation using chloride, deuterium and oxygen-18 profiles in the deep coastal sands of Western Australia. *J. Hydrol.* 81, 93-109.
- Simunek, J., Sejna, M., and van Genuchten, M.T., 1998. The HYDRUS-1D software package for simulating the one-dimensional movement of water, heat, and multiple solutes in variably-saturated media, version 2.0, IGWMC - TPS - 70, 202 pp., Int. Groundwater Model. Cent., Colo. Sch. of Mines, Golden, Colo.
- Stonestrom, D.A., Prudic, D.E., Laczniak, R.L., Akstin, K.C., Boyd, R.A., and Henkelman, K.K., 2003. Estimates of deep percolation beneath native vegetation, irrigated fields, and the Amargosa River channel, Amargosa Desert, Nye County, Nevada: U.S. Geological Survey Open-File Report 03-104.
- Tyler, S.W., Chapman, J.B., Conrad, S.H., Hammermeister, D.P., Blout, D.O., Miller, J.J., Sully, M.J., and Ginanni, J.M., 1996. Soil-water flux in the southern Great Basin, United States: temporal and spatial variations over the last 120,000 years. *Water Resour. Res.* 32, 1481-1499.
- Tyler, S.W., McKay, W.A., and Mihevc, T.M., 1992. Assessment of soil moisture movement in nuclear subsidence craters. *J. Hydrol.* 139, 159-181.
- van Devender, T.R., 1990. Late Quaternary vegetation and climate of the Chihuahuan Desert, United States and Mexico, in *Packrat Middens: The Last 40000 Years of Biotic Change*, edited by J. L. Betancourt, T. R. van Devender, and P. S. Martin, pp. 104—133, Univ. of Ariz. Press, Tucson.
- Walvoord, M.A., Plummer, M.A., Phillips, F.M., and Wolfsberg, A.V., 2002. Deep system hydrodynamics: 1. Equilibrium states and response times in thick desert

vadose zones, *Water Resour. Res.* 38, 1308, doi:10.1029/2001WR000824.

Winograd, I.J., 1981. Radioactive waste disposal in thick unsaturated zones. *Science* 212, 1457-1463.

Wood, J.L., and Andraski, B.J., 1995. Selected meteorological data for an arid site near Beatty, Nye County, Nevada, calendar years 1990-91: U.S. Geological Survey Open-File Report 94-489, 49 p.

CHAPTER 6

CONCLUSIONS

This dissertation is composed of four separate studies which are related to each other. Studies examined effects of soil physical properties, vegetation cover, and macropores on soil moisture variation of desert soils, the impacts of climate change on solute transport, paleoclimate and paleohydrology in southwestern Great Basin, and chloride transport in vadose zone of ADRS. Three of these studies focused on soil moisture change, and solute transport in the vadose zone of southwestern Great Basin. The fourth chapter evaluated paleoclimate and paleohydrology change in Owens Valley in the last 18 ka.

The simulated results from the soil moisture study indicate that the soil texture and vegetative cover have significant effects on the soil water content, while macropores have only slight effects on the soil water content at the NTS. Soil texture determines the soil's hydraulic properties and affects the retention and flow of water in the soil, which thereby affects the soil water content. In arid environments, plant growth enhances the loss of water from the soil. As a result, the soils with vegetation cover have less soil water content than the bare soils. The overall effect of soil texture on evaporation varies with the amount of available water.

The macropore flow increases the soil water content by 3.0% in sand and silty loam, and decreases the soil water content by 3.0% in the loamy sand. The combined effects of

vegetation and macropores on the soil water content are most significant in loamy sand and insignificant in sand.

Soil with macropores has higher effective hydraulic conductivity near saturation than soil without macropores. However, macropore flow contributions to soil water content varies among different soil textures. The simulated results with macropores show that sand and loamy sand with macropores have a slightly lower soil water content during periods of low precipitation, but have a larger difference during periods of high precipitation. This is because soils with macropores have a higher effective hydraulic conductivity near saturation. Water flows faster through soil with macropores than soil without macropores. High precipitation makes it possible for a higher water content, and therefore a more significant macropore flow.

Under current climatic conditions, the precipitation at the NTS is low throughout most of the year; macropore flow is insignificant. However, macropore flow could have been important in past pluvial periods and could be important in future possible high precipitation events.

The parameterization of the effective hydraulic conductivity shows promise in calculating soil water contents for soils with macropores. The simulations in this study show that soil texture, vegetative cover, and macropores interact with each other to influence the soil water content in arid regions.

Water fluxes from the in-situ measurements with tension infiltrometer, and Br dispersion coefficients obtained from displacement experiments in undisturbed soil cores were quite high. These high water fluxes are mainly results of coarse soil textures and

possibly from preferential flow, which was supported by the effluent data for the undisturbed cores.

One undisturbed soil core from the plant canopy area exhibited similar a transport characteristics to the cores from the interspace, which may not be typical for the soils under plant canopy, because the field measurements with the tension infiltrometer indicated a larger variation in hydraulic properties for the soils under canopy. It can be expected that large soil cores would better capture more information on the water movement and solute transport in structured soils. Multiple tracers could also be used to identify the contributions of preferential flow and matrix diffusion in structured soils.

The coupled catchment-lake model developed in this dissertation is capable of simulating lake extent as a function of modern climate and paleoclimate. The simulations on lake extent at 18 ka, 15 ka, 12 ka, 9 ka, 6 ka, and modern climate conditions are very compatible with observed or derived data. The annual precipitation and temperature of Owens Valley for these times are generally in agreement with the proxy data that are derived from Owens Valley and the places near Owens Valley. The accuracy of our quantitative estimates in paleotemperature and paleoprecipitation in Owens Valley is completely dependent on the elevation of paleo-shorelines and their chronology for the lakes. Therefore, estimates on paleotemperature and paleoprecipitation at 18 ka, 15 ka, 12 ka, 9 ka, and 6 ka are only effective for the geologic evidence used this study. There are two advantages for the coupled catchment-lake model developed in this dissertation. First, based on the proxy data, numerical values of paleotemperature/paleoprecipitation can be easily obtained by narrowing a large number of possible paleoclimatic combinations. Second, the model developed in this study is a physically based model,

thus it can be applied to any lake system if input parameters are available.

The simulation of chloride profile is improved with the modified version of the HYDRUS-1D computer code by using variable boundary conditions. The unclear assumptions in the CMB are avoided in simulations with the variable conditions. Based on the simulated results of local paleolake extents, the techniques preparing variable boundary conditions have been proved effective in this study. Simulated water flux at ADRS is ~ 0.016 mm/year upward at the base of the profile, which is consistent with previous studies. However, many uncertainties exist, and may have some effects on chloride transport, thus it is very critical to perform the uncertainty analysis in future studies.

APPENDIX I

PERMISSION OF ELSEVIER SCIENCE



ELSEVIER
7 July 2004

Our Ref: HW/jj/Jul04/J155

Weiquan Dong
University of Nevada, Las Vegas
4505 Maryland Parkway
Las Vegas 89154-4010
USA

Dear Weiquan Dong

**JOURNAL OF HYDROLOGY, Vol 275, No 3-, 2003, pp 162-181, Dong et al:
“Simulations on soil ...”**

As per your letter dated 6 July 2004, we hereby grant you permission to reprint the
aforementioned material at no charge **in your thesis** subject to the following conditions:

1. If any part of the material to be used (for example, figures) has appeared in our
publication with credit or acknowledgement to another source, permission must
also be sought from that source. If such permission is not obtained then that
material may not be included in your publication/copies.
2. Suitable acknowledgment to the source must be made, either as a footnote or in a
reference list at the end of your publication, as follows:

“Reprinted from Publication title, Vol number, Author(s), Title of article, Pages
No., Copyright (Year), with permission from Elsevier”.
3. Reproduction of this material is confined to the purpose for which permission is
hereby given.

4. This permission is granted for non-exclusive world **English** rights only. For other languages please reapply separately for each one required. Permission excludes use in an electronic form. Should you have a specific electronic project in mind please reapply for permission.
5. This includes permission for UMI to supply single copies, on demand, of the complete thesis. Should your thesis be published commercially, please reapply for permission.

Yours sincerely

A handwritten signature in black ink, appearing to read 'H Gainford', written in a cursive style.

Helen Gainford

Rights Manager

VITA

Graduate College
University of Nevada, Las Vegas

Weiquan Dong

Home Address:

1600 E. University Ave, Apt. #220
Las Vegas, NV 89119

Degrees:

Bachelor of Science, Geology, 1987
Chengdu University of Technology, China

Master of Science, Geochemistry, 1990
Guiyang Institute of Geochemistry, Chinese Academy of Sciences, China

Special Honors and Awards:

Excellent Thesis Award, Chinese Committee of Petrology, Mineralogy and
Geochemistry (CCPMG), 1990
Award of Scientific Achievement of GIGCAS, 1994
Chinese Academy of Sciences Scholarship, 1995

Publications:

- Chen, D., Dong, W., Qi, L., Chen, G., and Chen, X., 2004. Pb-Pb Ages for Doushantuo phosphorites constraints on early Metazoan evolution and glacial events during terminal Neoproterozoic in south China. *Precambrian Research* 132, 123-132.
- Chen, D., Dong, W., Qi, L., Chen, G., and Chen, X., 2003. REEs constrain paleoenvironment changes for Doushantuo phosphorites in Weng'an Mine, south China during terminal Proterozoic. *Chemical Geology* 201, 103-118.
- Lal, D., Harris, N.B., Sharma, K.K., Gu, Z., Ding, L., Liu, T., Dong, W., Caffee, M.W., and Jull, A.J.T., 2003. Erosion history of the Tibetan Plateau since the Last Interglacial: constraints from the first studies of cosmogenic ^{10}Be from Tibetan bedrock. *Earth and Planet. Sci. Lett.* 217, 33-42.
- Dong, W., Yu, Z., and Weber, D., 2003. Simulations on water variation in arid regions. *J. Hydrol.* 275, 165-181.
- Dong, W., Lal, D., Ransom, B., Berger, W., and Caffee, M. W., 2001. Marine biogeochemistries of Be and Al: A study based on cosmogenic ^{10}Be , Be and Al in

marine calcite, aragonite, and opal. Proc. Indian Acad. Sci. (Earth Planet. Sci.)
110, 95-102.

Dissertation Title: Extraction of Paleohydrology and Paleoclimate Proxies from Vadose
Zones and Paleolake Records in Southwestern Great Basin

Dissertation Examination Committee:

Chairperson, Dr. Zhongbo Yu, Ph. D.

Committee Member, Dr. Andrew D. Hanson, Ph. D.

Committee Member, Dr. David K. Kreamer, Ph. D.

Committee Member, Dr. Terry L. Spell, Ph. D.

Graduate Faculty Representative, Dr. Klaus J. Stetzenbach, Ph. D.